TOWARDS MONOLITHIC SEMICONDUCTOR PHOTONIC CRYSTAL PASSIVELY MODE LOCKED LASER FOR TWO-PHOTON MICROSCOPY

A DISSERTATION
SUBMITTED TO THE DEPARTMENT OF ELECTRICAL ENGINEERING
AND THE COMMITTEE ON GRADUATE STUDIES
OF STANFORD UNIVERSITY
IN PARTIAL FULFILLMENT OF THE REQUIREMENTS
FOR THE DEGREE OF
DOCTOR OF PHILOSOPHY

Altamash Janjua
March 2012

This dissertation is online at: http://purl.stanford.edu/pj798mk1986

I certify that I have read this dissertation and that, in my opinion, it is fully adequate in scope and quality as a dissertation for the degree of Doctor of Philosophy.

James Harris, Primary Adviser

I certify that I have read this dissertation and that, in my opinion, it is fully adequate in scope and quality as a dissertation for the degree of Doctor of Philosophy.

Shanhui Fan

I certify that I have read this dissertation and that, in my opinion, it is fully adequate in scope and quality as a dissertation for the degree of Doctor of Philosophy.

Mark Schnitzer

Approved for the Stanford University Committee on Graduate Studies.

Patricia J. Gumport, Vice Provost Graduate Education

This signature page was generated electronically upon submission of this dissertation in electronic format. An original signed hard copy of the signature page is on file in University Archives.

Altamash Janjua

I certify that I have read this dissertation and that, in my opinion, it is fully adequate in scope and quality as a dissertation for the degree of Doctor of Philosophy.

_____

James S. Harris, Principal Adviser

I certify that I have read this dissertation and that, in my opinion, it is fully adequate inscope and quality as a dissertation for the degree of Doctor of Philosophy.

_____

Mark Schnitzer, Co-Advisor

I certify that I have read this dissertation and that, in my opinion, it is fully adequate inscope and quality as a dissertation for the degree of Doctor of Philosophy.

_____

Shanhui Fan

Approved for the Stanford University Committee on Graduate Studies.

Abstract

Semiconductor Monolithic Passively Mode Locked Lasers (MMLLs) have been demonstrated and have a variety of applications including sensing, in optical communications and optical clock generation. The major advantage that these semiconductor light sources possess is their compact size, high efficiency, low cost and robustness. Also the ability to access different wavelengths using various semiconductor materials is a big advantage. The inability to get these lasers to operate at low repetition rates and the limited peak output power of the pulses are the two major limitations of these lasers. The repetition rate is inversely proportional to the semiconductor laser cavity length. The lowest repetition rate in current MMLLs is around 1GHz. This rate is limited by the complexity involved in the fabrication of centimeter long semiconductor laser cavities. The material loss, dispersion and carrier radiative recombination lifetime also limit the output repetition rate. Lower repetition rate lasers can be used in low frequency integrated optical circuits and also for imaging especially for Two-Photon Microscopy (TPM). TPM works by exciting florescence dyes using two photons instead of one. This requires pulsed lasers with high peak power and high energy per pulse. TPM is currently done by using expensive and bulky Ti:Sapphire mode locked lasers that can produce subpicosecond pulses at a repetition rate of order of 100 MHz. The possible use of semiconductor lasers for this application can transform this field by dramatically reducing the cost of imaging and allowing for dramatically smaller sized and more mobile imaging solutions.

One potential way to reduce the repetition rate of the lasers without increasing the physical cavity length is to incorporate a slow light photonic crystal structure inside the lasers cavity. Such a laser cavity will have a group index that is much larger than the material refractive index thereby giving a longer optical path length for the same physical length of the device. The incorporation of the photonic crystal will also allow the possibility to do dispersion engineering within the laser cavity and to enable pulse compression. Both these effects can increase the two-photon excitation efficiency for TPM. In this work we highlight the design and progress towards the development of a monolithic semiconductor photonic crystal passively mode locked laser for two-photon microscopy.

Acknowledgement

Alhumdulilah! All praise and thanks is for God. Everything that I have been able to accomplish is only because of His Will, Help and Guidance.

This work would not have been possible without the help of many people. I would like to thank all of them for their help and support. Firstly, I would like to thank my advisor and mentor Prof. James Harris. He was instrumental in my decision to pursue graduate studies in the field of optoelectronic devices. He provided the inspiration for this project and was my primary source of guidance throughout my stay at Stanford University. I would also like to thank my co-advisor Prof. Mark Schnitzer. He has been a constant driving force behind this project and provided me with the motivation to keep working in easy and difficult times. I am heavily indebted to both of my advisors for their constant guidance and support. My PhD studies at Stanford would not have been possible without their help. I would also like to thank Prof. Shanhui Fan for being an advisor on this project. I have leant a lot from him. His student Sunil Sandhu has been a source of advice throughout this work and I am very thankful to him as well. I would also like to thank Prof. Krishna Saraswat for being part of my oral defense committee. He was also my academic advisor during my MS studies and I am really obliged to him for his invaluable advice during my initial years at Stanford. I would like to thank the whole of Harris group. They were my family away from home and helped me throughout my stay at Stanford. Specifically I would like to acknowledge Sonny and Tomas for their precious help and support. I would also like to express thanks to all of my fellow group members in the Schnitzer group

for their help. I would like to specially thank Supriyo Sinha and Yiyang Gong for their very helpful advice. Lastly, I would also like to acknowledge the SNF and SNC staff. They were instrumental in making this work possible by keeping the SNF and SNC labs operational through their hard work.

Dedication

This work is dedicated to my parents, my wife and my son. Without their help, support and patience this work would not have been possible.

Table of Contents

Chapter 1

Introduction

We have come a long way since the discovery of lasers in 1960 [1]. Nowadays lasers are all around us. From telecommunications, to medicine, to agriculture, to CD and DVD players, to a computer mouse, laser applications are now incredibly widespread. Lasers are a source of high intensity optical power. The light output from a laser also has high degree of spatial and temporal coherence. These properties make lasers the only available solution for many problems. For example, lasers are used for welding and precise machining. The high optical power output from a laser can easily melt metals and since the light from a laser can be focused to very small dimensions, they are ideal candidates for precise welding of metals. For this reason lasers are now essential tools in the manufacturing of modern automobiles. The acronym LASER stands for Light Amplification through Stimulated Emission of Radiation. Every laser needs two basic components to work. It needs a gain medium that can allow for the optical excitation to grow over time through the stimulated emission of photons. Then to further increase the optical intensity we need to put the gain medium in a resonator cavity as illustrated in figure 1. The cavity preferentially makes the amplitude of particular wavelengths of light to grow very rapidly. These wavelengths, which are also called modes, are resonant with the cavity.

Introduction

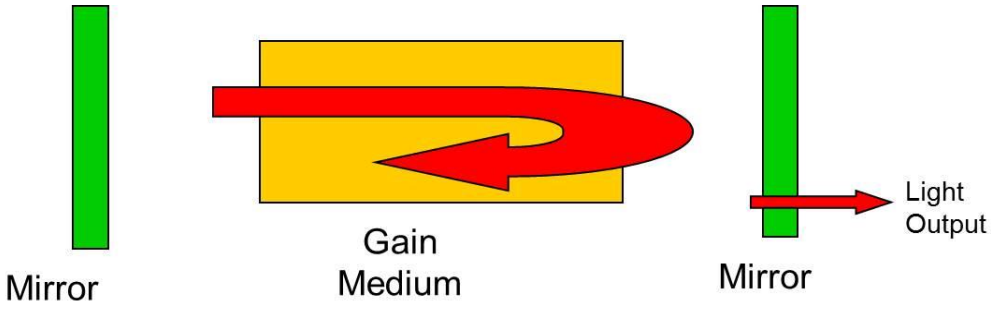

Figure 1: Components of a Laser

Semiconductors lasers are a very important class of lasers. These lasers are usually made from direct bandgap semiconductors like Gallium Arsenide (GaAs) and Indium Phosphide (InP). Inside a semiconductor the energy of the electron is distributed into bands of allowed energy states. At room temperature, the electrons reside in two bands separated by a range of forbidden energies. This forbidden range is called the bandgap. This is very different from what we have in metals as shown below in figure 2. The lower energy band is called the valence band and the upper band the conduction band.

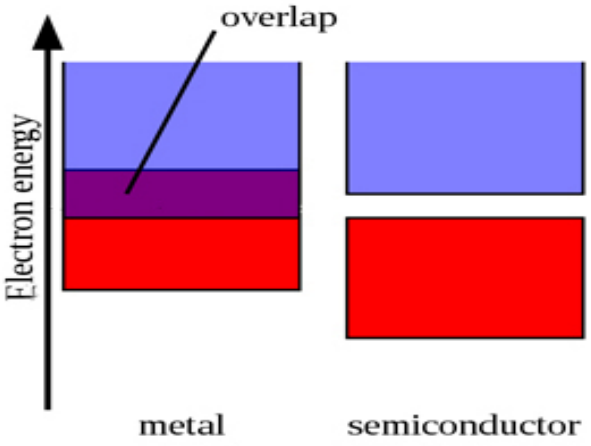

Figure 2: Electron energy levels in metal and semiconductor

Normally electrons fully populate the valence band and the conduction band is empty. However through thermal or optical excitation or through the incorporation of external elements called dopants, some electrons can be injected into the conduction band from the valence band. These electrons can later jump back into the empty states in the valence band with the possible emission of a photon, a quantum of light. The empty states are called holes and this type of electron-hole recombination is called radiative recombination. In this manner semiconductors can emit light. Direct bandgap semiconductors like GaAs and InP can emit light very efficiently. This is because in direct bandgap semiconductors the maximum of the valence band is at the same position in momentum space as the minimum in the conduction band. Most electrons lie at the conduction band minimum and correspondingly most holes are located at the valence band maximum. Therefore, a direct bandgap allows for very efficient electron-hole radiative recombination without any momentum change. In contrast in indirect bandgap semiconductors, electron hole recombination requires momentum exchange through the emission or absorption of momentum packets (quanta) called phonons. This makes the radiative recombination process very inefficient. Direct and indirect recombination of electron and holes is shown in figure 3 below [2].

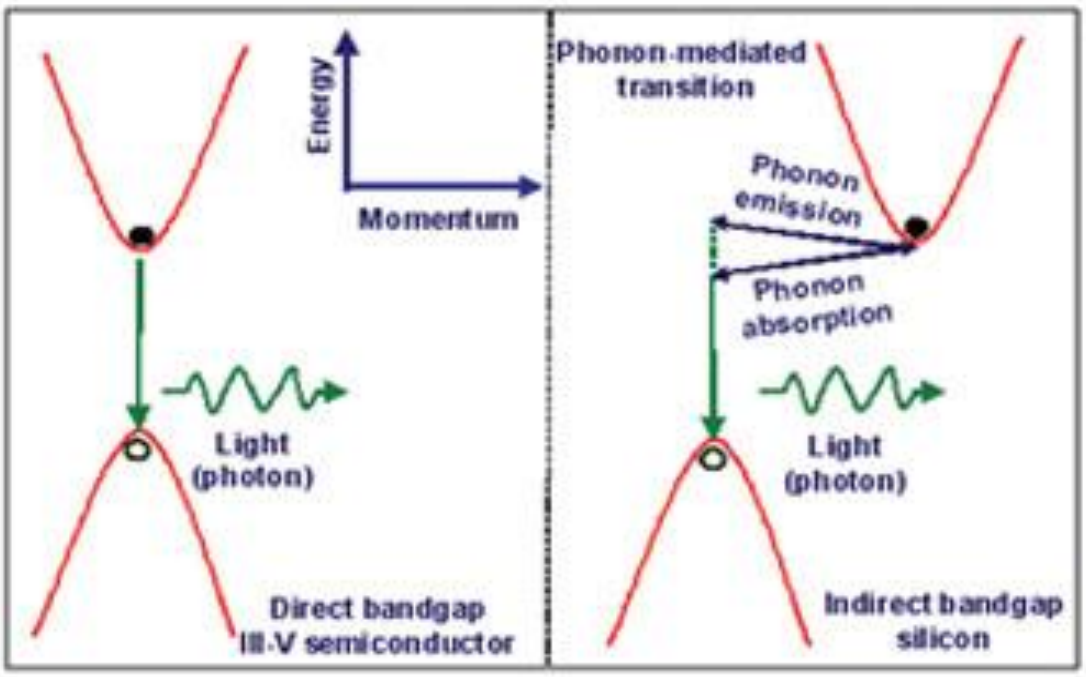

Figure 3: Direct semiconductors vs Indirect semiconductors [2]

Direct bandgap semiconductors under excitation can show optical gain. This happens when the electron population in the conduction band minimum is greater than the electron population in the valence band maximum, a condition called population inversion. The population of electrons and holes in the conduction and valence bands is statistically described by electron and hole Fermi levels. Population inversion requires the Fermi level separation to be greater than the bandgap of the semiconductor as shown in the equation below where is the E_g is the bandgap, F_n is the electron fermi level and F_p is the hole Fermi level.

$$E_g = F_n + F_p$$

Chapter 1

By creating a P-N diode in a direct semiconductor like GaAs, electrical injection of the device can easily be done. At the junction between the P and N doped regions, there is a large number of electrons and holes present when the device is forward biased. Under these conditions a significant number of electrons and holes can recombine and emit photons. This is how a simple Light Emitting Diode (LED) works. To get a semiconductor laser, however, we need to have better confinement of carriers to obtain a population inversion. Furthermore, we also need better optical confinement so that there is strong coupling between the optical wave and the recombining electrons and holes, thus insuring that the optical gain is sufficiently high to overcome the losses inside the cavity. Both of these objectives can be achieved in Separate Confinement Heterostructure (SCH) lasers. In SCH lasers multiple semiconductor layers are used to get optical and electrical confinement with strong overlap. In the middle there is a narrow layer of the smallest bandgap semiconductor, called the Quantum Well (QW) layer. This layer is surrounded by a layer of intermediate bandgap and high refractive index material and it is called the waveguide/confinement layer. The waveguide layer is in turn sandwiched by a large bandgap and low refractive index semiconductor layer on the top and thet bottom. These layers area called the top and bottom cladding layers, respectively. The top cladding is N-doped and the bottom cladding is P-doped. The waveguide and quantum well layer are usually undoped. A common material system that is used for SCH lasers consists of using Aluminum Gallium Arsenide ($Al_xGa_{1-x}As$) with high Aluminum (Al) content as the cladding layer, a low Al content $Al_xGa_{1-x}As$ layer as the waveguide layer and using GaAs as the QW layer. The layers

are grown epitaxially on a single crystal substrate like GaAs and they are covered on top by a highly doped cap contact layer. The SCH structure is shown below in figure 4.

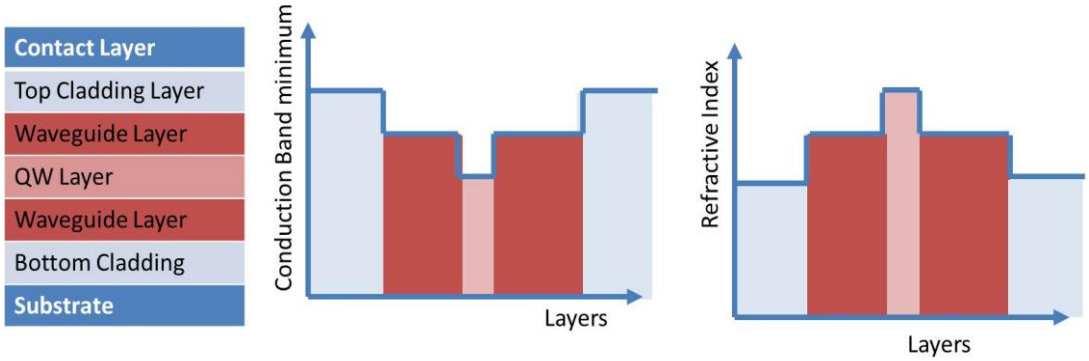

Figure 4: Wafer structure with bandgap distribution and refractive index profile

The SCH combination provides both optical confinement and electrical confinement. The lowest bandgap QW layer traps both electrons and holes in a common region. This makes achieving population inversion much easier. Simultaneously, the difference in refractive index between the waveguide layer and cladding layer confines light by total internal reflection. The light is now confined to the location where we have population inversion and this increases the optical gain. The last element needed to make a laser is to create a resonator. This can be done by cleaving the semiconductor. The cleaved ends are both perfectly parallel and smooth enough to make good mirror facets. These facets now enclose the semiconductor gain region and we have a laser.

Modelocked Lasers

Common lasers usually output light continuosly as long as the excitation is present. An electrically pumped lasers will output light as long as the input current is on. However lasers can also output pulses of light. The easiest way to do that would be to pulse the excitation source. For example in injection pulsed lasers, modulating the electrical current will modulate the output light. In Q-switched lasers the cavity loss is modulated and this gives pulsed operation. Mode locked lasers are a more interesting type of pulsed lasers. These lasers pulse intrinsicly and produce ultrashort pulses. These ultrashort pulses also have very high peak optical power since for the same average output power the light is now being concentrated into very narrow pulse periods instead of being output continuosly. The pulse repitition rate of mode locked lasers is inversely proportionaly to cavity length. So the smaller the laser cavity, the higher the repitition rate. Also the pulses themselves are very narrow, of the order of few picoseconds (ps) or less. Semiconductor mode locked lasers are very interesting because they can provide ps pulses at very high repition rates while being very compact, cheap and robust [3,4].

Mode locked lasers have a variety of applications. Very large mode locked lasers are being used to achieve nuclear fusion. They are also used for micromachining and in surgery because they can deliver large amount of heat precisely to very small areas. Mode locked lasers are also used for imaging, especially in Two Photon Micrscopy (TPM). Semiconductor mode locked lasers due to their small size and low cost are ideal candidates for both on-chip and off-chip optical communications [5].

They are also useful for optical clock generation and Wavelength Division Multiplexing [6,7].

Two Photon Microscopy

Conventional microscopy uses one-photon absorption to excite fluorescence. A fluorescent dye is illuminated by photons that have energy equal to the difference in energies between the ground and excited state of the fluorescent dye molecule. The dye absorbs the photon and reaches an excited state. On decay from the excited state, the dye emits a photon that is slightly red shifted due to the Stokes shift.

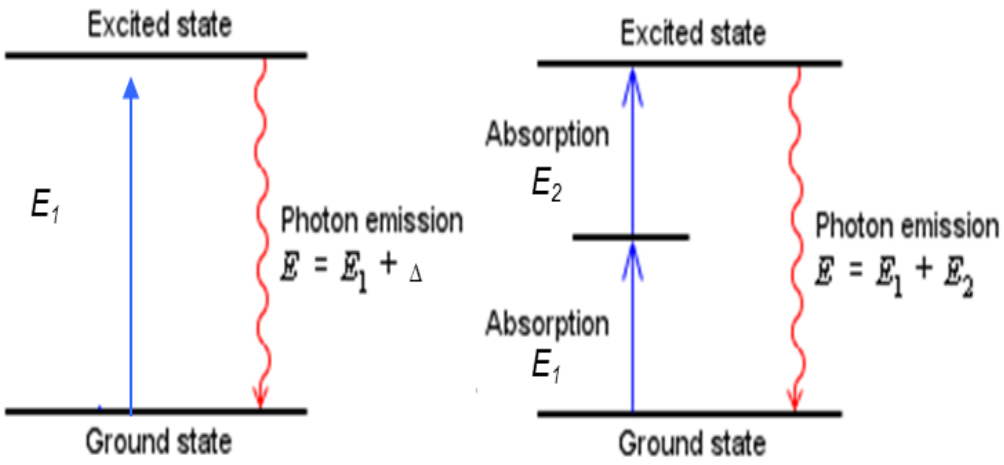

Figure 5: One-photon excitation and two-photon excitation

In Two Photon Microscopy (TPM), the dye is excited by the simultaneous absorption of two photons, each with nearly half the energy of the energy difference illustrated in figure 5 above. Since simultaneous absorption of two photons is required, the fluorescence is proportional to the square of the intensity of the excitation light.

Due to this square dependence, TPM requires high peak intensity that is usually done by using mode locked lasers. The pulses from these lasers have sufficiently high peak power to excite significant two-photon fluorescence. The technique is a scanning imaging technique where the laser pulses are scanned over the specimen. Figure 6 below, taken from reference [8], shows a typical two photon system.

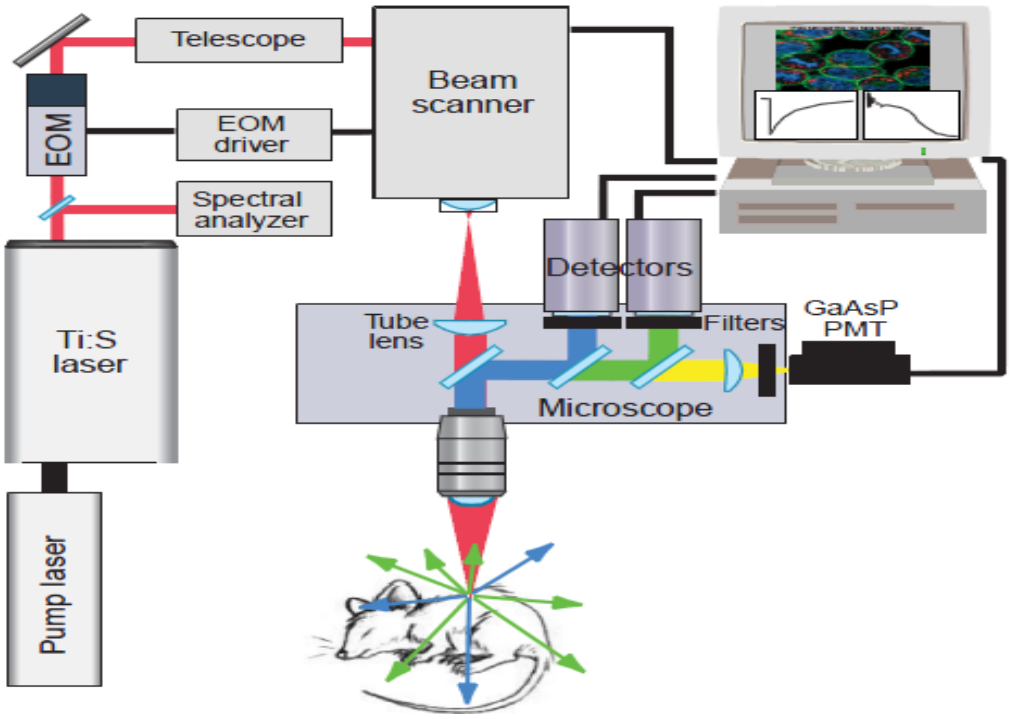

Figure 6: Two Photon Microscopy system [8]

Usually TPM is done using rather large and expensive Ti: Sapphire lasers. The intensity of the laser is controlled by using Electro Optic Modulators (EOM). A telescope lens is used to adjust the beam size. The light is then focused onto a small focal spot using a collection of lenses. This focal spot can be scanned in the X-Y directions over the specimen to be imaged using beam scanners. The lenses also allow

for the movement of the focal point in the Z direction thus allowing tomographic cross sectioning. A dichroic mirror splits the input and fluorescent light. Using sensitive large area photomultiplier tubes (PMTs) as detectors, efficient collection of fluorescent photons is made possible.

Two-photon microscopy has many advantages over one-photon microscopy. First, the wavelength of the excitation light and the fluorescent light are very different and this makes the separation of the input photons from the output photons much easier. Also in TPM, the fluorescence signal only comes from a tiny volume where the light is focused since only in that region is the intensity high enough to produce significant two-photon excitation. This is very different from one-photon microscopy where fluorescence can be generated anywhere along the incident path of the excitation light. This is clearly shown in figure 7 below.

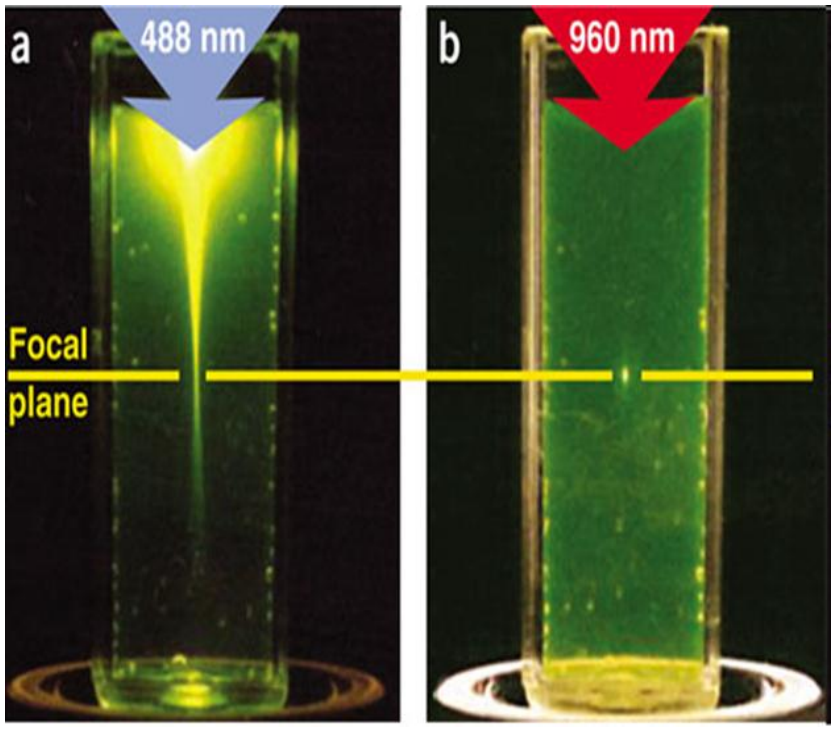

Figure 7: (a) One-photon excitation (b) and Two-photon excitation [8]

In the one-photon case on the left, fluorescence is generated in a much larger volume. Whereas in the two-photon case, shown on the right, noticeable fluorescence only originates from a small volume in the focal plane of incident light. This localized excitation allows cross sectioning. 3D image stacks can be collected in TPM since light can be scanned over multiple focal planes at different depths. Since TPM is done with longer wavelength light, the incident light can penetrate much deeper since it is absorbed and scattered less than the higher energy photons required for one-photon fluorescence. Also since the fluorescence comes from a tiny localized focal volume, all the useful fluorescence photons can be collected. This allows for the possibility of much deeper imaging in TPM.

References for Chapter 1

[1] T. Maiman, “Stimulated Optical Radiation in Ruby”, Nature 187, 493, 1960.

[2] Bahram Jalali, “Silicon Lasers, Physics and Technology Forefronts”, APS news, volume 15, number 3, March 2006.

[3] E.A.Avrutin, J.H.Marsh and E.L.Portnoi, “Monolithic and multi-gigahertz mode-locked semiconductor lasers: constructions, experiments, models and applications”, IEEE Proceedings on Optoelectronics, volume 147, number 4, August 2000.

[4]Dennis j. Derickson, Roger J. Helkey, Alan Mar, Judy R. Karin, John G. Wasserbauer, and John E. Bowers, “Short pulse generation using multisegment mode-locked semiconductor lasers”, IEEE Journal of Quantum Electronics, volume 28, number 10, October 1992.

[5] Alexander W. Fang, Brian R. Koch, Kian-Giap Gan, Hyundai Park, Richard Jones, Oded Cohen, Mario J. Paniccia, Daniel J. Blumenthal, and John E. Bowers, “A racetrack mode-locked silicon evanescent laser”, Optics Express, volume 16, issue 2, pp. 1393-1398, 2008.

[6] P. Delfyett, D. Hartman, and S. Z. Ahmad, “Optical Clock Distribution Using a Mode-Locked Semiconductor Laser Diode System,” Journal of Lightwave Technology, volume 9, pp. 1646, 1991.

[7] R. Logan, “All-optical heterodyne RF signal generation using a mode-locked laser frequency comb: theory and experiments,” IEEE MTT-S Digest 3, pp. 1741, 2000.

[8] Warren R Zipfel, Rebecca M Williams and Watt W Webb, “Nonlinear magic: multiphoton microscopy in the biosciences”, Nature Biotechnology 21, pp. 1369 – 1377, 2003.

Chapter 2

Theory

Our proposed device combines the device physics of edge emitting, passively mode locked lasers with the nanophotonics of slow light photonic crystals. To understand the device working principles, we need to study the theory behind mode locking in general and passive mode locking in particular. We also need to study the physics of photonic crystals and understand the design process to engineer them. This chapter discusses these two areas.

Mode Locking

For lasing to occur, we need to have a medium that shows optical gain and we need to enclose it in a resonator. A direct bandgap semiconductor like GaAs can serve both of these purposes. A semiconductor shows optical gain over some wavelength/frequency range called its gain bandwidth (see top of figure 1). At the same time, the semiconductor laser cavity formed by the cleaved laser facets, is resonant to a few particular wavelengths called the cavity modes. The resonant modes are those modes for which the length of the cavity (L) is an integer multiple of half the wavelength (λ).

$$\lambda = \frac{2 * L}{n * m}$$

In the equation above, ***n*** is the group refractive index and ***m*** is the integer mode number. Only for those cavity modes that fall within the gain bandwidth can lasing occur (see bottom of figure 1). These modes experience optical gain and are also resonant with the cavity. For a mode to lase, the total optical gain must be greater than the total optical loss for that mode. Under high enough excitation, some modes do experience net optical gain and they start lasing. This is explained in the figure below.

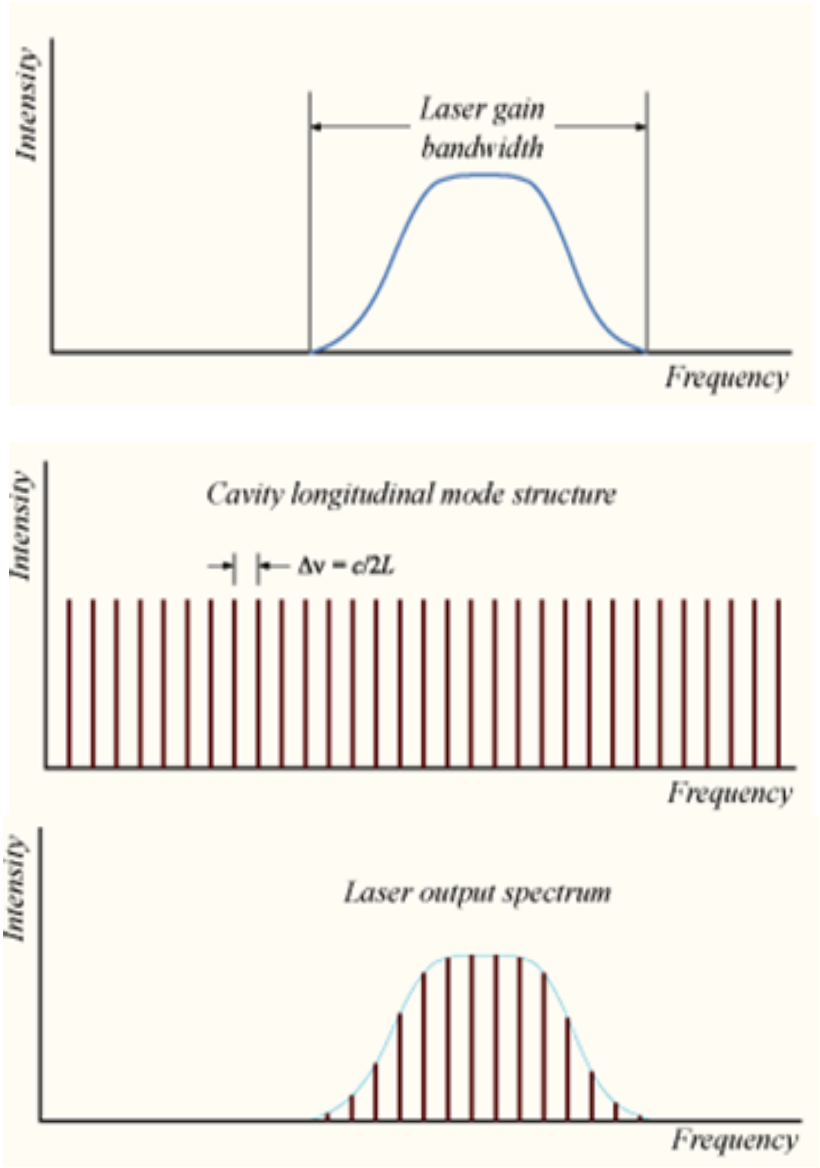

Figure 1: (Top) Lasing bandwidth, (Middle) Cavity modes, (Bottom) Laser spectrum

Theory

A normal laser operating in Continuous Wave (CW) mode will have all of these modes lasing in a random fashion. The resulting output of light is a random fluctuation of intensity over some average value. In mode locked operation all the lasing modes are locked together *in phase*. They have a constant fixed phase relationship between them. These modes can then interfere constructively and this constructive interference of the modes results in the light output being pulsed. This mode of operation can also be understood through knowledge of Fourier series.

$$f(x) = a_0 + \sum_{n=1}^{\infty} \left(a_n \cos \frac{n\pi x}{L} + b_n \sin \frac{n\pi x}{L} \right)$$

The equation above is the definition of a Fourier series. The equation states that any periodic function ***f(x)*** can be obtained by summing a bunch of sinusoids that have frequencies that are integer multiples of the frequency of the periodic function itself. a_0, a_n and b_n are weighting constants. Therefore a periodic train of square pulses can be obtained by the combining a few sinusoids, each having a frequency that is an integer multiple of the square pulse train frequency. This is exactly what is happening in a mode locked laser. The cavity modes have frequencies that are integer multiples of the inverse roundtrip time. When the laser is mode locked these modes are lasing in unison, locked together, and therefore the output of the laser is a periodic train of pulses that have a period that is equal to the cavity round trip time.

$$R = \frac{c}{2 \times L \times n}$$

In the equation above ***R*** is the repetition rate of the laser, ***c*** is the speed of light, ***L*** is the length of the cavity, and ***n*** is the refractive index of the semiconductor material.

Passively Mode Locked Semiconductor Lasers

Semiconductor mode locked lasers can serve as effective, compact, cheap and robust sources for ultrashort pulses. They can also provide very high repetition rates since compact monolithic devices can be easily fabricated using conventional lithography. There are three types of mode locked lasers: active, passive and hybrid. Actively mode locked lasers are single segment devices where the injection current driving the laser is periodically modulated. The periodic variation of the input current causes the cavity modes to lock together over time and under steady state conditions the laser can output short light pulses periodically. In passively mode locked lasers a new element, the saturable absorber, is incorporated into the laser cavity. This is shown in figure 2 below [1].

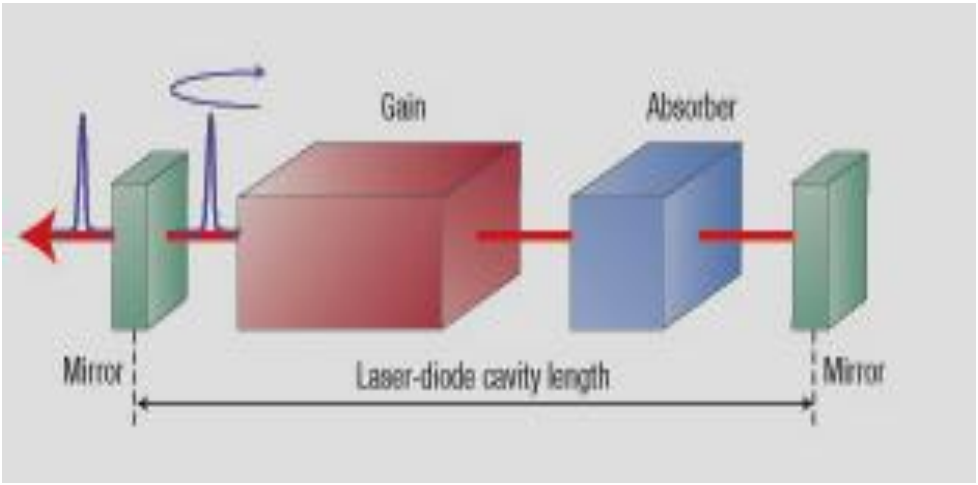

Figure 2: Passively mode locked laser structure

Theory

The purpose of the Saturable Absorber (SA) is to establish the fixed phase relationship between the cavity modes that is needed for mode locking. The SA section introduces controlled loss inside the laser cavity and performs pulse shaping. When a passively mode locked laser is turned on, the light intensity within the cavity consists of random fluctuations. These fluctuations grow over time due to the cavity gain. Most of these fluctuations are not high enough to saturate the SA and they experience net loss inside the laser cavity. However, some fluctuations grow large enough to saturate the SA. These large fluctuations now experience net gain on each pass through the cavity since the SA loss has been saturated. They eventually become the output pulses. Under steady state, only a single pulse travels inside the laser cavity and all the smaller fluctuations decay over time and die out.

For a segment to serve as a SA, it needs to satisfy three conditions [2]. First the energy of the laser pulse (E_p) should be able to saturate the SA.

$$E_P > 4F_{SA}A_{SA}$$

In the equation above, F_{SA} is the energy fluence (J/cm^2) needed to saturate the SA and A_{SA} is the cross-sectional area of the SA. The factor of 4 just signifies the fact that the pulse energy needs to be much greater than the energy required to saturate the SA. If this condition is not met the pulses will not grow over time and the laser will not mode lock. The second condition is that the gain of the laser should not saturate before the SA loss saturates. As the optical intensity grows inside the laser cavity, it starts to saturate the loss inside the SA. The SA loss is usually due to absorption of photons. This absorption cannot grow indefinitely and after a particular level of

optical fluence no further absorption is possible and the SA saturates. The gain of the cavity is also limited and begins to saturate at high optical intensity. Higher light intensity causes an increase in stimulated emission. This reduces the population inversion and thereby reduces the available gain. For the pulses to grow, they should experience a net gain window which means that the pulse has to saturate the SA before the gain saturates. This ensures that the pulse increases during each round trip within the cavity. This condition is shown below where $E_{Sat, GAIN}$ is the saturation energy level of the gain and $E_{Sat, SA}$ is the saturation energy of the SA.

$$E_{Sat, GAIN} > E_{Sat, SA}$$

Finally the SA needs to recover in time so that it can perform pulse shaping on each pass. This is true if the recovery time of the SA (T_{SA}) is much smaller than the cavity round trip time (T_{RR}). Similarly, the gain recovery time (T_{GAIN}) also needs to be smaller than the T_{RR}. This ensures that the pulses can grow and also get shaped during each pass within the laser cavity.

$$T_{RR} > 4T_{SA}, 4T_{GAIN}$$

Figure 3 below shows how the SA shapes pulses. When the leading edge of the pulse hits the SA, it starts to get absorbed by it. This compresses the pulse from the leading edge. At the same time, the incident pulse fluence also starts to saturate the SA. The SA loss begins to decrease and eventually it saturates. After that, the pulse can travel through the SA without getting further absorbed. The gain also eventually

saturates but this needs to happen after the SA has saturated. This creates a net gain window for the pulse peak power to grow. When the pulse starts to exit the SA section, the SA begins to recover. It can now absorb part of the trailing edge of the pulse and this compresses the pulse from the rear edge. After the pulse has exited, the SA section soon reaches its original state. For mode locking to happen, this needs to happen fast enough and before the pulse hits the SA on its next round trip.

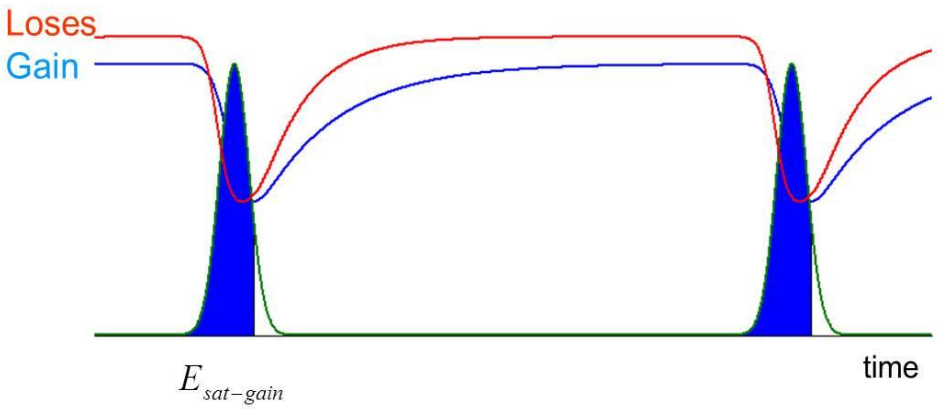

Figure 3: Behavior of Gain and Loss in passive mode locking

A reverse biased QW section of the laser can serve as an effective SA since it satisfies all of the conditions stated above. Furthermore, such a section can be easily incorporated into a monolithic device through simple fabrication steps. QW lasers are generally one section devices with one top electrode. This electrode is forward biased for the laser to be pumped electrically. If we split this top electrode into two pieces, which are sufficiently electrically insulated from each other, it becomes possible to reverse bias one section (SA)and forward bias the other section (laser). Such a two section laser can function as a compact passively mode locked laser as illustrated in figure 4.

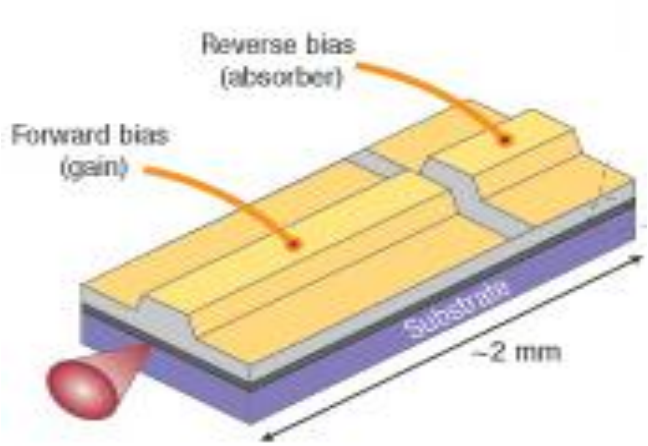

Figure 4: Monolithic passively mode locked laser architecture [1]

Quantum Dots (QDs) lasers can also be passively mode locked. A reverse biased QD section can serve as a better SA region. QDs have a faster recovery time and can provide narrower pulses [2]. However, there is complexity in the difficulty in growing good quality QDs laser wafers.

Semiconductor mode locked lasers for TPM

TPM is conventionally done using large and expensive Ti:Sapphire mode locked lasers. These lasers operate at 80MHz and produce 250 femtoseconds (fs) wide pulses. ~10mW of average power is used for most imaging experiments for TPM and this translates into ~125 picojoule (pJ) per pulse. Comparatively, monolithic semiconductor passively mode locked lasers (MMLLs) usually operate at much higher repetition rates, greater than 1GHz. They also have broader pulses which are few

picoseconds wide and they provide only a few 10s pJ per pulse. TPM fluorescence intensity is inversely proportional to the product of repetition rate and pulse width for a constant average power [3]. Therefore, current MMLLs are not useful for TPM. The possible use of semiconductor MMLLs for TPM can have some major advantages. First, MMLLs will be much cheaper than Ti:Sapphire lasers and this will make TPM solutions far more affordable and more accessible. Second, MMLLs are very light and compact. This will increase the mobility of conventional TPM systems. More importantly, compact and light lasers will allow for the incorporation of these lasers onto miniaturized microscopy solutions like the one shown below that has been designed by the Schnitzer lab at Stanford [4, 5]. These microscopes allow in vivo imaging in live freely moving animals. Cheap MMLLs packaged together into mass produced miniature microscopes will make parallel imaging experiments feasible and practical. This can usher in a new age in microscopy.

Figure 5: Photo of one-photon microscope for in vivo imaging of freely moving mice designed in Schnitzer lab, Stanford [5]

To make MMLLs feasible for TPM, we need to reduce the repetition rate of these lasers and we also have to decrease the temporal widths of the laser pulses. The repetition rate of MMLLs is limited due to the difficulty associated with the fabrication of long devices that are greater than a few centimeters in length. Self Phase Modulation (SPM) and dispersion effects also make mode locking difficult in longer devices. Similarly, narrow laser pulses are more suitable for TPM. However due to dispersion, the pulses in MMLLs are usually greater than 1 ps. This effect is exacerbated in larger devices. Lower repetition rate, at the same average power, results in higher energy per pulse. Similarly, a sharper pulse also means higher peak power of the pulse. Both these effects increase TPM fluorescence.

Photonic Crystals

In recent years, nanophotonics has attracted a lot of interest and attention in the research community. Traditionally photonics has dealt with micron scale features to control the flow of light. However over the last two decades a lot of work has been done to control the propagation of light using engineering at the nanoscale. By engineering the macroscopic dielectric constant of a medium and creating a periodicity in it comparable to the wavelength of light, we can finely control the propagation of light inside that medium. Such materials are called Photonic Crystals (PC) due to their similarity with semiconductor crystals. In semiconductor crystals the periodic arrangement of atoms creates a periodic variation in the electrostatic potential that is seen by the electrons. The propagation of electrons through such periodic potential is described by the electronic band structure, which can be understood through quantum

mechanics. Photonic Crystals (PCs) are the optical counterparts of semiconductor crystals. In PCs, in place of the periodic arrangements of atoms, we create a periodic variation in the dielectric constant of the material. Like the electronic band structure, the propagation of light through PCs can be explained through an optical band structure. The optical band structure is obtained by solving Maxwell's equations [6]. There are also numerous other similarities between semiconductor and photonic crystals. In semiconductors we have an energy bandgap for electrons. Electrons with energy inside the bandgap range cannot travel through the semiconductor crystal. Similarly in some PCs, we have a photonic bandgap and similarly photons that have energy or frequency that fall within the photonic bandgap are forbidden to propagate inside the PC. Also, in both the photonic and electronic band structures, the slope of the bands describes the group velocity of the photons and electrons respectively.

The propagation of light through any medium is governed by the four Maxwell's equations shown below.

$$\nabla \cdot \mathrm{H}(\mathrm{r},t) = 0 \qquad \nabla \times \mathrm{E}(\mathrm{r},t) + \mu_0 \frac{\partial \mathrm{H}(\mathrm{r},t)}{\partial t} = 0$$

$$\nabla \cdot [\varepsilon(\mathrm{r})\mathrm{E}(\mathrm{r},t)] = 0 \quad \nabla \times \mathrm{H}(\mathrm{r},t) - \varepsilon_0 \varepsilon(\mathrm{r}) \frac{\partial \mathrm{E}(\mathrm{r},t)}{\partial t} = 0.$$

In the equations above, ***B*** is the magnetic flux, ***E*** is the electric flux, ***D*** is the electrical displacement field and ***H*** is the magnetic induction field, $\boldsymbol{\varepsilon}$ is the dielectric constant, $\boldsymbol{\mu}$ is the magnetic permeability, ***r*** is the position vector and ***t*** is time.

After some algebraic manipulation and simplification of the four Maxwell's equation shown above, we can obtain the master equation that is shown below. It is from the master equation that we get the photonic band structure of medium.

$$\nabla \times \left(\frac{1}{\varepsilon(\mathbf{r})} \nabla \times \mathbf{H}(\mathbf{r}) \right) = \left(\frac{\omega}{c} \right)^2 \mathbf{H}(\mathbf{r})$$

Photonic Band Structure

By solving the master equation we can calculate the photonic band structure for a medium. This equation is mostly solved numerically. As a simple example, light propagation through a medium of uniform dielectric constant can be described by a constant velocity in all directions. The speed of propagation is equal to the speed of light divided by the refractive index of the material. The band structure for such a medium is shown below.

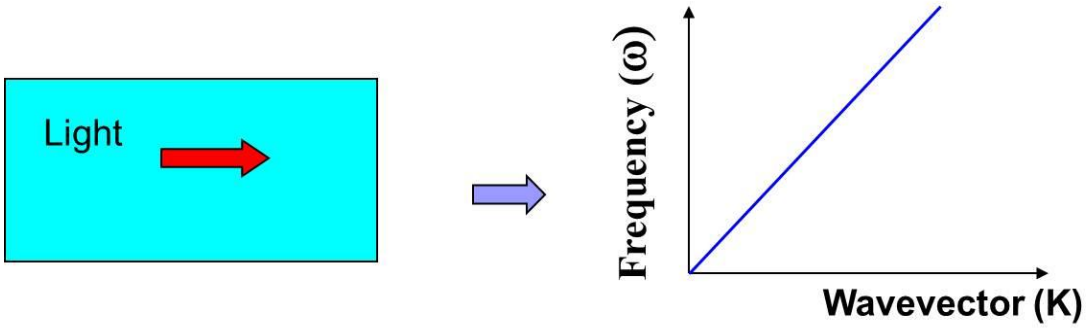

Figure 6: Band structure for a uniform medium

The band structure is plotted with the frequency ($\boldsymbol{\omega}$) of light on the Y-axis and the momentum or wavevector ($\boldsymbol{K}$) on X-axis. This plot is also called the dispersion

diagram. The blue line above, also called a band, is straight in the case of a uniform dielectric slab. This is because the slope of the line is equal to the inverse of group index. In the case of a uniform slab, the group index (n_g) is equal to the refractive index.

$$Slope = \frac{d\omega}{dK} = \frac{1}{n_g}$$

Each point on a band is an allowed electromagnetic mode that can propagate inside the slab. In the more complex case of a periodic array of infinite dielectric rods in a uniform medium, the band structure is naturally more complicated.

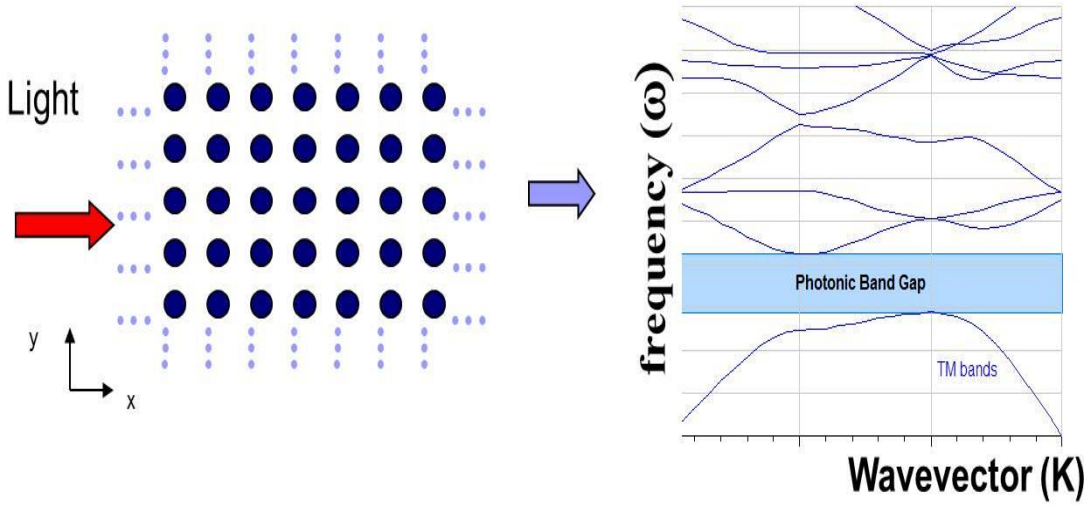

Figure 7: Dispersion diagram for a periodic array of dielectric rods in air

The dispersion diagram now has multiple bands, as shown by the blue lines. For a 2D periodic structure, which is uniform in the third dimension, we can divide the solution of the master equation into two sets of bands according to their polarizations.

The TE band has two electric field components along the X and Y orientations respectively and a single magnetic field component along the Z direction. The X, Y and Z directions are shown on the left in figure 7 above. The other set of bands is called the TM bands. It has two magnetic field components along the X and Y directions and the single electric field component in this case is along the Z direction. The plot on the right side of figure 7 shows the TM band structure. As is evident in the plot, the TM band structure is now much more complex as compared to the case of a uniform slab. There are many more bands and most have non-constant slopes. An interesting feature of the plot above is the existence of the photonic bandgap in the TM band structure. The band gap shows that for the dielectric distribution of rods shown above, TM polarized light with frequency falling within the band gap cannot travel in the medium.

In 2D, a triangular lattice of holes in a dielectric slab can provide us with bandgap for both the TE and TM bands. There is also a frequency range where these gaps overlap. If the incident light has frequency in this range, then irrespective of its polarization, it will not be able to propagate through the structure. If the light is incident from outside on the slab it will be totally reflected back by the structure. Figure 8 below, which is taken from the reference text [6], shows the band structure for such a 2D photonic crystal. In the figure, the triangular lattice of holes is shown in the inset on bottom right. The *k*-axis is a little more complicated and consists of points that are present in the first irreducible Brillouin zone (BZ). The inset at the bottom middle of the figure shows the first BZ. The appendix of the text [6] gives a good

description of the reciprocal lattice and the BZ. The plot clearly shows the presence of a photonic band gap for both the TE and TM polarizations of light.

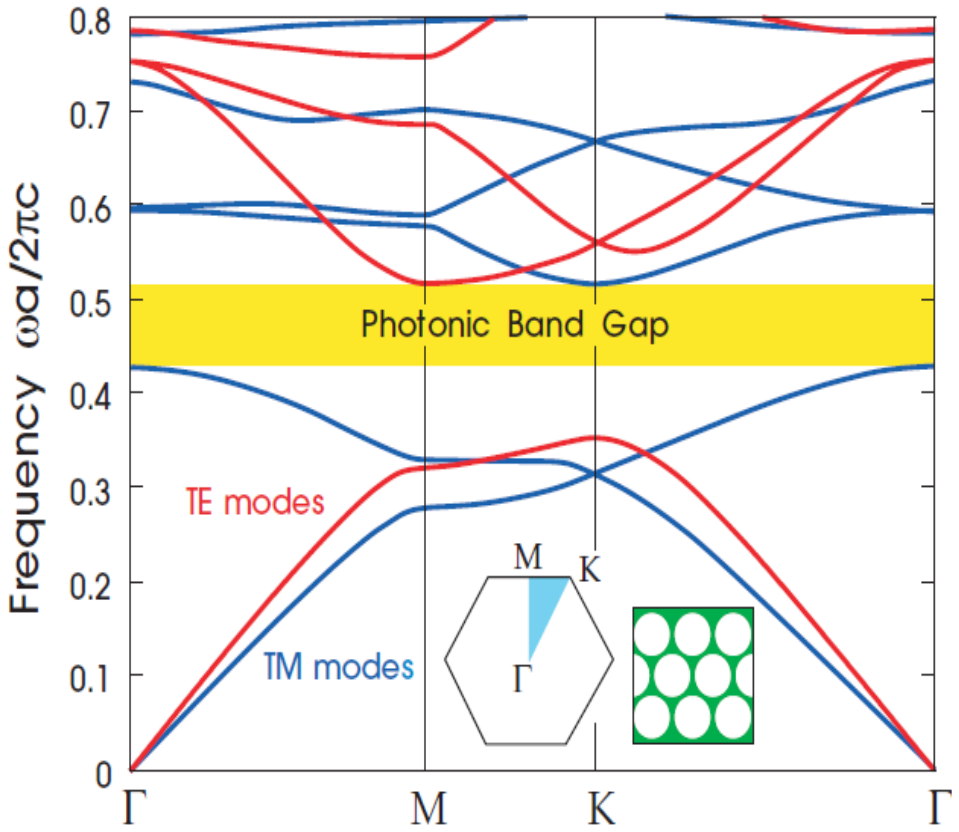

Figure 8: TE and TM band structure for a triangular lattice of holes [6]

Slow Light Photonic Crystals Slabs

The discussion above was about structures that are infinitely uniform in the Z-direction. In practice, we have finite slabs. These structures show periodicity in the two directions in plane of the slab but they have finite thickness in the other direction. Light propagation in such structures can also be described by the dispersion diagram. A complication in such structures is the fact that light does not necessarily have to be

confined inside the slab. Light that will be totally internally reflected can stay inside the slab, whereas the rest can leak out of the slab. This is shown on the dispersion diagram by the light cone. Modes or parts of the bands that fall below the light line are confined to the slab by total internal reflection and are relatively lossless. Modes that fall above the light line are not confined to the slab and hence are lossy. The plot below shows the band structure of a typical 2D slab.

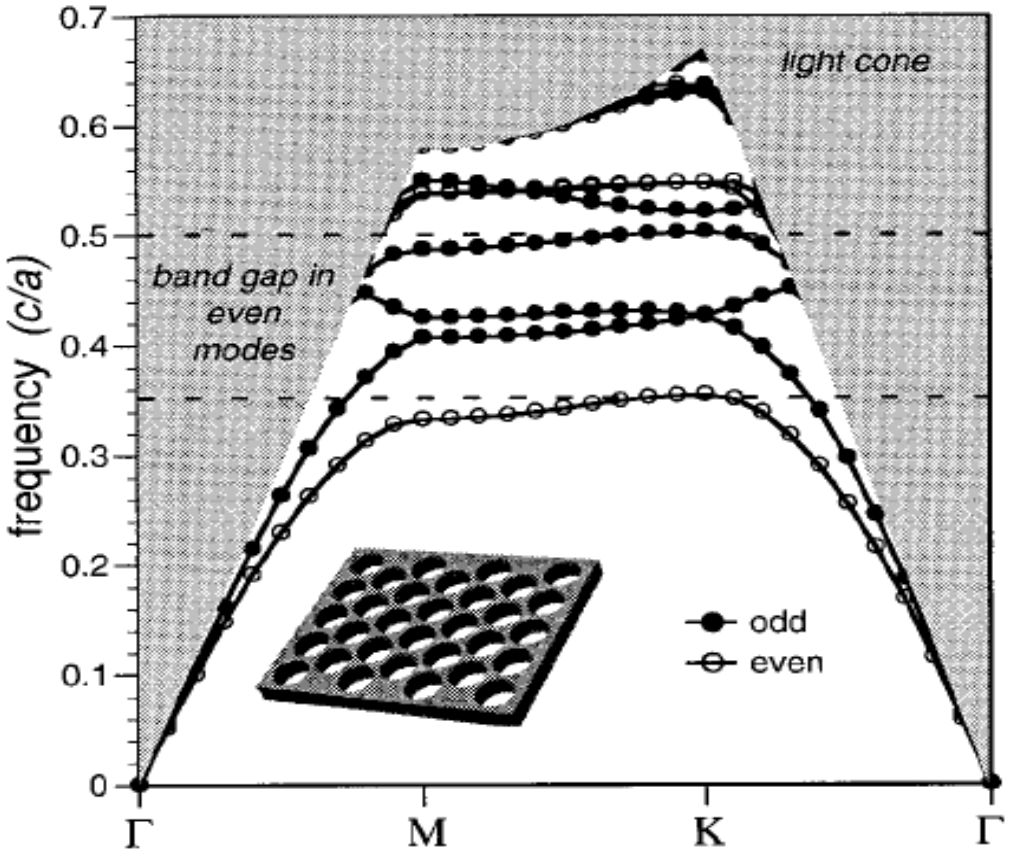

Figure 9: Dispersion diagram of a slab with a 2D triangular lattice of holes

Another difference in the case of finite slabs is the fact that the modes can no longer be classified as TE or TM due to the finite Z extent of the slab. Instead the

modes are now labeled as even or odd. The even modes are like the TE modes. They have even symmetry across the mirror plane of symmetry of the slab. The odd modes, similarly, are like the TM modes. They have odd symmetry across the mirror plane.

One thing that is very obvious in 2D structures is that the bands generally become shallow near the edges of the BZ. The edges of the BZ are denoted by the specially labeled points such as the Γ, X, M, and K in the dispersion plots. As was discussed before, the slope of a band is inversely related to the group index. The low slope at these points therefore corresponds to regions of high group indices. Light that has frequency that falls near the band edges will experience a group index that is much greater than the refractive index of the material. Consequently such incident light pulses will travel far more slowly through the structure.

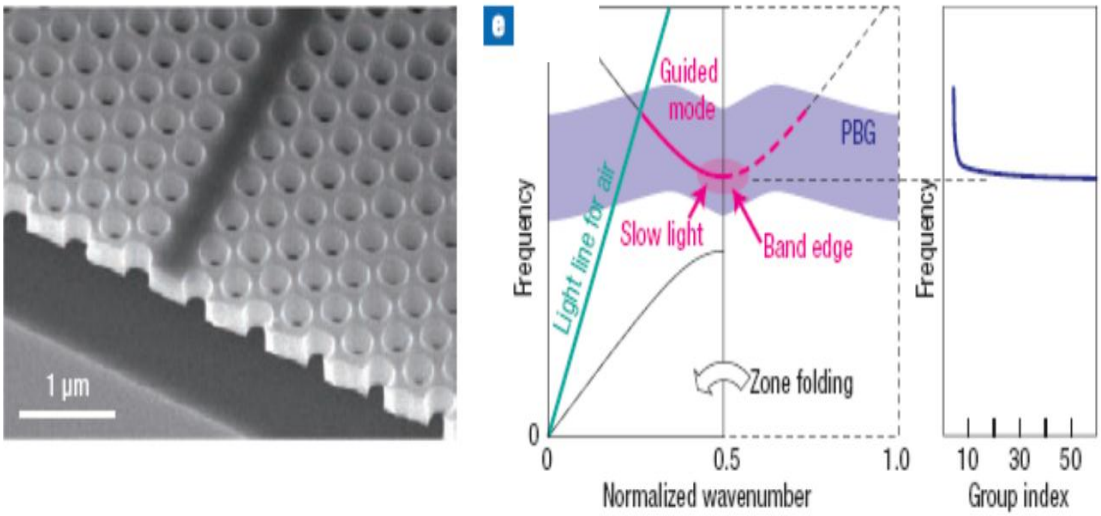

Figure 10: Slow Light Photonic Crystal Slabs [7]

Figure 10 above, taken from reference [7], highlights all of these points. The slab is a thin hanging film of Silicon surrounded by air. The picture on the left is a

Scanning Electron Microscope (SEM) image of the film. A triangular array of holes or air columns is defined using E-Beam lithography followed by chemical etching. The band structure of such a film is shown in the middle plot of the figure. The triangular lattice of holes produces a photonic bandgap (colored grey in the plot and labeled PBG). One new feature in the band structure is the defect band inside the band gap, shown in pink. The defect band arises because of the row of missing holes in the middle of the lattice. This missing row of holes is called a Photonic Crystal Waveguide (PCWG). Light that travels in this waveguide is confined in the vertical direction by total internal reflection. In the lateral direction, the photonic crystal on either side of the waveguide does not allow the light to spread out if its frequency falls within the bandgap. The plot on the right shows the group velocity inside the waveguide, which corresponds to the slope of the defect band at various points. As can be seen in the plot, near the band edge the waveguide shows very high group index. In similar PCWG structures researchers have been able to experimentally show group indices as high as 300 [8]. This highlights the important point that light pulses of particular frequencies will travel at a much slower speed through these slow light PCWGs as compared to normal waveguides. Above the light line the propagating modes in PCWGs may not be tightly vertically confined to the PC slab. Such modes will experience significant propagation loss. However these modes can also show slow light phenomenon [9].

Monolithic photonic crystal passively mode locked lasers

We need to design a monolithic passively mode locked laser that is suitable for TPM. Such a laser will be cheap since it uses semiconductor technology. It will also be compact and light weight. This will allow us to integrate the lasers into the tiny Schnitzer lab microscopes discussed beforehand. Such semiconductor lasers will make TPM solution very cheap and mobile and will also allow for parallel and live imaging in freely moving animals. The lasers commonly used for TPM usually operate around 100 MHz but monolithic passively mode locked semiconductor lasers usually have repetition rates in excess of 1GHz. Therefore, we need to reduce the frequency of these lasers to make them more effective for TPM. The proposed solution in this thesis work is a new a device: a "monolithic photonic crystal passively mode locked laser". As the same suggests our goal is to incorporate a photonic crystal within the device structure of a monolithic passively mode locked semiconductor laser. Figure 11 below shows the proposed device.

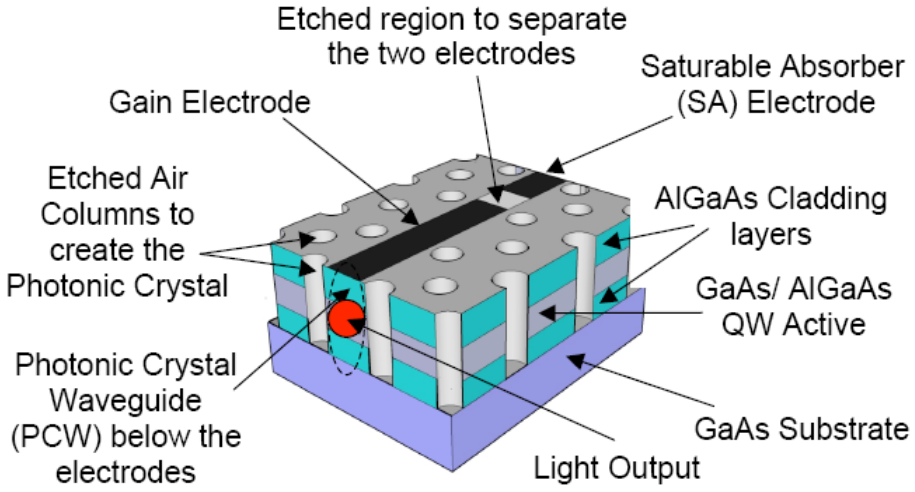

Figure 11: Monolithic photonic crystal passively mode locked laser

The device is very similar to the traditional MMLL structure, which is a two section device. The top electrode, shown in black, is split into two parts which are electrically isolated. The longer portion can be forward biased to serve as the gain section of the device and the smaller portion is reverse biased to serve as the SA. Proper electrical isolation between the two electrodes will ensure that they do not short out with each other. The novel feature of the device is that on each side of the electrode we write and etch a triangular lattice of holes. This will provide us with a PCWG below the electrode. The depth of the photonic crystal holes is a design parameter that can be optimized. Ideally we want the holes to penetrate all the way through the top cladding layer, the waveguide layer and the bottom cladding layer of the laser wafer. However, there are certain design and fabrication issues that need to be addressed while deciding on the depth of the holes.

Incorporating a photonic crystal within the laser cavity will provide us with many advantages. First, a mode locked laser cavity that is also a slow light PCWG will have a much higher group index. This means that for the same physical length of the device we will now have a much longer optical length and hence a lower repetition rate laser. A GaAs based MMLL needs to have a ~ 4cm long cavity to get a repetition rate of ~1 GHz. With a group index of 50 we can shrink the same device to 3mm in length. Such a device will be small and light enough for a small animal like a mouse to carry around on its head. In addition, PCWGs also show many other interesting properties. The dispersion properties of such waveguides can be fine-tuned to provide pulse compression, pulse shaping and mode shaping capabilities. All of these features can improve our laser performance. For example, the ability to compress pulses will

increase the pulse peak power and make the laser more suited for TPM. Since semiconductor lasers have enough bandwidth to provide pulse widths of few hundred femtoseconds, there is a lot of potential to do intra-cavity pulse compression.

References for Chapter 2

[1] E. U. Rafailov and M. A. Cataluna, “Mode-locked quantum-dot lasers”, Nature Photonics, volume 1, pp. 395 – 401, 2007.

[2] Rafael Aldaz, “Towards monolithic integration of mode-locked vertical cavity surface emitting laser”, Thesis, Electrical Engineering, Stanford University, 2007.

[3] Fritjof Helmchen and Winfried Denk, “ Deep tissue two-photon microscopy”, Nature Methods, volume 2, number 12, December 2005.

[4] W. Piyawattanametha, E.D. Cocker, L.D. Burns, R.P. Barretto, J.C. Jung, H. Ra, O. Solgaard, M.J. Schnitzer, “ In vivo brain imaging using a portable 2.9 g two-photon microscope based on a microelectromechanical systems scanning mirror”, Optics Letters, 34(15), pp.2309-11, 2007.

[5] K.K Ghosh, L.D. Burns, E.D. Cocker, A. Nimmerjahn, Y. Ziv, A.E Gamal, M.J. Schnitzer, “Miniaturized integration of a fluorescence microscope”, Nature Methods, 8(10), pp.871-8, 2011.

[6] John D. Joannopoulus, Steven G. Johnson, Joshua N. Winn, Robert Meade, “Photonic Crystals: Molding the flow of light”, Second Edition, 2008.

[7] Toshihiko Baba, “Slow light in Photonic Crytsals”, Nature Photonics, volume 2, August 2008.

[8] Yurii A. Vlasov1, Martin O’Boyle1, Hendrik F. Hamann1 & Sharee J. McNab, “Active control of slow light on a chip with photonic crystal waveguides”, Nature, volume 438-3, November 2005.

[9] Kazuaki Kiyota, Tomofumi Kise, Noriyuki Yokouchi, Toshihide Ide, Toshihiko Baba, “Various low group velocity effects in photonic crystal line defect waveguides and their demonstration by laser oscillation”, Applied Physics Letters, 88, 201904, May 2006.

Chapter 3

Device modeling and simulations

The first step towards the design of our laser was to perform device simulations. The proposed device combines the micro-photonics of conventional edge emitting mode locked lasers with the nanophotonics of PCs. Both these fields have their own specialized device simulations tools. A comprehensive simulation of our complete device would be an extensive project in itself. Since the focus of our research work was on device design and fabrication, therefore, fairly early on it was decided that this path would not be pursued. We decided to do independent simulations of the MMLL part and the PC part. Along the way we also did some feasibility studies to make sure that our integrated device would be able to deliver satisfactory performance.

The motivation for the project was derived from past simulation work done by a sister group at Stanford University. In that work, an actively mode locked semiconductor laser incorporating Coupled Resonator Optical Waveguides (CROWs) was simulated [1]. CROWs are quite similar to PCWGs and they also show slow light phenomena like PCWGs. The device that was simulated is shown in figure 1 below. The simulation results showed that by using the CROW structure and utilizing the slow light effect, the repetition rate of a mode locked laser can be reduced drastically. The simulated device had a physical length of 75um and yet it operated at 15GHz repetition rate. This device length is an order of magnitude smaller than the physical

length of few mms required by conventional semiconductor mode locked lasers to achieve the same operating frequency.

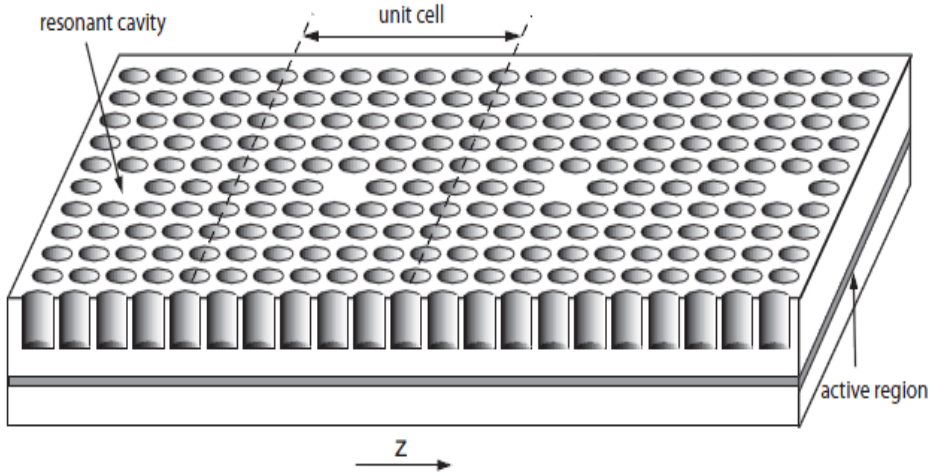

Figure 1: CROW actively mode locked laser [1]

Relevant simulation work on a slow light photonic crystal mode locked laser was also published last year. The device simulated was very similar to our design and used a PCWG to obtain the slow light effect [2].

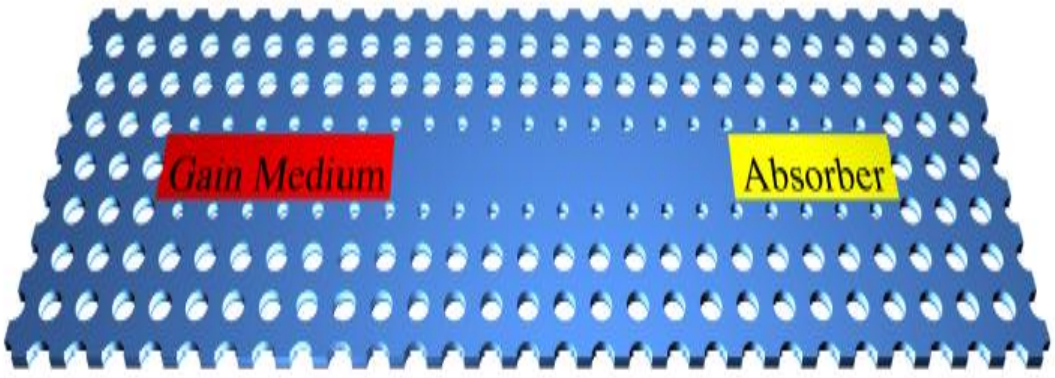

Figure 2: Slow light PCWG mode locked laser [2]

The published results highlighted that the slow light photonic crystal mode locked laser was able to show length reduction or slow down factor of about 20. The simulated laser could also generate sub-picosecond pulses.

Mode locked laser simulation

The laser design and simulations were done using PICWave, a commercial Time Domain Travelling Wave (TDTW) simulator made by Photon Design [3]. PICWave provides excellent support for passively mode locked lasers. It was used to optimize the various laser design parameters present. For example, the simulator's modal analysis tool allowed us to optimize the waveguide design and the thickness of the different wafer layers.

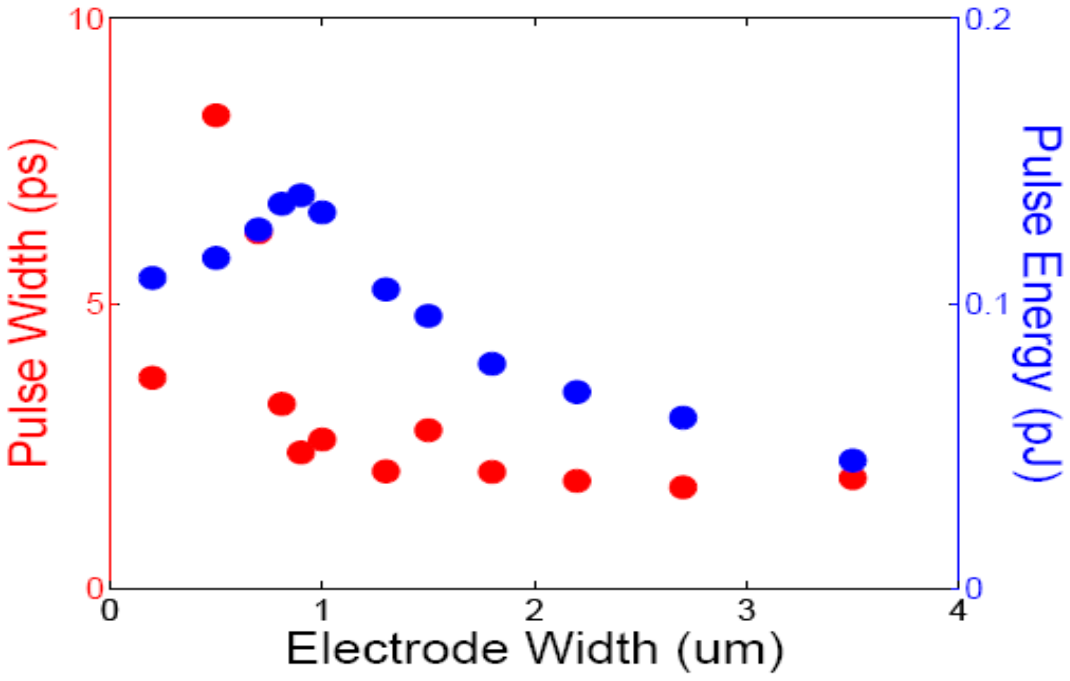

Figure 3: Effect of varying electrode width on laser pulse width and energy

One parameter involved in laser design is the width of the top electrode. The plot above shows the simulation results that were used to optimize the width of this electrode. Another variable of concern is the length of the SA section. Changing the length of this section affects the pulse width and the pulse energy since longer SA section means more loss inside the laser cavity. The plot below shows the results of such simulations

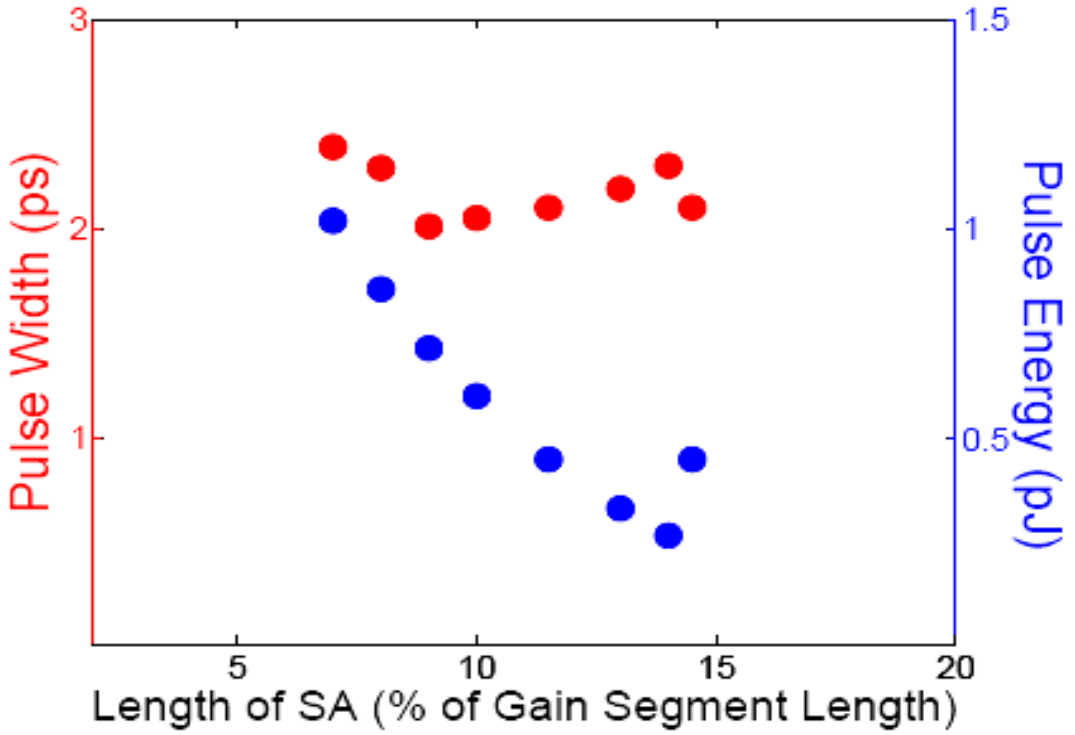

Figure 4: Effect of the length of the SA sections on laser pulse width and energy

To model the slow light effect we slightly changed the group index model of the simulator. This allowed us to study the first order effects of higher group index on mode locking. The simulations confirmed that even at high values of group index mode locking was possible without pulse breakup. However, the simulations also

showed that the pulses got broader as the index increased as shown in the plot below. This was an issue of concern for us and we attributed it to the higher dispersion present inside a laser cavity of high group index.

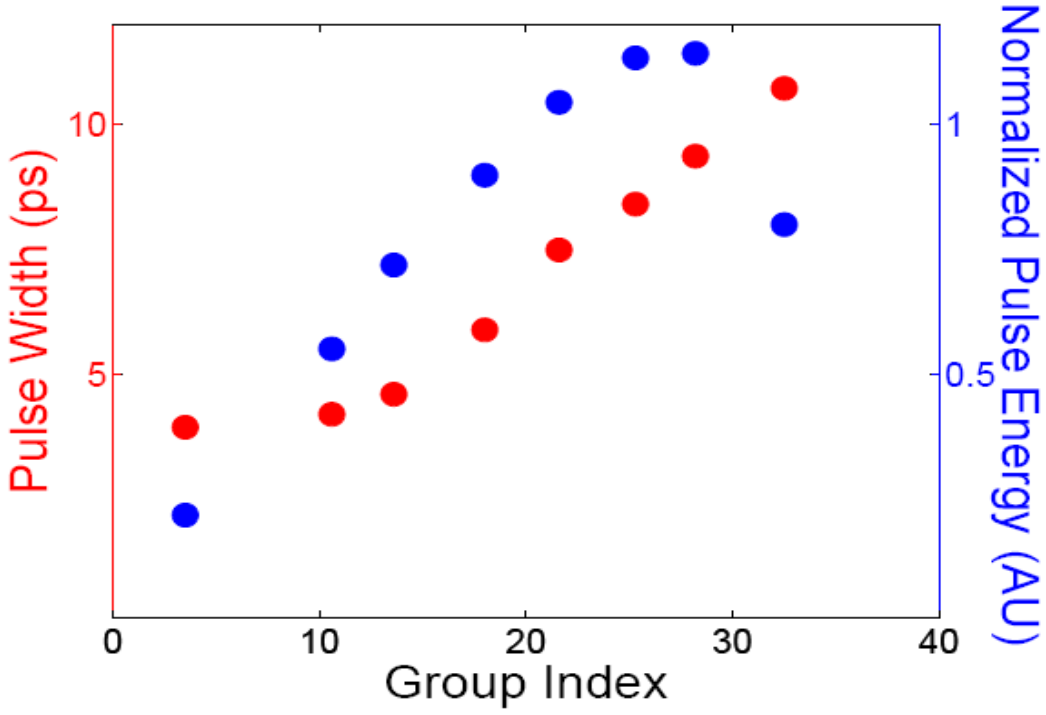

Figure 5: The effect of high group index on laser pulse width and energy

Picosecond TPM study

As noted above, our PICWave simulations showed that dispersion in a slow light MMLL can cause pulse broadening. Broader pulses decrease two-photon excitation strength and are a cause of concern. Therefore, we needed to check that in case our slow light laser is unable to generate sub-picosecond pulses, would it still be useful for TPM. To study this I did imaging experiments in collaboration with Tony Zhang of

the Schnitzer group. In the experiment we used a conventional TPM setup with a Ti:Sapphire mode locked laser to image pollen grains. But instead of using the pulses directly, we propagated them through a grating pair that allowed us to temporally expand the pulses. The experimental results we got alleviated our concerns. The figure below shows the two-photon images of the pollen grains. Using constant laser power we were able to image the pollen grains with pulses up to 8ps width. As can be seen below, the resolution of the images does decrease as the pulses become wider but still the features of the pollen grain are discernible. The results gave us the confidence that even though our lasers might not be able to perform as good as the conventional TPM lasers, they can still be useful. The advantage of our lasers would be the reduced size and potential for much lower cost. Published literature shows that TPM can be done using picosecond pulses [4]. In fact, picosecond pulses can sometimes be more useful because they produce lower photo-damage and photo-bleaching effects [5].

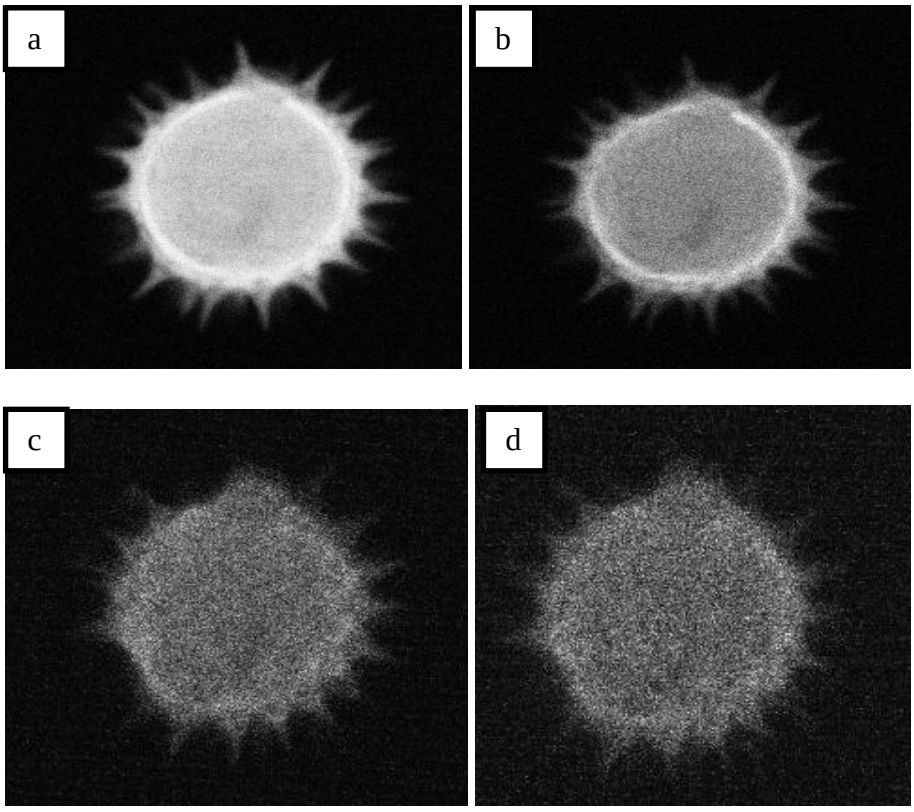

Figure 6: Pollen grains imaged using TPM system with varying pulse widths

a) 250fs original pulses b) 1.3ps pulses c) 6.5ps pulses d) 8.5ps pulses

Photonic crystal simulations

The simulation and design of the photonic crystal part was pursued independently of the laser simulations. Initially we used the free band solver software MPB by MIT to design and simulate the PC [6]. Later on we started using the commercial package CrystalWave by Photon Design to continue the PC design and simulation work [7]. The simulator provided us with an interactive GUI that allowed us to solve for the band structure and do Finite Difference Time Domain (FDTD) simulations within one platform. Bulk 3D PC band-solver simulations were performed. We always simulated

a PC consisting of a triangular lattice of holes. To minimize simulation time, we mostly solved for only the TE modes. In semiconductor edge emitting laser structures, the TE modes are far more dominant than the TM modes during lasing action. This is for two reasons. First, the mirrors formed by the semiconductor facets show better reflectivity to TE polarization compared to TM polarization. This results in the TE modes seeing lower loss. Second, the electric fields of the TE modes also see higher gain since they are aligned with the plane of the QWs. Both these effect make the laser light output predominantly of TE polarization.

Simulations were done to figure out the lattice constant and the radius of the holes for our triangular lattice. We also modeled the effect of varying the cladding thickness and the cladding index on the width of the photonic bandgap. A major design challenge that we faced throughout out our work was the fact that we needed to integrate the photonic crystal inside a conventional semiconductor MMLL structure. This severely restricted the design space for our PCs. For example the index of the cladding is an important variable of concern for PC slabs. Ideally, PC slabs are fabricated in such fashion that they are either freely hanging membranes in air or they are surrounded by very low index cladding material, like silicon dioxide. Having a low index cladding increases the optical confinement of the optical modes within the PC slab. The plots below show how varying the cladding index from 2.5 to 1.5 increases the size of the gap between the first and second bands between the M and K points. However, in our laser design, we were restricted to using the cladding layer of our laser wafer that is $Al_xGa_{1-x}As$. Now the Aluminum (Al) content of this layer can be increased to reduce the cladding index, but even with 100% Al the index only reaches

a minimum of around 3. Furthermore, even having such a high concentration of Al is problematic itself since it makes the cladding layer prone to oxidation. When the PC holes are etched into such a cladding layer, the layer can oxidize into a variant of Aluminum Oxide (Al_xO_y). Such oxides are usually non-conductive and they destroy the laser epitaxy.

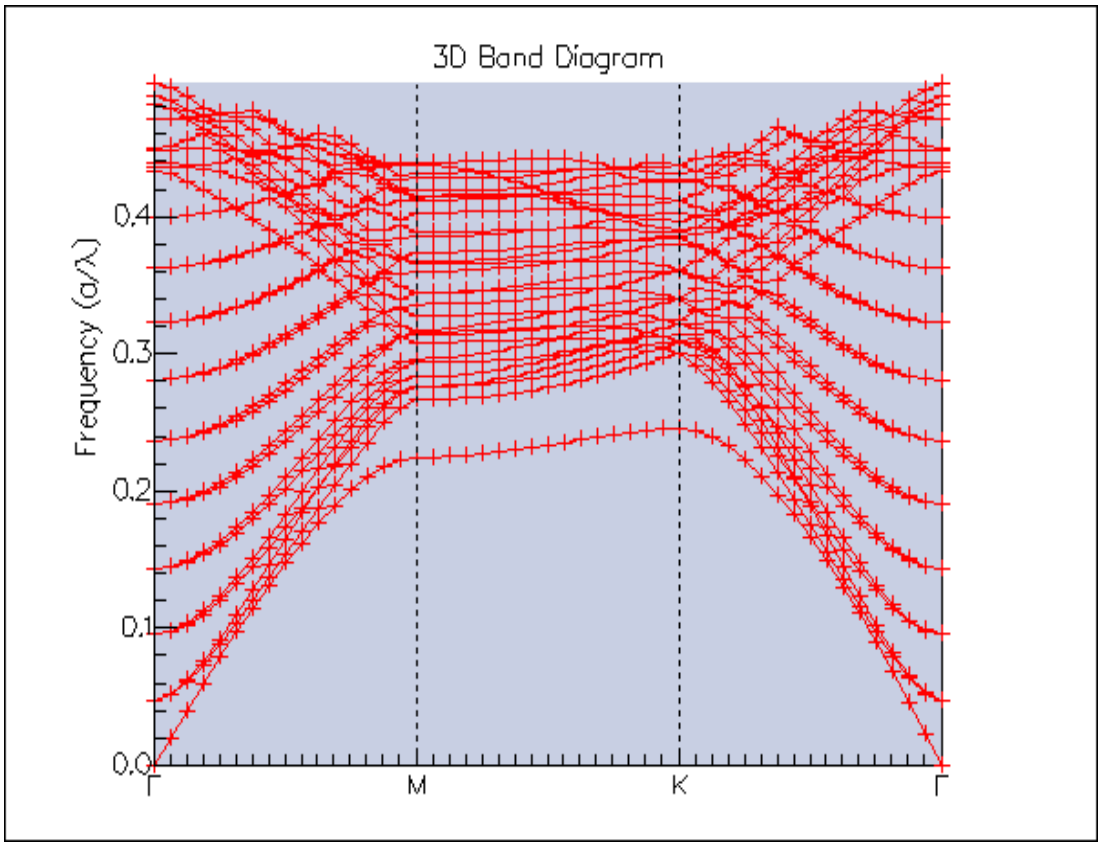

Figure 7(a): Band structure with a cladding index of 2.5

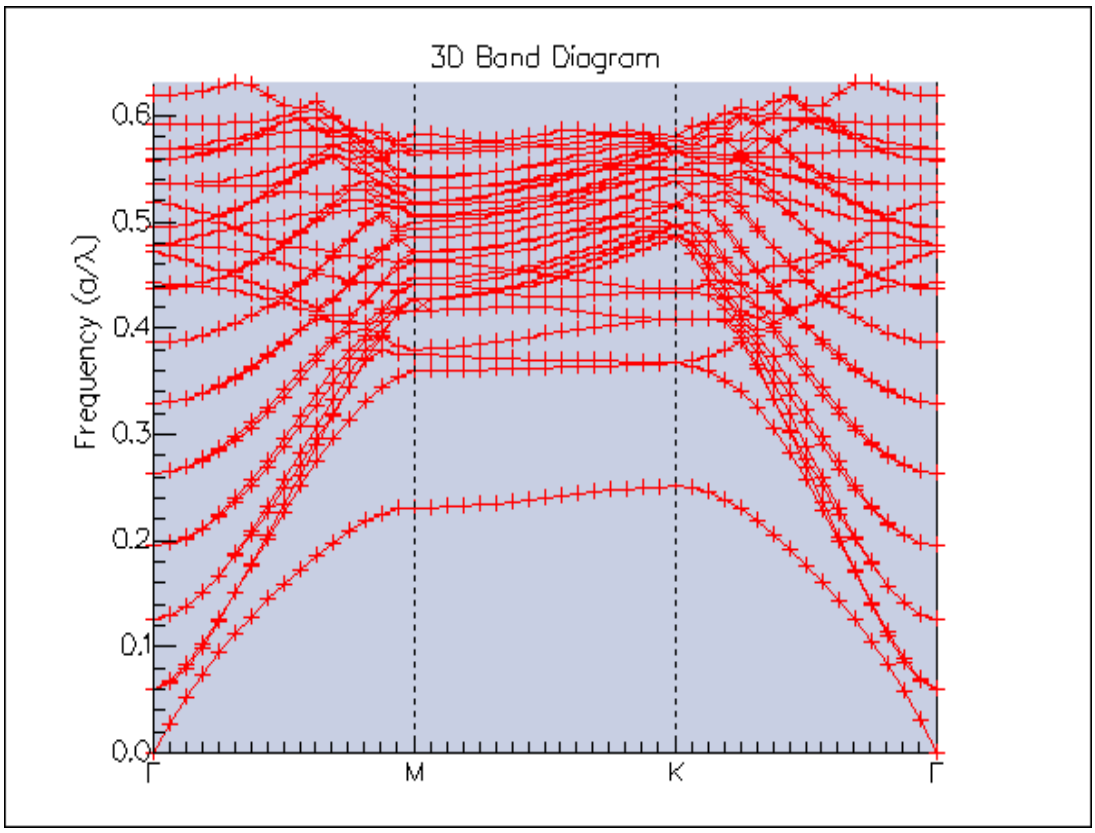

Figure 7(b): Band structure with a cladding index of 1.5

Another design challenge we faced was the thickness of the cladding layer. In semiconductor laser design, the upper and lower cladding thicknesses are made sufficiently large (>1um) such that the absorption loss from the top metal contact layer and the substrate at the bottom, are minimized. However, for our PC laser we have to etch holes through these layers. Therefore, due to fabrication limitations, we needed to reduce the layer thickness to much smaller values. Simulations were performed to study the effects of reducing the cladding thickness. In this regard, FDTD simulations using CrystalWave provided useful insight. In our simulations we varied the depth of the PC holes and simulated the effect of such partially etched holes on light

propagation through the PC waveguide. For example, in our first set of fabricated devices the PC was etched to a depth just barely below the top cladding layer. The etched holes went only a few 10s of nm deep into the waveguide layer. We needed to see how such a PC waveguide will behave and in this regards the FDTD simulations provided useful results.

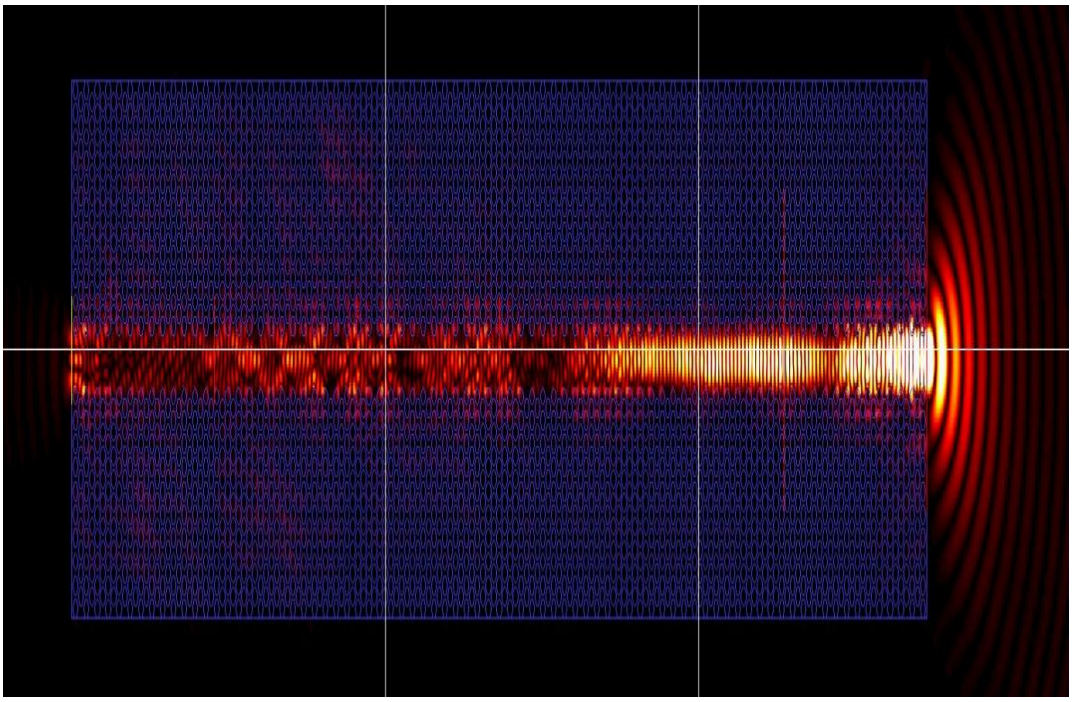

Figure 8: FDTD simulation of our waveguide showing good optical confinement within the PCWG even with shallow etched holes

Modeling nonlinearity

Another issue of concern for our slow light lasers is the fact that when optical pulses propagate through a slow light waveguide, they are compressed spatially and temporally. This means that inside a slow light waveguide, locally higher optical

intensities are present. Nonlinear effects, like Self Focusing and Self Phase Modulation (SPM) become more prominent at higher optical intensities. These effects can deform/break pulses and also prevent mode locking. Therefore the nonlinearity present in our slow light waveguide was a cause of concern and it had to be modeled. The B integral is one measure of the nonlinear effects present inside a waveguide. It is often used to characterize mode locked lasers. The B integral equation is shown below [8].

$$B = \frac{2 \times \pi}{\lambda} \int n_2 I(z) dz$$

In the equation above, λ is the wavelength of operation (the target wavelength for our lasers was 880nm), n_2 is the non-linear index of the material and I is the peak intensity of light inside the cavity or waveguide [9]. The B integral is the cumulative sum of the total non-linear effects in the path propagated by light. Mode locked lasers usually have B integral of a few 10s. That was also the case for our laser.

To study this issue further, I used a waveguide simulator that used the Split-Step Fourier Method to model nonlinearities. The simulator was developed by Supriyo Sinha in the Schnitzer group. The simulator allowed me to study the effects of high group indices on pulse propagation. High group index was modeled as an increase in the optical path length of the waveguide and also as an increase in the nonlinear index. As expected, the simulator did show that higher group indices reduce the peak power of pulses that can propagate through the waveguide without pulse break up. However,

to our satisfaction the simulation results did indicate that pulses with energy of ~10pJ/pulse and peak power of ~10W were possible at high values of group index. TPM can be performed using such pulses.

References for Chapter 3

[1] Yang Liu, ZhengWang, Minghui Han, Shanhui Fan,and Robert Dutton, "Mode-locking of monolithic laser diodes incorporating coupled-resonator optical waveguides", Optics Express 4539, volume 13, number 12, 13 June 2005.

[2] Mikkel Heuck, Søren Blaaberg and Jesper Mørk, "Theory of passively mode-locked photonic crystal semiconductor lasers", Optics Express, volume 18, issue 17, pp. 18003-18014, 2010.

[3] PICWave, Photon Design Inc., www.photond.com/products/picwave.htm

[4] J. Bewersdorf and S.W. Hell, "picosecond pulsed two-photon imaging with repetition rates of 200 and 400 MHz", Journal of Microscopy, volume 191, part 1, pp. 28-38, July 1998.

[5] H J Koester, D Baur, R Uhl, and S W Hell, "Ca2+ fluorescence imaging with pico- and femtosecond two-photon excitation: signal and photodamage", Biophysical Journal, volume 77, pp. 2226-2236, October 1999.

[6]MIT Photonic-Bands, MIT MPB, http://ab-initio.mit.edu/wiki/index.php/MIT_Photonic_Bands

[7] CrystalWave, Photon Design Inc.,

http://www.photond.com/products/crystalwave.htm

[8]AnthonyE. Seigman, “Lasers”, page 386, University Science Books, 1986.

[9]Mansoor Sheik-Bahac, David Crichton Hutchings, David J. Hagan, Eric W. Van Stryland, “Dispersion of bound electronics nonlinear refraction in solids”, IEEE Journal of Quantum Electronics, volume 27, number 6, June 1991.

Chapter 4

Device fabrication

In this chapter we discuss in detail the steps involved in the fabrication of our slow light laser. The first step in this regard was to epitaxially grow the laser wafer. The wafer was then processed using various lithographic, etching, and deposition tools to define the laser structures. Many fabrication challenges were faced and we devised novel solutions to overcome them. This chapter comprehensively discusses this fabrication process.

Wafer epitaxy

The first step involved in the fabrication of our device was the epitaxial growth of the laser wafer. The first wafer that we grew was the same as the wafer grown by J. F. Martins-Filho et al. for their mode locked lasers [1]. This was a four quantum well laser wafer and it was used by the authors to fabricate collision pulse mode locked lasers operating at 860nm. The wafer structure with the various layer thicknesses is shown below. Our research group has five Molecular Beam Epitaxy (MBE) chambers. Tomas Sarmiento, a fellow Harris group member, grew this wafer using one of these MBE chambers.

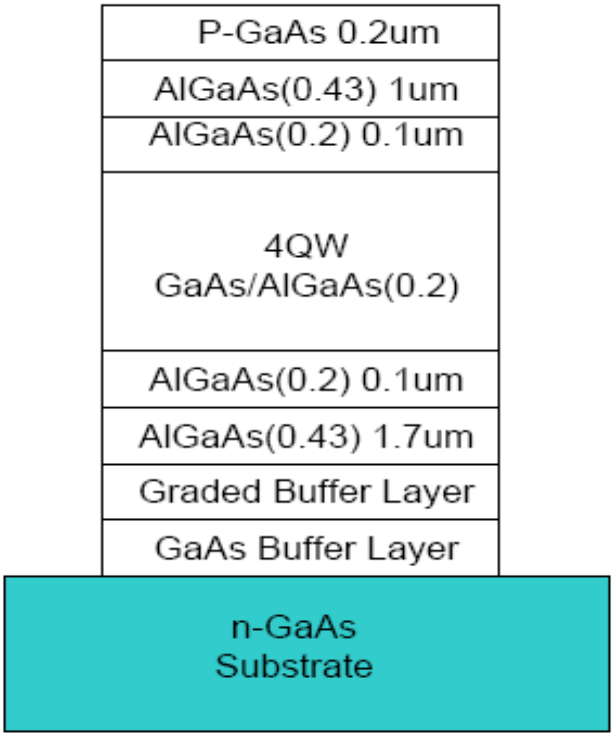

Figure 1: Epitaxial structure of the first laser wafer [1]

The top cap layer was p-doped $2x10^{19}$ $cm^{-3}$and the top 1um thick cladding was also p-doped $2.2x10^{17}$ cm^{-3}. The four quantum wells and the top and bottom waveguide layers were not doped. The bottom cladding was n-doped $1.4x10^{17}$ cm^{-3}. Edge emitting and passively mode locked laser structures were fabricated from this wafer. During the characterization of the lasers fabricated from this wafer, we faced two major problems: high contact resistance and laser roll-off due to device heating. This was due to the low doping level used in the cap and cladding layers. We therefore decided to use much higher doping levels in our second revision of the laser wafer. Another problem present in wafer 1was the thickness of the cladding and cap layer.

Device fabrication

We were limited by the etching capability present in our fabrication facility and the large thickness of the top cladding layer did not allow for the etched PC holes to reach the waveguide layer. Therefore, the thickness of the top cladding needed to be reduced. However, the tradeoff involved in reducing the cladding thickness is the corresponding increase in absorption losses due to the proximity of the top metal contact with the waveguide layer. The second wafer was grown using Molecular Organic Chemical Vapor Deposition (MOCVD), by Shuwei Chiu, a visiting research scientist in our group. The laser structure is shown below.

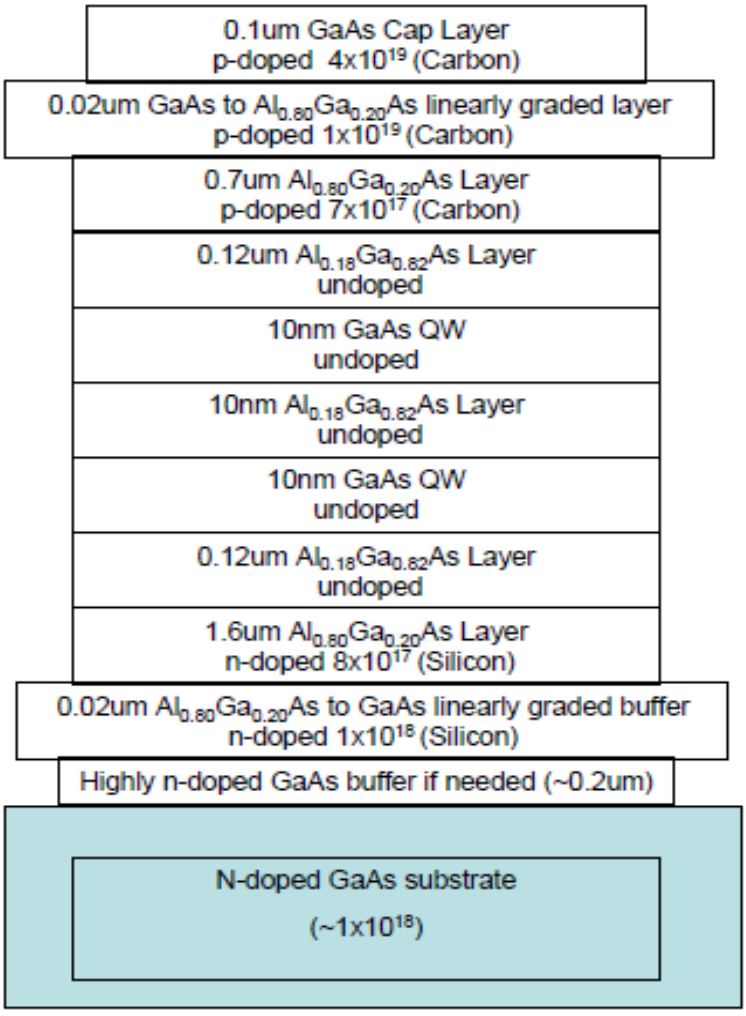

Figure 2: Epitaxial structure of the second laser wafer

In this wafer we decreased the thickness of the top cladding and the cap layer. We also increased the doping levels to reduce the device series resistance. The higher doping level allowed us to reduce the thickness of the cap layer and still get a good top p-contact. To reduce the thickness of the cladding layer even further we did some modal simulations to model the absorption loss. The results are shown in the graph below. As the plot suggests, the top cladding thickness can be decreased to about 300nm, after which the loss increases very rapidly and soon becomes too far high for any lasing to occur.

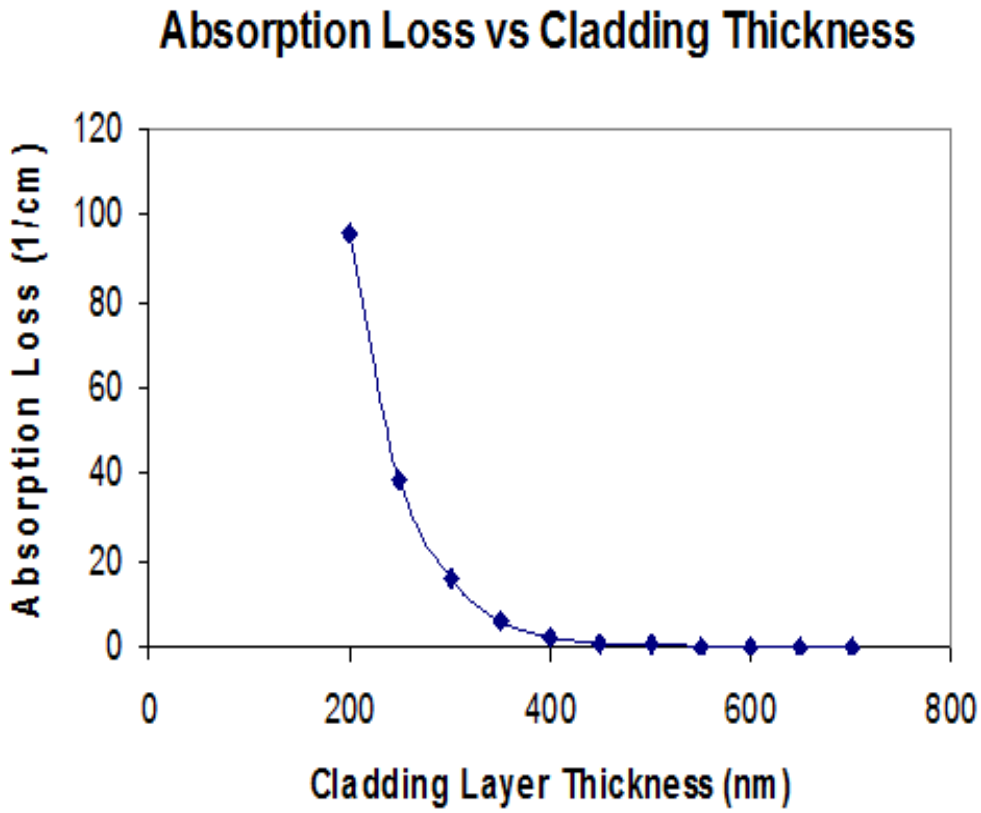

Figure 3: Effect on absorption loss due to reduction in top cladding thickness

Device fabrication

The third laser wafer was also grown using MOCVD, courtesy of Shuwei. Our photonic crystal lasers were fabricated using this wafer. The epitaxial structure of the wafer is shown below.

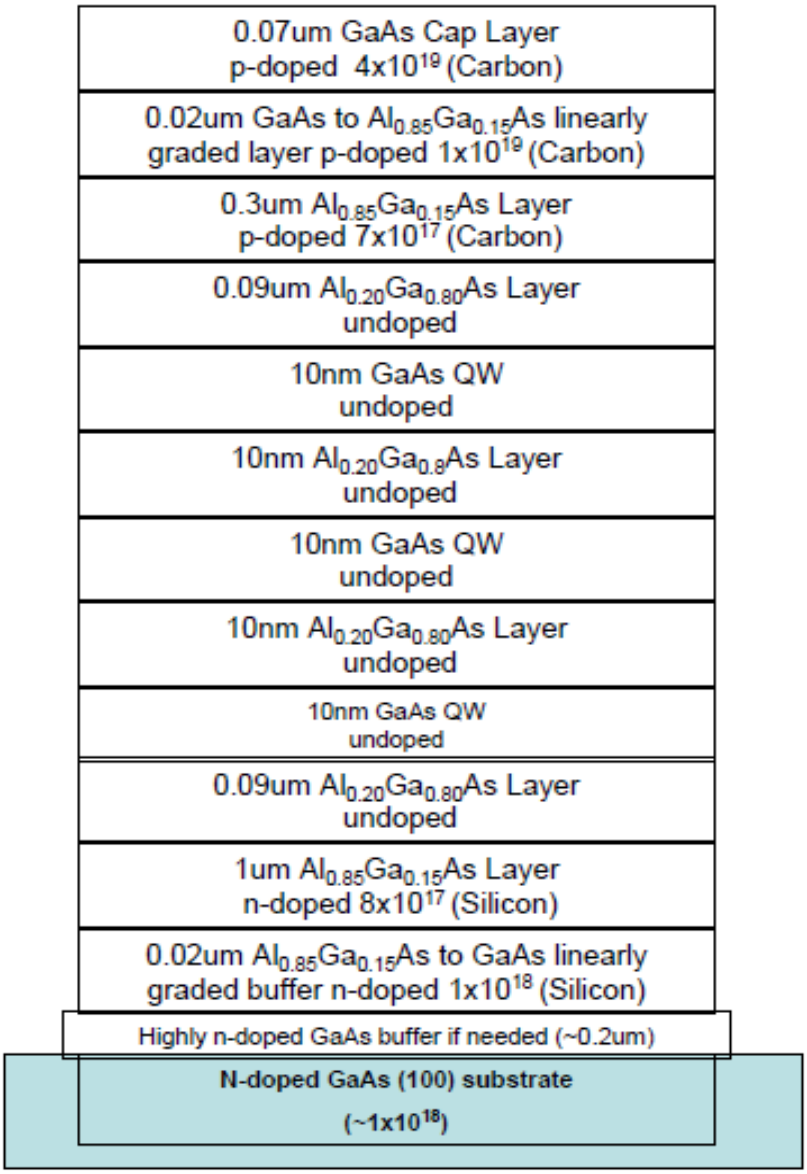

Figure 4: Epitaxial structure of third laser wafer

The lasers fabricated from this wafer showed very good optical and electrical properties with fairly low thresholds. This highlights the fact that there is potential to further decrease the thickness of the top cladding down to 200-250nm and still have manageable levels of absorption loss. Nevertheless, we did not pursue this possibility. The scattering loss due to the photonic crystal holes was a big source of concern for us and we wanted to first minimize the other sources of loss, including the absorption loss.

Laser fabrication

The fabrication of our lasers was done at the Stanford Nanofabrication Facility (SNF). The process flow was revised and refined over time. It combined both optical lithography and E-Beam lithography techniques. Device fabrication starts after the growth of the laser wafer. The laser wafer is first broken into small pieces, each of which is fabricated individually into lasers. The pieces are cleaned using solvents and then they are baked at 200C for 2 minutes to drive off the solvents. After that ZEP-520A E-beam resist is spun on the wafer at 5000 RPM for a target film thickness of 300nm. The pieces are then exposed using Jeol JBX 6300 E-beam writer operating at 100KeV. The top rectangular p-electrodes are written with widths ranging from 250 nm to 3um. The standard exposure dose for the resist was fine-tuned and found out to be 250uC/cm^2 ± 10%. After exposure, the pieces are developed using a 40s dip in Xylenes, a 30s dip in 25% MIBK:75% IPA mixture solution and then a 30s dip in IPA. Top metal p-contact is then deposited using an electron beam evaporator

followed by metal liftoff. Our standard p-contact consists of 20nm of Titanium, 20nm of Platinum and 200nm of Gold, deposited in that order. The pieces are then cleaned to remove excess resist. Metal electrode lines that serve as our p-contact are now present on the front/top surface of the laser wafer piece. These metal lines are then used as hard masks to etch shallow mesas on the front side of the wafer. This etching also removes the top conducting cap layer adjacent to the metal lines. The etching is performed using Plasma Quest ECR plasma etcher (PQuest). The etched mesas help in achieving good current confinement for our lasers. The pieces are then cleaned and ZEP-520A is again spun on them. This time the E-beam writer is used to write PC lattices on the pieces. Figure 5 below shows these steps.

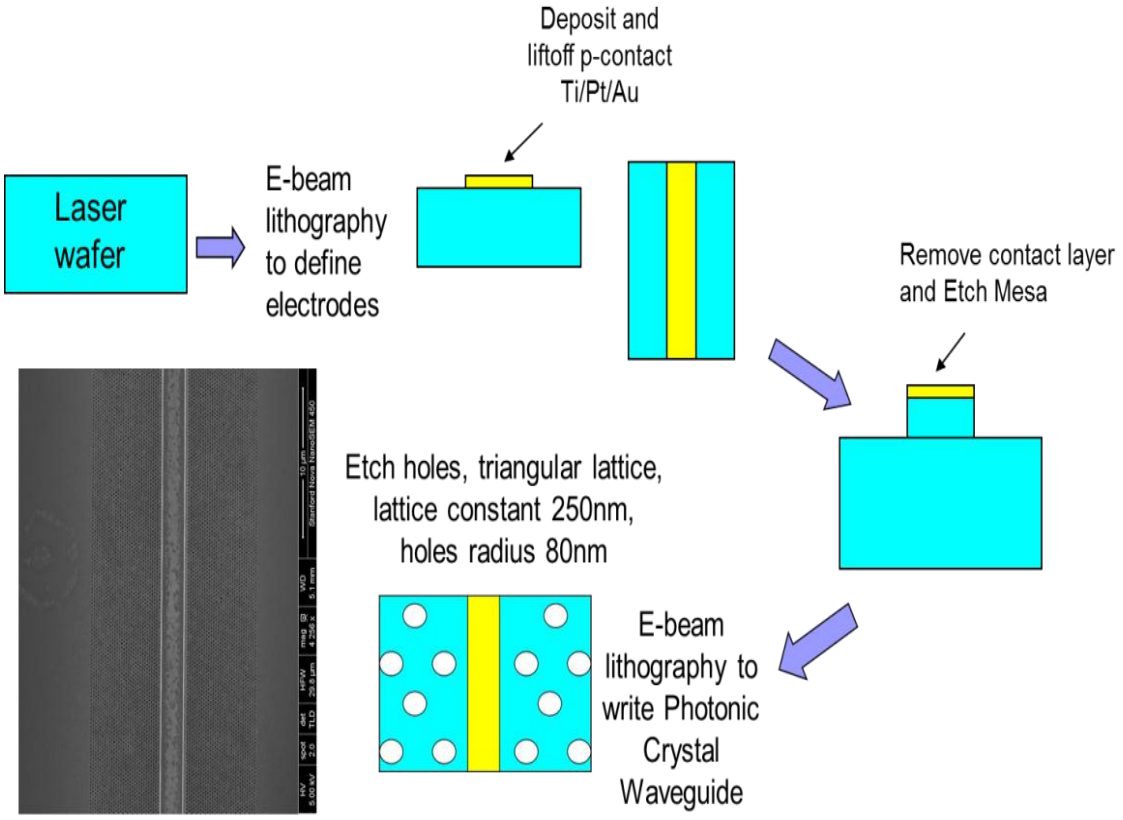

Figure 5: Laser fabrication steps (I)

The PC arrays written are triangular lattices of holes which are centered on the metal contacts. These arrays extend for more than 10 periods on either side of the metal lines. Patterns with different holes widths and lattice constants are written on different pieces. After the E-beam exposure, the pieces are developed and then etched using PQuest. This time, PC holes are etched on either side of the metal contact. The metal lines again serve as effective etch masks and a strip free of holes is formed underneath each metal line. This region serves as our waveguide.

Figure 6 below is a Scanning Electron Microscope (SEM) image that shows the PC aligned with the top p-electrode.

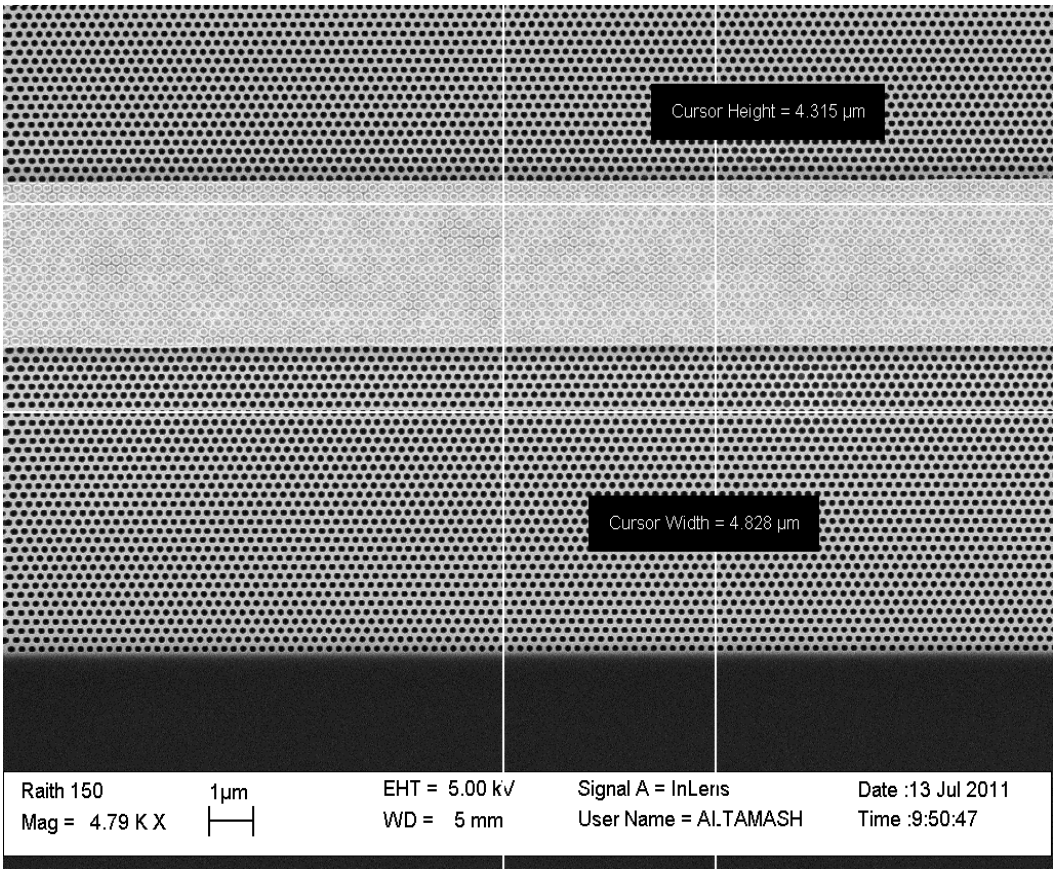

Figure 6: SEM image showing PC holes on either side of the top metal p-electrode

The PC holes on either side of the electrode are very clearly visible. The white stripe in the center is the top metal p-electrode. The faint holes on the metal stripe are small etched features that do not extend through the metal layers. After etching the PC, the piece is then coated with silicon dioxide for electrical passivation. 120nm of Silicon dioxide is deposited using Plasma Enhanced Chemical Vapor Deposition (PECVD). Using E-beam lithography followed by Dry Reactive Ion Etching (DRIE), contact windows are opened on the deposited oxide. These contact windows provide access to the p-contact metal stripes below the oxide. Standard optical lithography is then used to define bonding pads. Metal liftoff is performed to deposit the bonding pads that are in electrical contact with the p-electrodes through the contact windows. These steps are shown in figure 7 below.

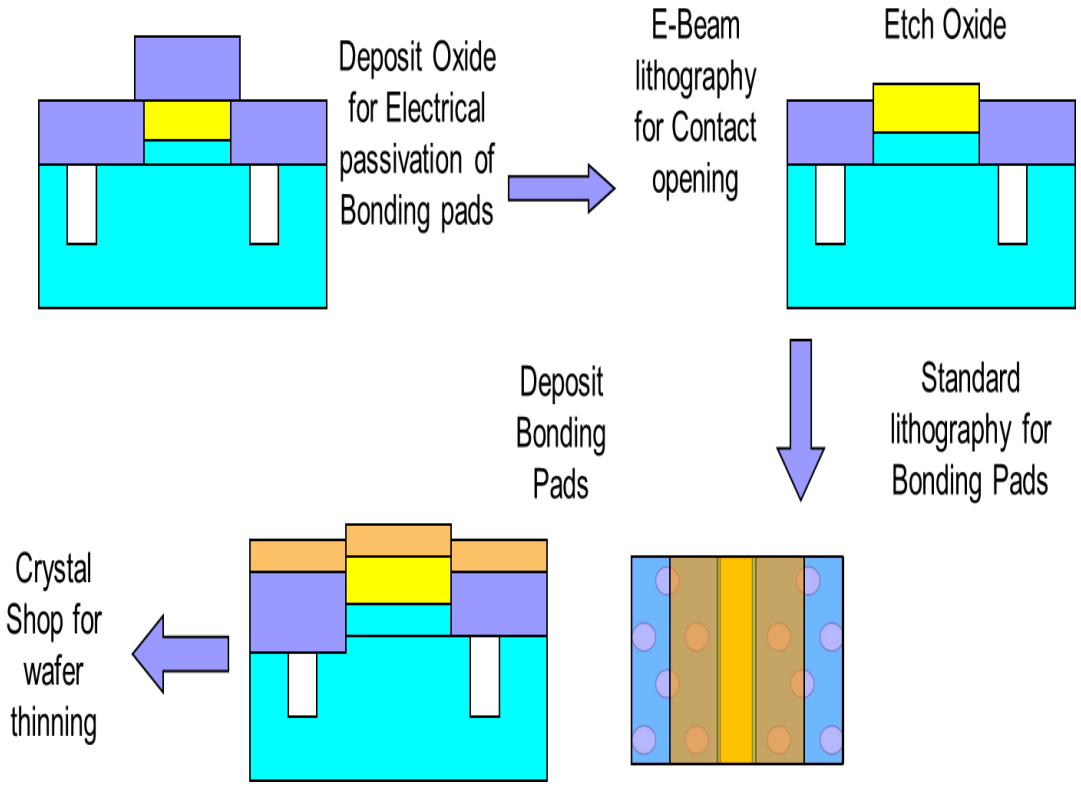

Figure 7: Laser fabrication steps (II)

After the deposition of bonding pads, the pieces are sent to the Crystal Shop on Stanford campus for wafer thinning and polishing. The substrate is thinned down to a total thickness of 200um. This is done so that the lasers can be easily cleaved. After the thinning of the wafer pieces, the back n-contact is deposited on the bottom/back side of the pieces. This contact consists of 40nm of Gold, 12.5nm of Germanium, 12.5nm of Nickel and 200nm of Gold deposited in that order. The back contact is then annealed using a RTA at 410C for 60s. The lasers are then manually cleaved. After cleaving, the lasers are mounted on copper heat sinks using Indium solder. This bonding facilitates the heat exchange from the lasers and improves laser performance.

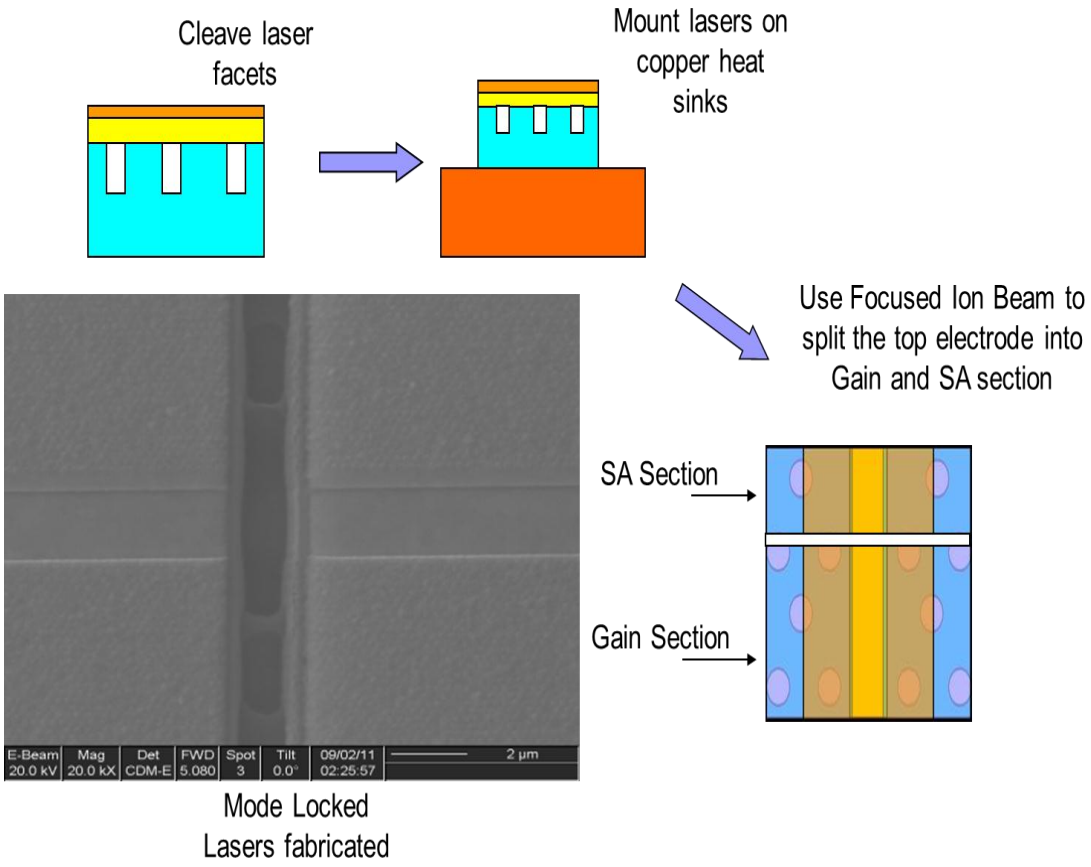

Figure 8: Laser fabrication steps (III)

Device fabrication

These steps complete the fabrication of narrow waveguide photonic crystal edge emitting lasers. To make a mode locked laser, we need to split the top electrode into two parts to create separate gain and the SA sections. These two sections also need to be sufficiently electrical isolated. Conventionally, these two sections in a semiconductor mode locked laser are defined through optical lithography and then the laser is precisely cleaved to control the length of the two sections accurately. However, in the absence of a precise cleaving tool, we had to come up with an alternative solution to prevent the time expensive option of shipping the pieces to outside vendors. We achieved this using Focused Ion Beam (FIB) milling. FIB provides the ability to machine and drill features at the nanometer scale with high accuracy. After mounting our lasers onto copper heat sinks, we used FIB to split the top bonding pads and the p-electrodes into two parts. This created a two segment device. By changing the FIB beam current and ion energy the depth of the mill can be precisely controlled. This allowed us to achieve good electrical isolation between the SA and gain sections. These steps are shown are figure 8 above. The SEM picture below shows how the FIB milling looks. As can be seen in the picture below, the FIB cut is very clean and can be placed accurately. This technique also allowed us to create different length SA sections on the same laser bar. FIB milling is the final step involved in the fabrication of our mode locked lasers.

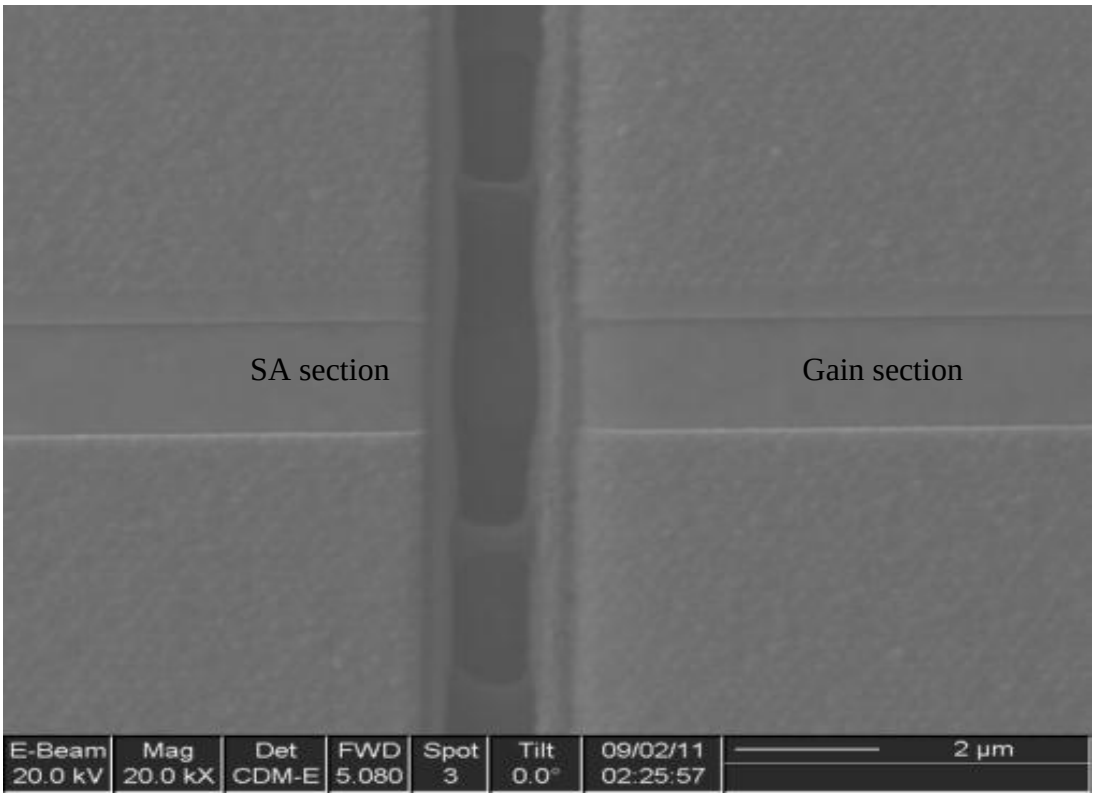

Figure 9: SEM image of the FIB mill to separate the SA and gain section

Fabrication challenges

We faced many obstacles during the course of our device fabrication. Some of these problems are discussed as follows. Since our fabrication process involved a lot of E-beam writing, the first step was to choose a suitable E-beam resist. For our work ZEP520A resist produced the best results. Various concentrations of PMMA were tried but they did not perform to our satisfaction. Since we were writing large area PCs, which extended over multiple millimeters, we had to use a resist that had a moderate to low exposure dose to minimize exposure times. In this regards ZEP520A was very advantageous because of its low exposure dose. The resist consistently

produced good resolution exposures and it also showed good etch resistance. Additionally, the intrinsic undercut of ZEP after exposure was also beneficial for metal liftoff.

Combining the micron scale laser diode lithography with the nanometer scale PC lithography was a serious design challenge. The extent of each PC array was nearly 20um x 8mm per laser electrode. One exposure took nearly 2 hours on the Raith-150 E-beam system available in SNF and this made the laser fabrication process very slow. A faster E-beam writer became a necessity for our work. Jeol JBX 6300 E-beam writer was installed during this project and was an ideal tool in this regard.

Learning to etch the PC pattern properly also took a lot of experience and time. Our target wavelength of 880nm was much smaller than the telecommunication wavelength of 1.55um at which a majority of PC research work was done in the past. This meant that our PC holes were much smaller and correspondingly the patterns were far more difficult to fabricate. To make the problem worse, we wanted to etch very deep holes that went through the top cladding. To achieve this, we tried three different hard masks: Silicon dioxide, Silicon nitride and Chrome. However, these hard masks did not provide us with any performance boost in comparison to ZEP520A. The primary reason for this was the unavailability of a good GaAs etcher in SNF. The table copied below is taken from the literature and compares the relative performance of different etchers [2].

Technique	Chemistry	Performance
RIE	CH_4	AR≈2
	$CH_4/Ar/H_2$	AR≈2
ECR-RIE	Cl_2/Ar	AR=8 cylindro-conical
	Cl_2	AR≈2
ICP-RIE	$SiCl_4(/Ar)$	AR=14 cylindro-conical
	Cl_2	AR≈10
	Cl_2/O_2 250 °C	AR=16 cylindro-conical cylindrical
	Cl_2/N_2	AR≈8
	$Cl_2/Ar/N_2(/He)$	AR=16 conical
	Cl_2/Xe	AR≈5 cones swelled cylinders
	Hi/Xe	AR=13 conical
CAIBE	Ar/Cl_2	AR≈18-20 cylindro-conical
FIB	–	low AR

Figure 10: Table comparing the performance of various etchers

The Aspect Ratio (AR) of the fabricated PC is defined as the ratio of the depth of the etched holes to the diameter of the holes. As is illustrated in the table above, the aspect ratio attainable using an ECP-RIE etcher like PQuest is limited to ~ 2. For our 200nm wide holes, we were limited to etch depths of ~400nm. The ideal etcher for our device would be a Chemical Assisted Ion Beam Etching (CAIBE) tool. The unavailability of such an etcher was a serious constraint for us. After PC etching, we

performed cross section SEMs to characterize the etch profile of our holes. A SEM image is shown in figure 11 below.

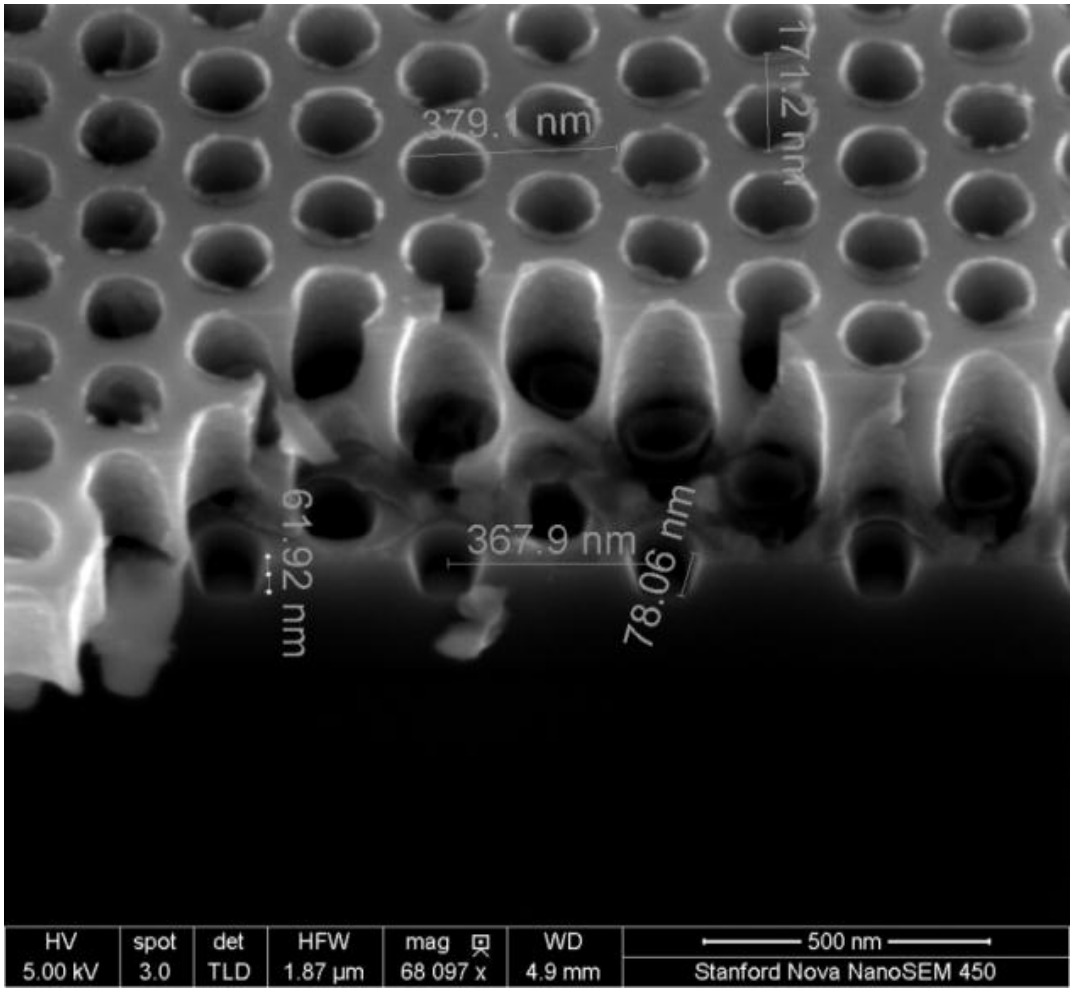

Figure 11: Cross-section SEM image showing the depth profile of the PC holes.

Another concern during device fabrication was the possibility of the deposited metal getting into the PC holes. This would place metal in close proximity to the waveguide layer which would result in a large increase in the laser cavity loss. The deposited passivation oxide mitigated this problem to a manageable extent by covering

the holes partially. The proper method to solve this problem is to planarize the holes by filling them with polyamide before depositing any metal [3]. The excess polyamide on top of the holes can be removed by Oxygen plasma etching. This prevents the metal from getting into the holes during deposition. Further work is being pursued in this domain.

References for Chapter 4

[1] J.F. Martins-Filho, C.N. Ironside and J.S. Roberts, “Quantum well AlGaAs/GaAs monolithic colliding pulse modelocked laser”, Electronic Letters, volume 29, number 12, June 1993.

[2] Audrey Berrier, InP-based photonic crystals: Processing, Material properties and Dispersion effects, Thesis, KTH, Sweden, 2008.

[3] Lin Zhu, Philip Chak, Joyce K.S. Poon, Guy A. DeRose, Amnon Yariv and Axel Scherer, “ Electrically-pumped, broad-area, single-mode photonic crystal lasers”, Optics Express 5966,volume 15, number 10, May 2007.

Chapter 5

Laser characterization

The characterization of our lasers involved multiple electrical and optical measurements. This testing work allowed us to understand the laser quality of lasers and also diagnose any problems that may be present. For example, from the current-voltage characteristics of the lasers, we can easily understand the quality of the laser metal contacts. Similarly, the laser light output needs to be characterized to study the spectral properties of lasers. These measurements require a wide variety of test equipment. This chapter discusses our laser characterization work in detail.

Characterization setup

The laser characterization work was done in our group's optics lab. After mounting the lasers on copper heat-sinks, the sinks are glued onto TEC cooled stations. Current is injected into a laser using a probe station with multiple electrical probes, as shown in figure 1 below. The lasers can be driven in two modes: pulsed mode and continuous wave (CW) mode. In pulsed mode, a pulse generator drives the laser using current pulses which are 10-100μs wide. Pulsed testing of lasers is performed first to make sure that thermal heating of the devices is not an issue. Once pulsed mode lasing has been validated, CW testing is then performed. In CW mode, the laser is driven by continuous current input. CW lasing is harder to achieve since in CW operation the

lasers can show early thermal roll-off. Thermal roll-off is the decrease in light output due to the heating up of the active region of the lasers. As the optical intensity builds up inside a laser cavity, the active region starts to heat up. Ohmic heating of the device due to the drive current can also cause heating. Device heating leads to the non-localization of the carriers (electrons and holes) at the energy band minimum inside the quantum well. This leads to a decrease in population inversion which reduces stimulated emission and can eventually stop lasing. If the device has not reached threshold, lasing may not occur at all.

The current flowing through the laser diode and the voltage across it is measured using an oscilloscope. These measurements provide us with the V-I curve, the voltage vs. current plot, of the laser. The V-I curve tells us about the quality of the laser's electrical contacts and also gives information about possible device heating and shorting issues. Light from the laser is collected by an integrating sphere and directed onto the photodetector, Thorlabs PDA 55 (shown in figure 1 below). The photodetector is connected to the oscilloscope to measure the incident light power. This measurement gives us the light vs. current graph, also called the L-I curve of the laser. The L-I curve tells us about the onset of lasing. Below threshold the light output from the laser is primarily spontaneous emission and it increases linearly with increasing current. As soon as the laser crosses the threshold current value, the light output from the laser increases exponentially and this can be seen as a sharp kink in the L-I curve with a rapid increase in light output thereafter.

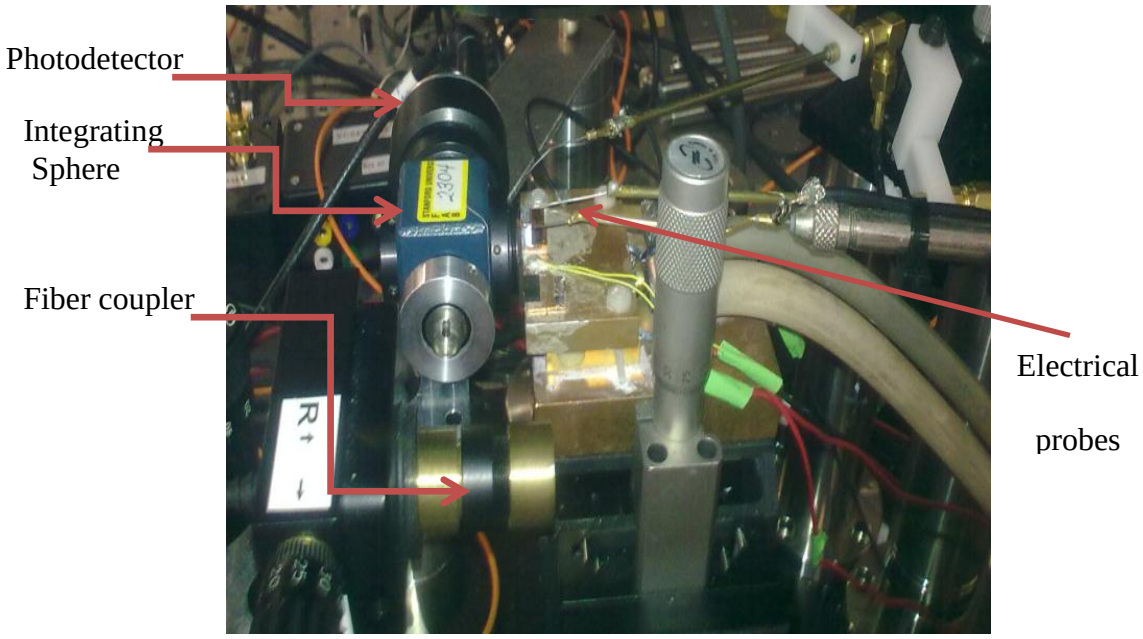

Figure 1: Actual photo of the setup

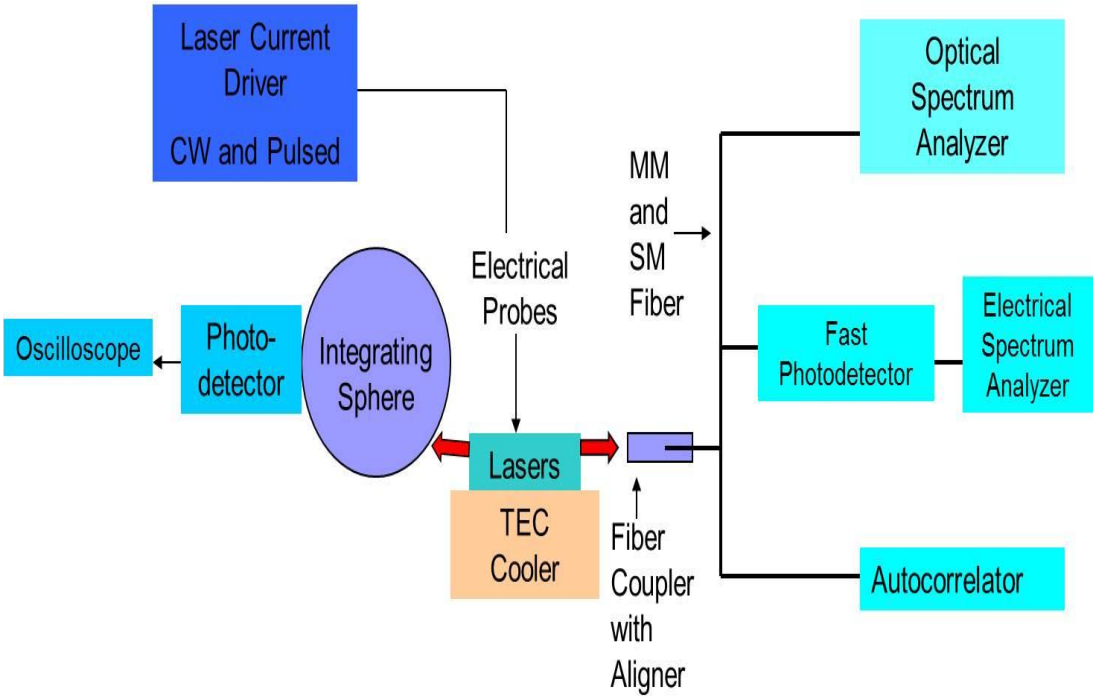

Figure 2: Laser testing setup

The laser light can also be focused into either Single Mode (SM) or Multi-Mode (MM) optical fibers. This is done by using a customized fiber coupler attached to a precise XYZ movement stage. Using the optical fiber the light can be directed into a spectrum analyzer. The spectrum analyzer characterizes the spectral properties of the laser. It shows the relative intensity of various wavelengths that are present in the output of the laser. We are in process of building a custom autocorrelator for our mode locked lasers. Using the optical fiber we will be able to couple the laser light output into this autocorrelator. We are also planning to incorporate a fast picosecond detector into our testing setup. This will allow for the pulsed output from our mode locked lasers to be characterized by Electrical Spectrum Analyzer (ESA). Figure 2 above shows the complete setup.

Photonic Crystal Lasers

The first step towards the fabrication of our proposed slow light mode locked laser was the incorporation of the Photonic Crystal (PC) into an edge emitting laser structure. Related work has been done before [1]. In that work, a square PC lattice was used as a 2D Distributed Bragg Reflector (DBR) mirror to make a single mode laser [2]. The first set of novel devices that we fabricated were narrow waveguide lasers with a 2D triangular lattice PC etched on either side of the top p-electrode. The electrode was 3um wide and the PC on either side of the electrode extended for 7.5 um or ~15 periods. The device is shown in figure 3 below. This SEM image was taken before the passivation oxide and bonding pads had been deposited. The laser p-

electrode is the white strip in the center and the PC on either side of the electrode can be seen clearly.

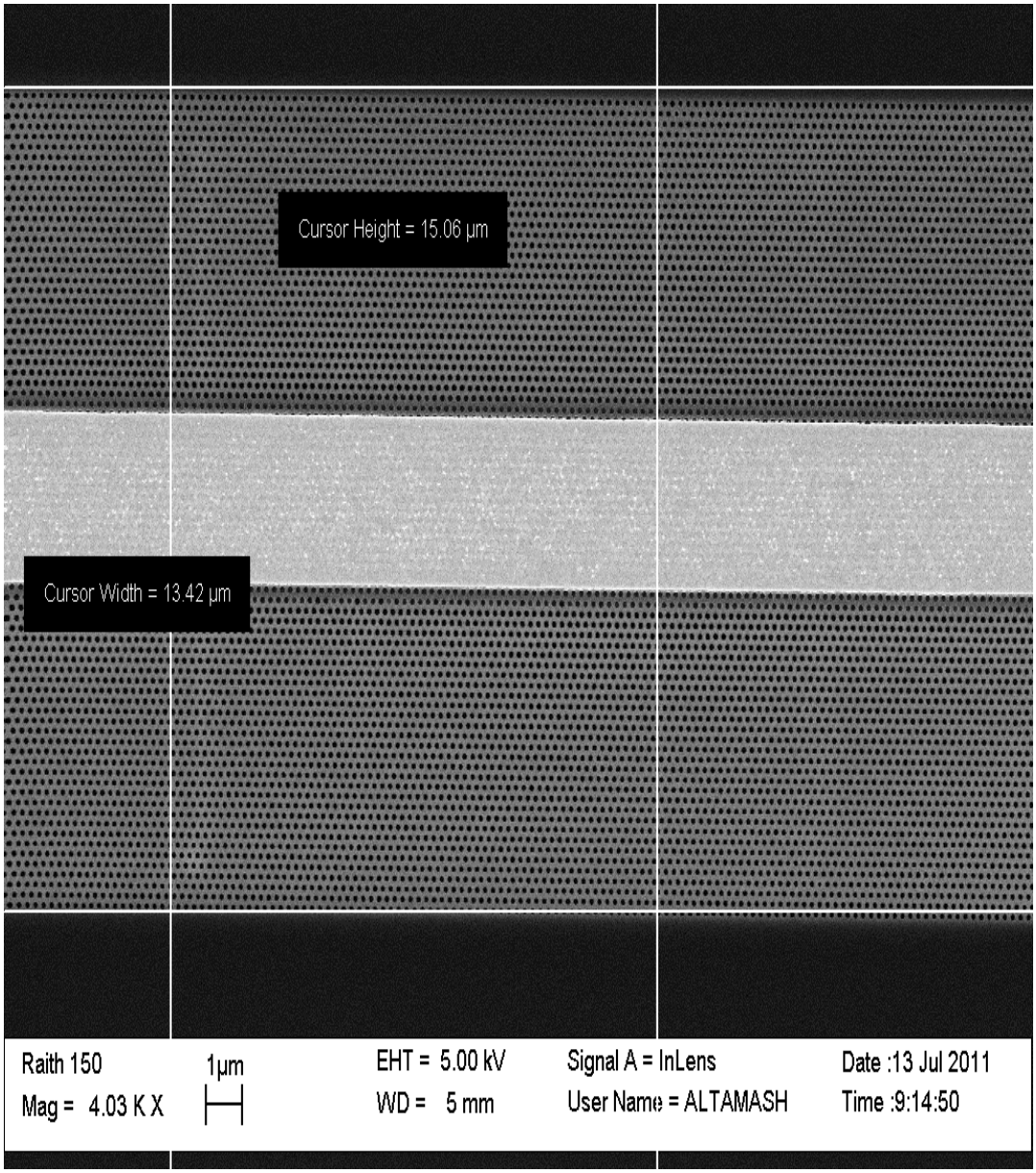

Figure 3: Photonic Crystal laser

The I-V curve shown below is typical of our photonic crystal lasers. The lasers exhibit low contact resistance. This is highlighted by the fact that the voltage across

the diode does not reach large values even at high drive current values. Also, the curve is smooth without any kinks. This is representative of good electrical injection into the laser and shows the absence of any short or open circuits due to poor contact/bonding pad deposition or bad probes connections.

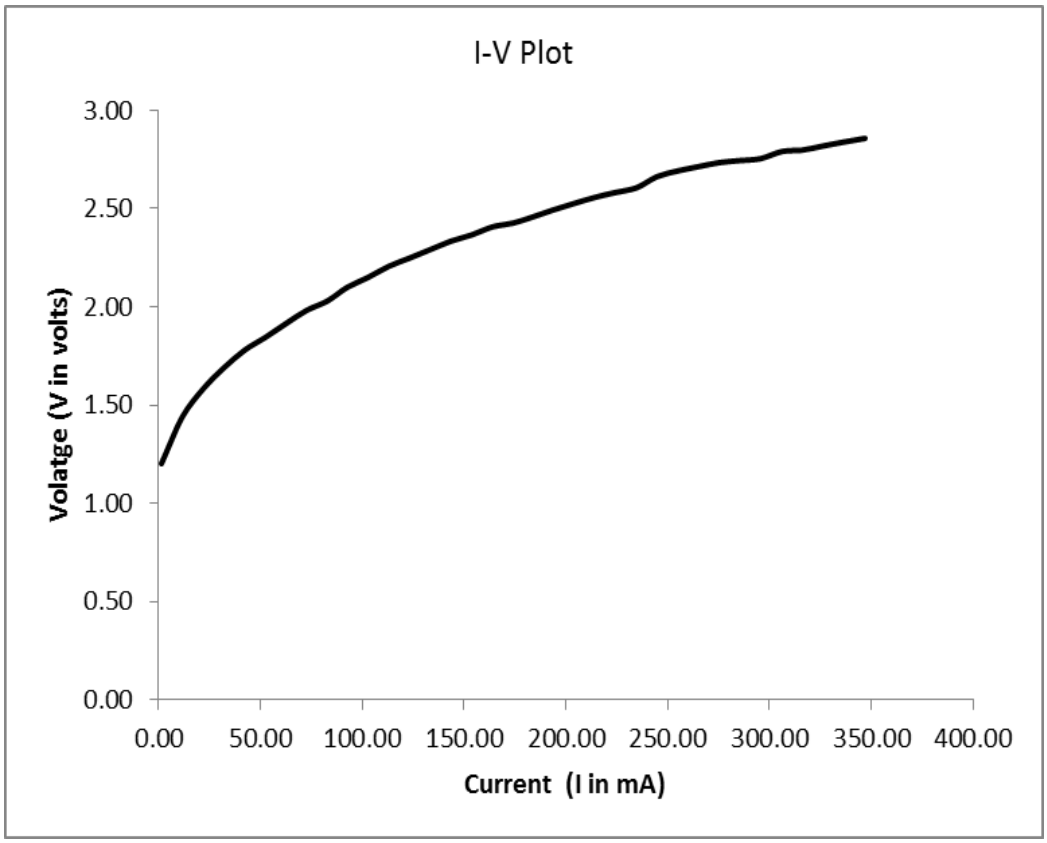

Figure 4: I-V plot of a PC laser

The performance of the PC lasers was compared to simple gain guided lasers. Gain guided lasers have a similar top p-electrode but they do not have any etched mesa or etched PC holes. This means such lasers have poor or no current confinement. The L-I plots for the two types of lasers are shown in figure 5 (a) and 5 (b) below.

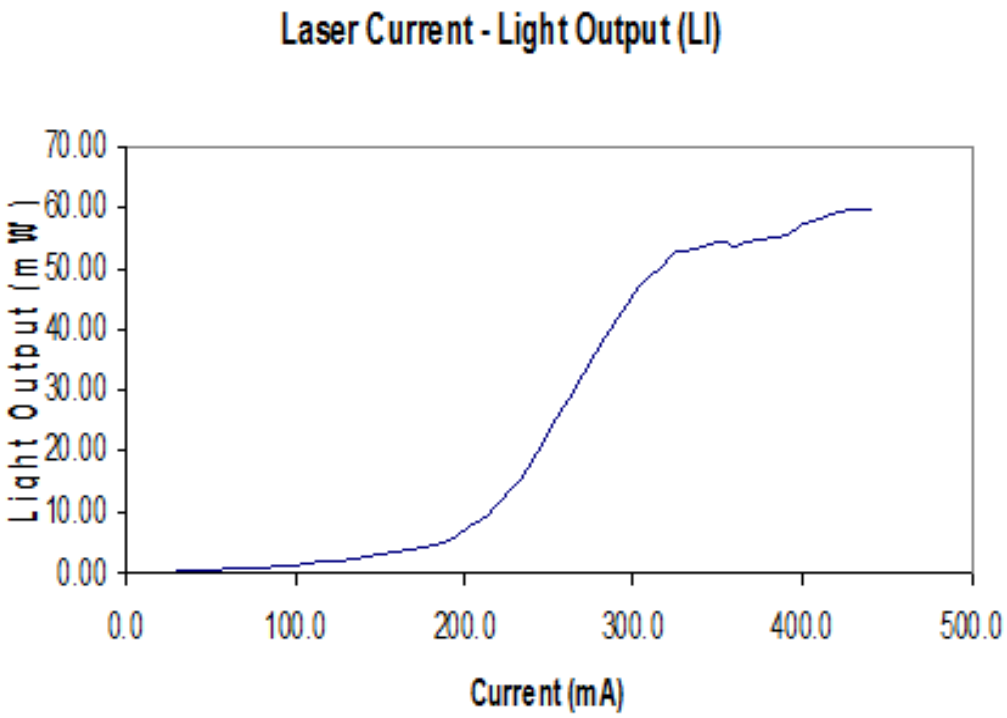

Figure 5 (a) : L-I curve of gain guided laser without PC

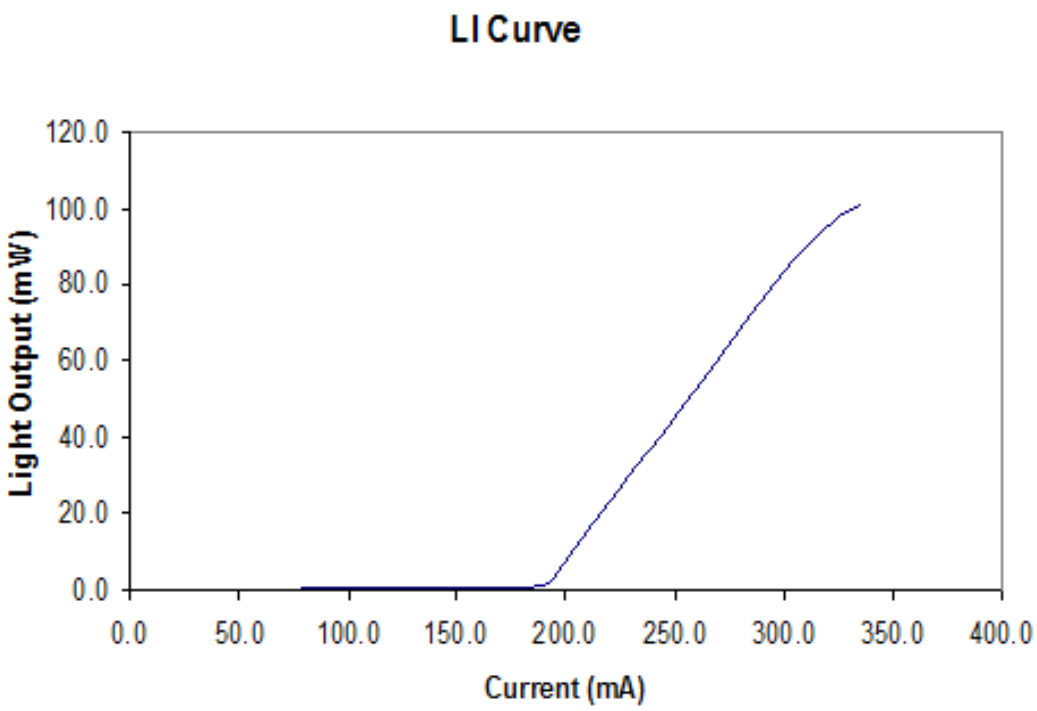

Figure 5 (b) : L-I curve of Photonic Crystal laser

The L-I curve of the PC laser looks much better. It shows a clear threshold kink. The better performance of the PC lasers can be explained by the better current and optical confinement due to the etched holes. The etched holes of the PC remove a significant part of the top conducting layer of the laser wafer. Also the thin veins of the triangular lattice make this region a region of high electrical resistance. This prevents the lateral diffusion of current on either side of the electrode and thereby provides current confinement. The PC also provides optical confinement. This happens due to Bragg scattering from the holes and a difference in effective index between the waveguide and the PC region. The optical spectra of the two types of lasers show even greater differences. This can be seen in figure 6 below.

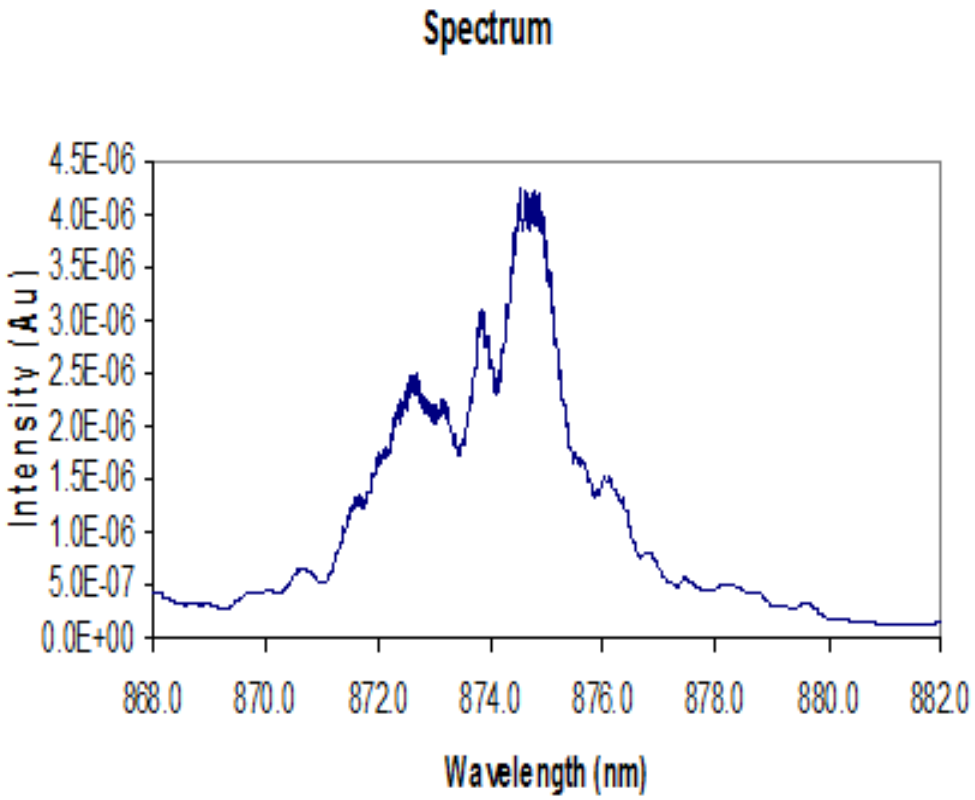

Figure 6 (a): Optical Spectrum of gain guided laser

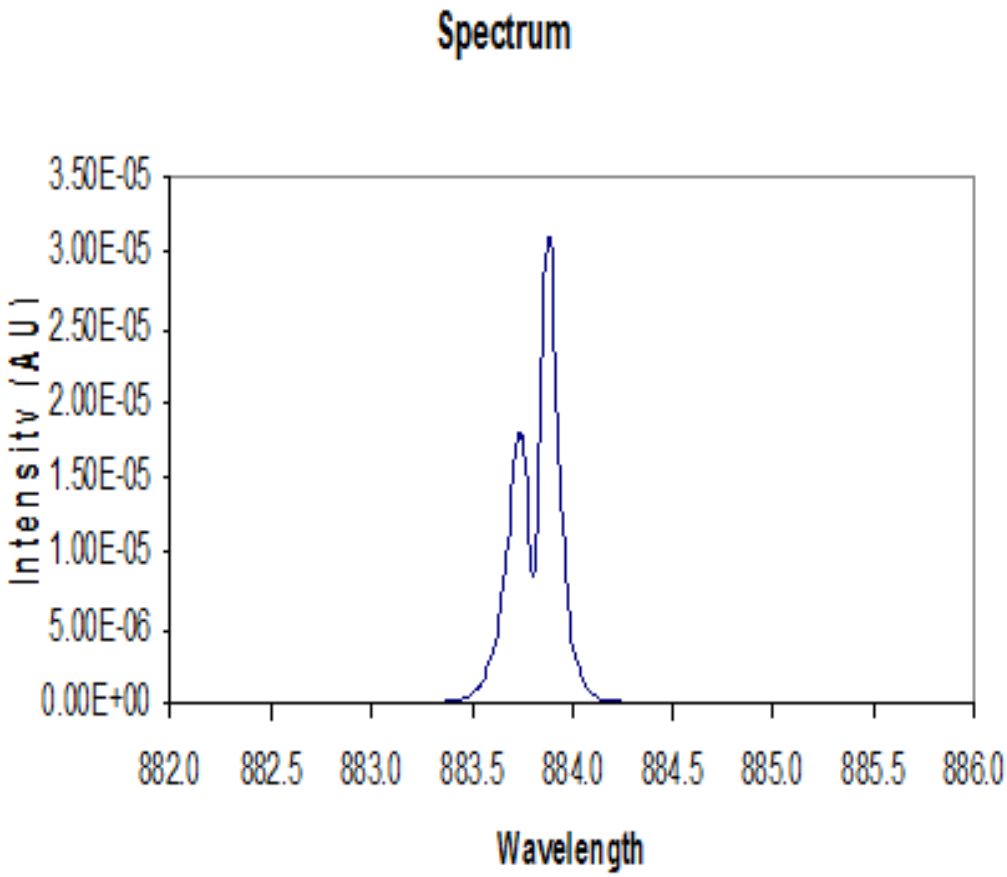

Figure 6 (b): Optical Spectrum of PC laser

Both these lasers are operating at similar drive current levels. As can be seen above, the spectrum of the PC lasers has much narrower linewidth. The spectrum is also red-shifted by nearly 10 nm. These interesting results show that the PC is interacting with the optical mode inside the laser cavity. Both kinds of lasers are assumed to be lasing in a single lateral mode near threshold due to the narrow width of the electrode [3].

Varying the PC hole radii

PC lasers were fabricated with the same lattice constant but with varying hole radii. The plot shows the effect of the hole size on the threshold current.

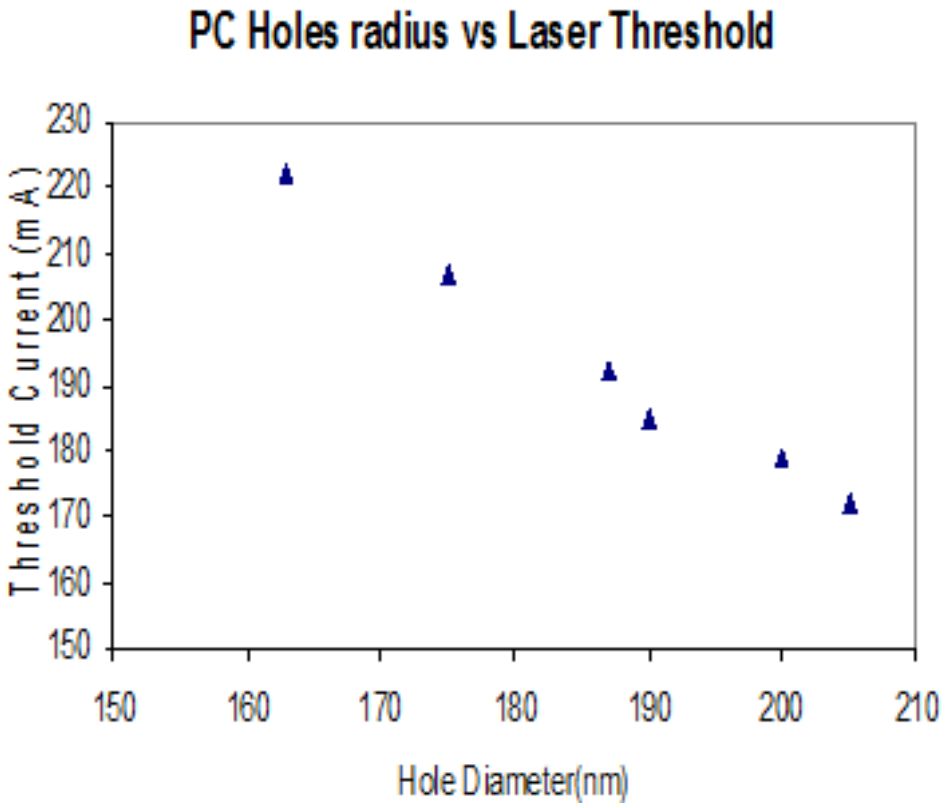

Figure 7: Effect of hole diameter on the laser threshold

The plot above shows that increasing the hole diameter decreases the threshold current of the PC lasers. Larger holes make it difficult for the current to penetrate through the region where the PC has been etched. This increases the resistance of that region and helps in confining the current to the region below the p-contact. Furthermore, larger holes also provide more optical confinement. Both these factors

improve laser performance. The effect of holes diameter on lasing spectrum was even noticeable. The spectrum changed shape and was also shifted.

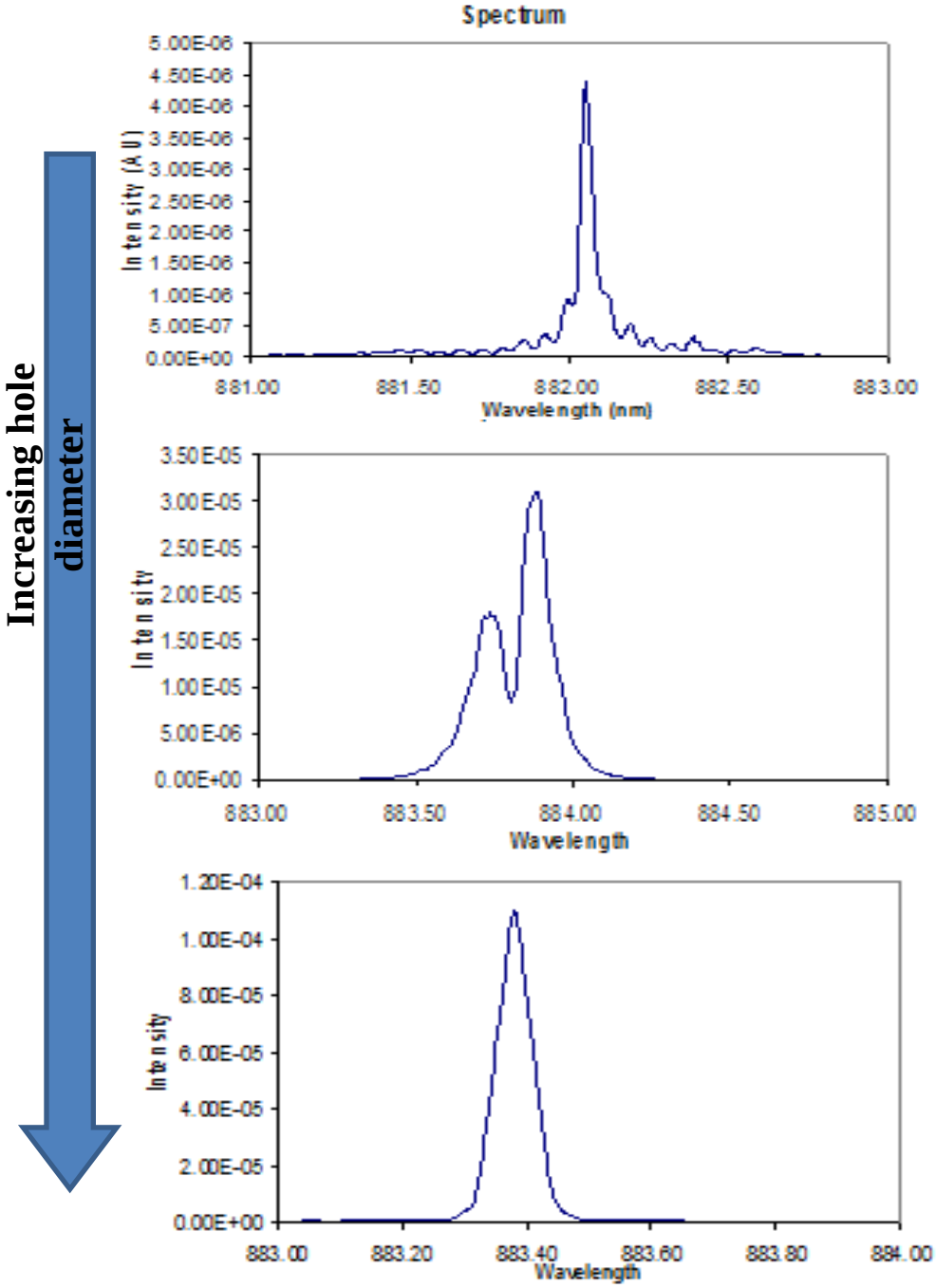

Figure 8: Effect of varying holes size on the spectrum

Lasers were also fabricated that had an etched mesa for better current confinement. Such lasers were fabricated using the second epitaxial wafer. In that wafer, the top cladding was sufficiently thick to allow for etching of a mesa before the photonic crystal was etched. The etched mesa was much more effective in preventing lateral current diffusion and these lasers showed much lower threshold current density. The etched mesa reduced the effective current density by as much as 2.5 times from $7kA/cm^2$ to $3kA/cm^2$. One issue in fabricating such lasers was the uneven spinning of the E-beam resist. This can be attributed to the etched mesas which created topographical features on the front side of the wafer. A non-uniform film of resist made it more difficult to write clear PC patterns and often the rows of holes next to the mesa were exposed improperly. This can be seen in the SEM picture below. Pre-coating the laser pieces with HMDS before spinning ZEP proved beneficial.

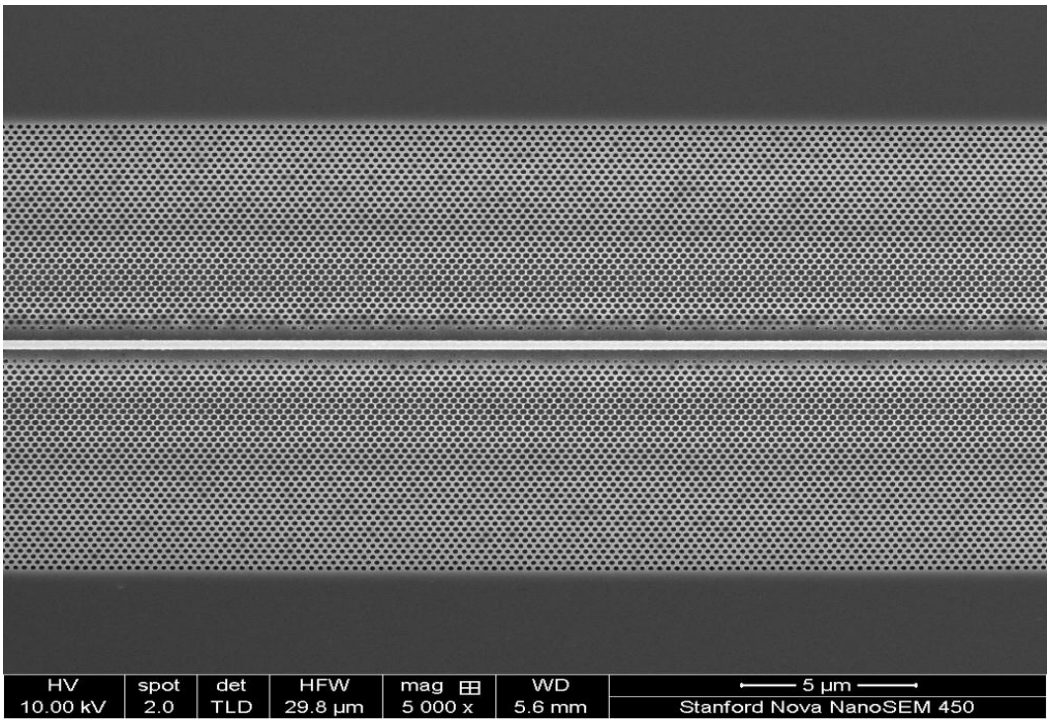

Figure 9: PC laser with an etched mesa

Mode locked PC lasers

If the separation between the SA section and the gain section is defined by lithography, a precise cleave is necessary to control the length the two sections. As has been stated before, we did not have access to a precise laser wafer cleaver on campus. Manual cleaving did not provide us with the required precision level and this resulted in some lasers having very long SA sections and others having very short ones. This problem can be seen in the picture below.

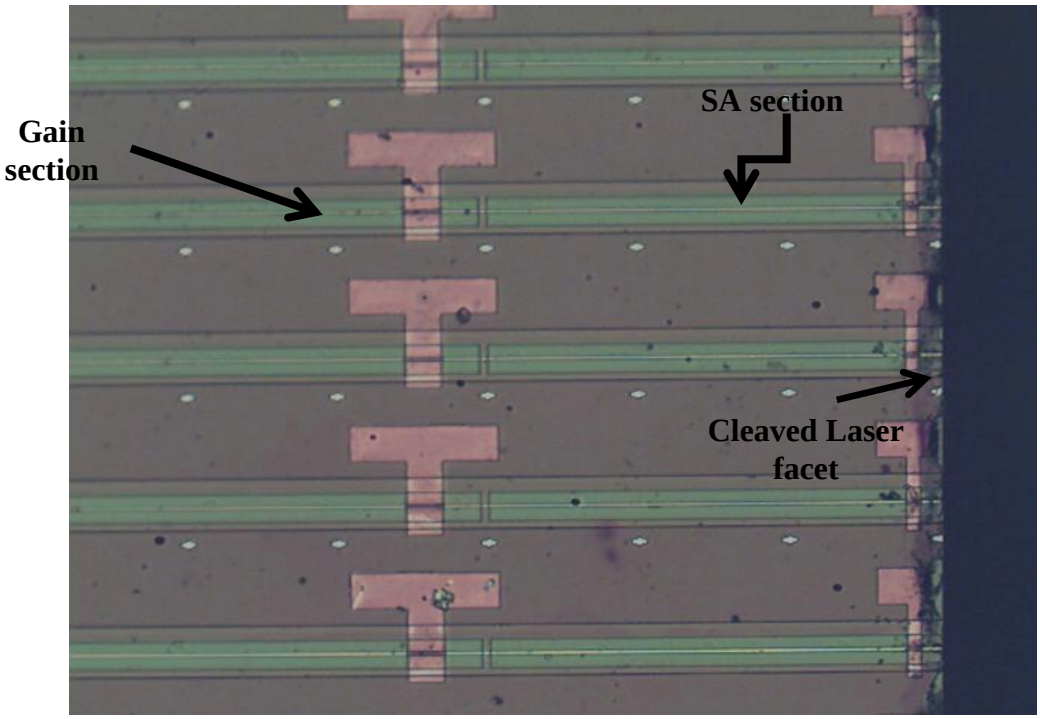

Figure 10: Picture of mode locked laser

In lasers that had very long SA sections, as soon as we put a small reverse bias on the SA section, the lasers stopped lasing. This is shown in the L-I curves in figure 11 below. Without the reverse bias on the SA the laser shows a clear threshold kink. In

contrast, when we apply a small reverse bias, the laser rolls off before threshold is reached. This can be explained by the fact, that a long SA section introduces too much loss into the laser cavity. The gain of the laser is not sufficient to compensate for this loss and therefore the laser never reaches threshold.

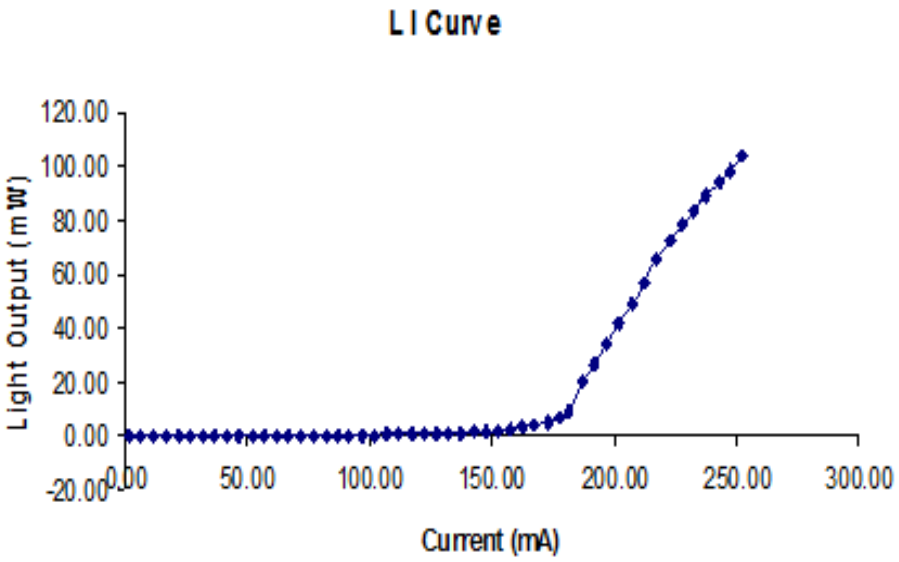

Figure 11(a): L-I curve without any reverse bias showing clear kink and lasing

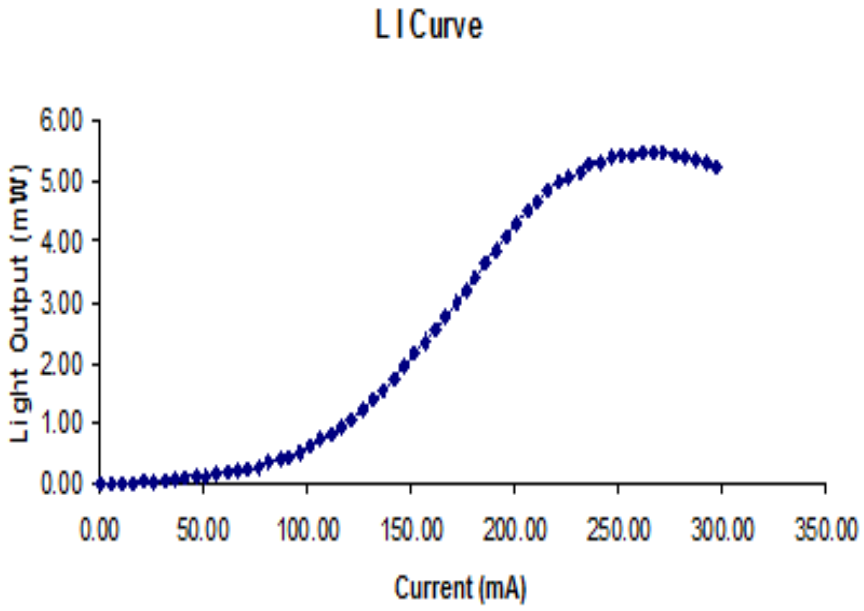

Figure 11(b): L-I curve with applied reverse bias of -1V showing no lasing

We wanted to keep the entire laser processing in-house and wanted to avoid the use of off-campus cleaving facilities. Therefore we decided to use Focused Ion Beam (FIB) milling to split our top electrode into two sections. FIB uses Gallium ions with high kinetic for micromachining. These ions have sufficient kinetic energy to cause the physical removal of the material on which the ion flux is incident. The flux can be controlled by tuning the ion current. Higher current means greater flux and this leads to quicker milling. However, at high currents the ion beam is larger and it may not be suitable for precise nanometer scale ion millings. The time of exposure to the ion beam can be used to control the ion milling depth. Longer exposure leads to deeper physical ablation. Our goal was to use the ion flux to create a sufficiently deep trench that produces good electrical isolation between the two laser sections. We found out that this can be easily achieved through FIB milling. The SEM pictures below show the well-defined clean cuts that can be obtained through FIB milling.

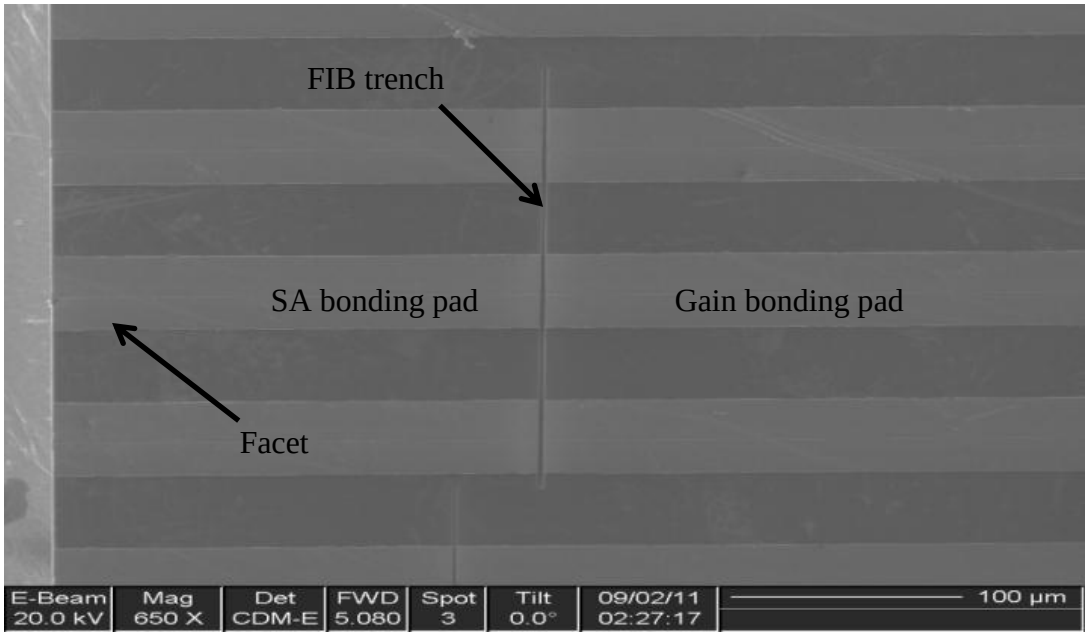

Figure 12(a): SEM image of the top bonding pads with the FIB trench

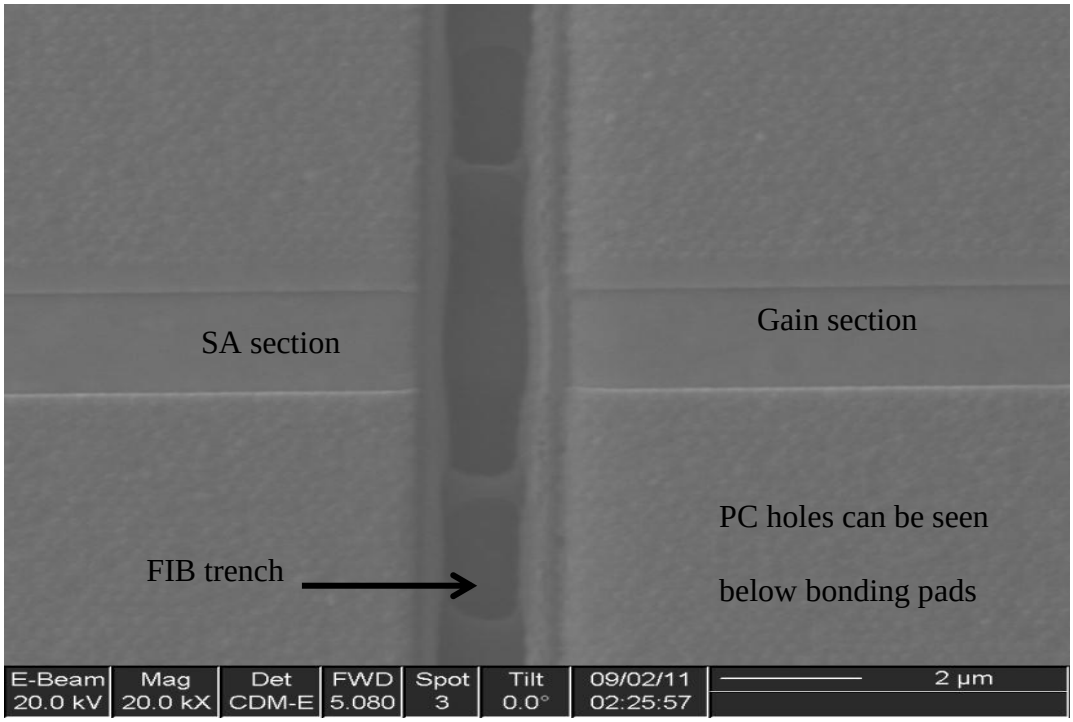

Figure 12(b): SEM image of the FIB milled trench

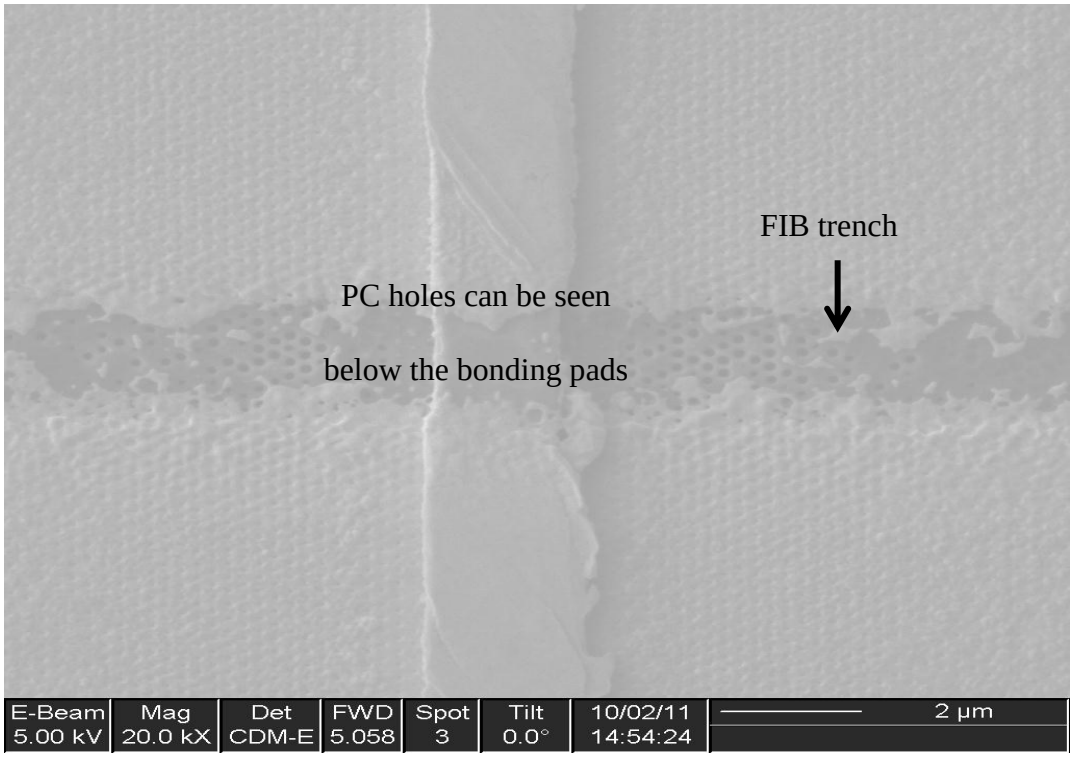

Figure 12(c): SEM image showing the PC holes in the trench area

The FIB milling was performed after the laser bar had been cleaved and mounted on the heat sinks. Etching the trenches was the last step of our fabrication process. This allowed us to accurately control the lengths of the gain and SA section. FIB also provided us with the capability to make lasers with different SA lengths on the same laser bar. The laser I-V curves allowed us to check the quality of electrical isolation achieved through FIB milling. The I-V curves were normal and showed no signs of electrical shorts between the gain and SA section.

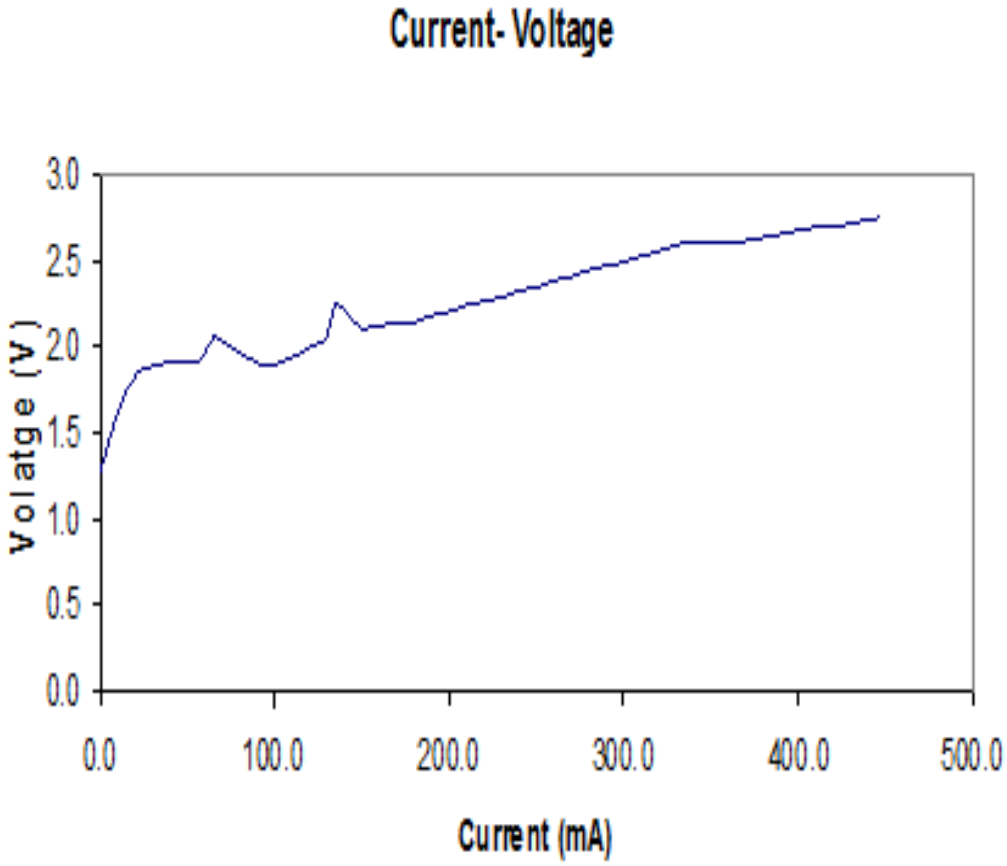

Figure 13: I-V curve of FIB milled mode locked laser showing good electrical isolation between the SA and gain section

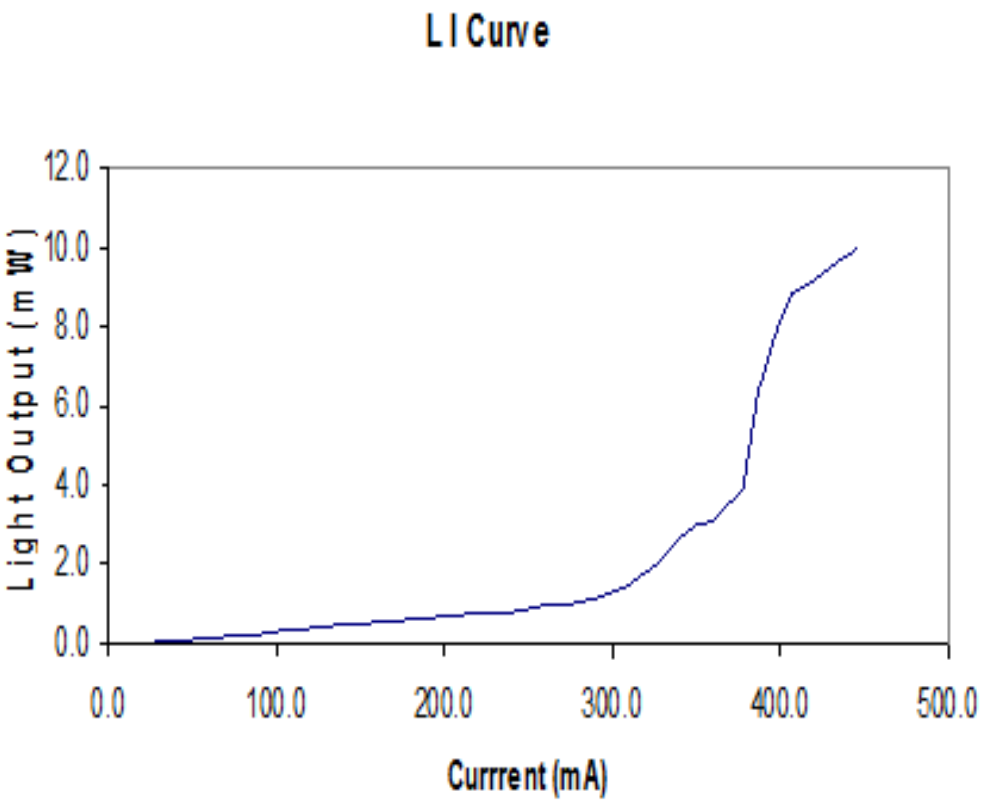

Figure 14: L-I curve for a FIB milled mode locked laser

The L-I curve for a typical FIB milled mode locked laser is shown in figure 14 above. The laser shows lasing even with reverse bias applied to the SA section. As a laser mode locks, the SA section saturates and this is shown by an additional kink in the L-I curve above threshold. The slope of the L-I curve after SA saturation is lower than before saturation, signifying a lower effective threshold. This is because of the fact that after the SA has saturated the total loss inside the laser cavity is reduced. The L-I curve for our PC mode locked lasers, shown in figure 14 above, also shows some kinks. However, the results are not conclusive. Further laser characterization work is in progress.

References for Chapter 5

[1] Lin Zhu, “Photonic Crystal Bragg Lasers: Design, Fabrication, and Characterization”, Thesis, Caltech, 2008.

[2] Lin Zhu, Xiankai Sun, Guy A. DeRose, Axel Scherer and Amnon Yariv, “Room temperature continuous wave operation of single-mode, edge-emitting photonic crystal Bragg lasers”, Optics Express 502, volume 16, number 2, January 2008.

[3] Peter Vasil′ev, Ultrafast diode lasers: fundamentals and applications, Chapter 1, Boston Artech House, 1995.

Chapter 6

Future work

Due to time limitations this thesis work could not incorporate a lot of design modifications, improvements and new ideas. This chapter discusses some of the future work that is in progress. It also highlights some new avenue towards which future research work can be directed.

PC laser improvements

In this thesis work we fabricated and demonstrated novel narrow waveguide edge emitting lasers with integrated 2D photonic crystal structures. These lasers show very interesting properties and need to be examined in more detail. Work is in progress to study how the PC affects the electrical and spectral properties of these lasers. In this regard, we are looking into a few design variables and trying to find out how they affect the lasing properties. One such variable is the width of the p-electrode of the lasers. We have fabricated lasers where the width of the top p-electrode varies from 250nm to 3um. The SEM pictures of lasers with electrode width of 276nm and with width of 2um are shown in figure 1. CW lasing has been observed in lasers with electrode widths down to 2um. Pulsed lasing has been seen in lasers with even smaller electrodes. The laser performance decreases sharply as the width of the electrode is decreased. One explanation of this observation is the sharp reduction in current

confinement as the width of the electrode is decreased. Reduced current confinement means that there are fewer carriers inside the active region to bring about population inversion and lasing. This will lead to higher threshold current and the laser may not lase at all if the threshold is too high due to device heating. As a possible solution to this problem we are looking into ion implantation to improve the current confinement. By using proton bombardment, the resistivity of the region adjacent to the electrode can be increased. This will reduce the lateral diffusion of current and will lead to better lasing performance.

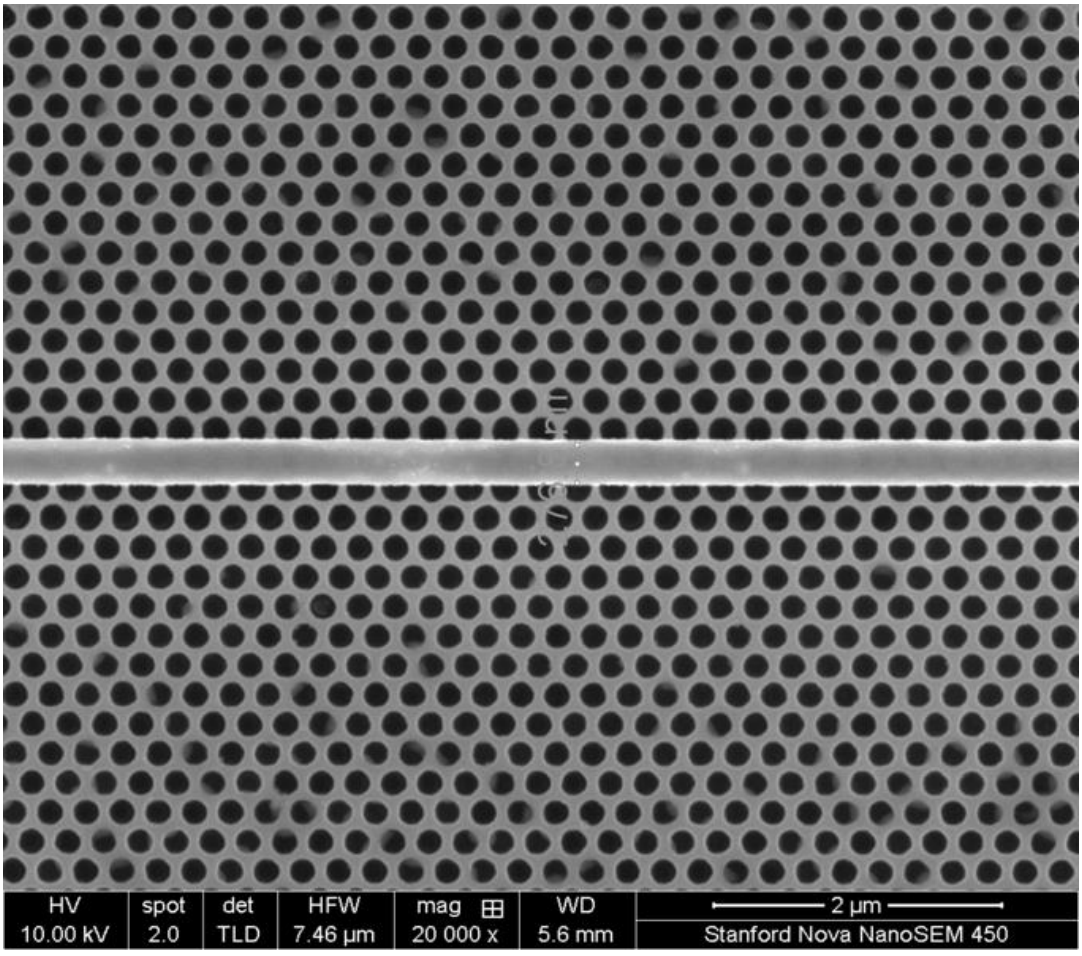

Figure 1(a): PC laser with 276nm wide electrode

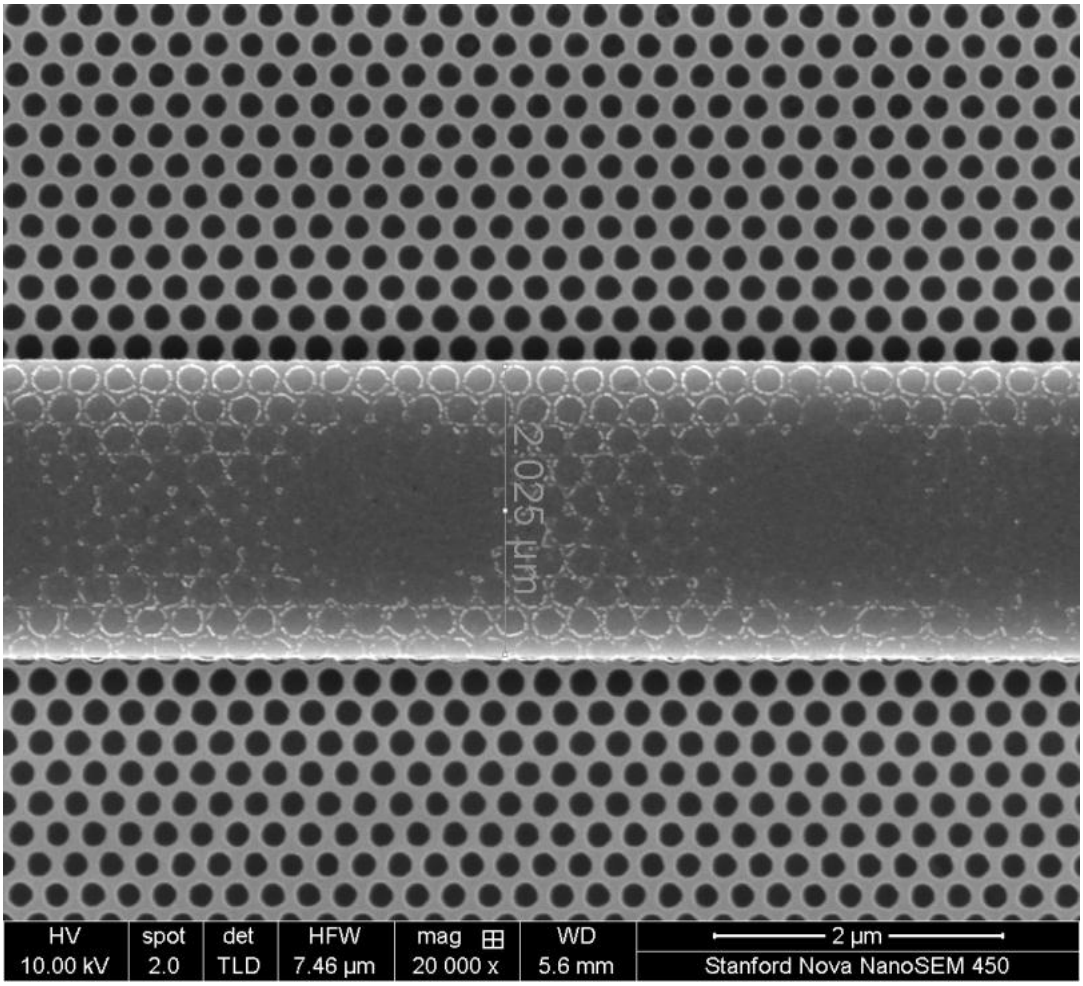

Figure 1(b): PC laser with 2um wide electrode

In addition to the width of the electrode, there are many other design parameters that can be varied and they can potentially lead to novel interesting results. One very interesting possibility is to make a single mode laser using this 2D triangular lattice of holes. As has been discussed before, the PC lasers had a much narrower linewidth as compared to the lasers without the PC. Some PC lasers show less than 0.2nm wide laser linewidth as shown in the figure 2 below. This can allow for making of a single mode laser by simply reducing the length of the device to 1mm or below.

The decrease in device length will increase the longitudinal mode spacing and this coupled with narrower linewidth can result in a single mode laser. As compared to Distributed Feedback (DFB) lasers and Distributed Bragg Reflecting (DBR) lasers, this will be a much easier and more robust way to make single mode lasers. We have fabricated some lasers that can possibly be single mode lasers. We are arranging for a high resolution spectrum analyzer to confirm our findings.

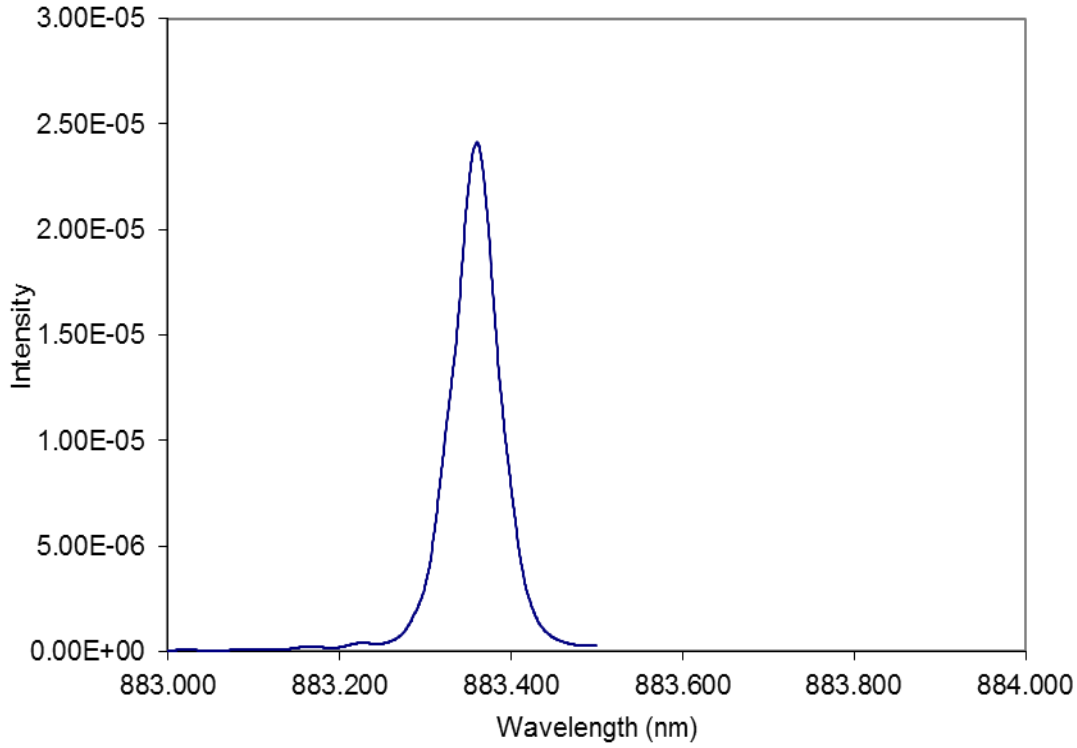

Figure 2: Narrow linewidth shown by our PC laser

Other possible device modifications include studying the effects of changing lattice constants on the lasing properties. Also, different PC lattice types like square,

rectangular or hexagonal lattices can be incorporated into our lasers as well. Such lasers can show interesting electrical and spectral properties.

Mode locked laser improvements

The fabrication of Photonic Crystal mode locked lasers has also been completed. However, the characterization work on these lasers is in progress and for this we are upgrading our testing setup to incorporate an autocorrelator and a fast detector. We are also fabricating new devices to characterize the effects of the slow light PC on the mode locking behavior. In this domain we have a lot of variables that can be engineered and their effects can be studied in detail. The following is a list of some of the design variables upon which we are focusing.

I. PC hole radius
II. Laser electrode width
III. Lattice constant and fill factor
IV. Lattice type: Triangular, square, rectangular etc.
V. Sectioning the PC array

All these variables and many more can be changed to achieve novel device properties. For example, PC waveguides can be engineered to allow for dispersion free propagation of light as shown in figure 3 taken from reference [1]. By systematically changing the radius and/or position of a few rows of holes, a dispersion free wavelength range can be obtained. The incorporation of such a feature into our mode locked laser will be of great advantage.

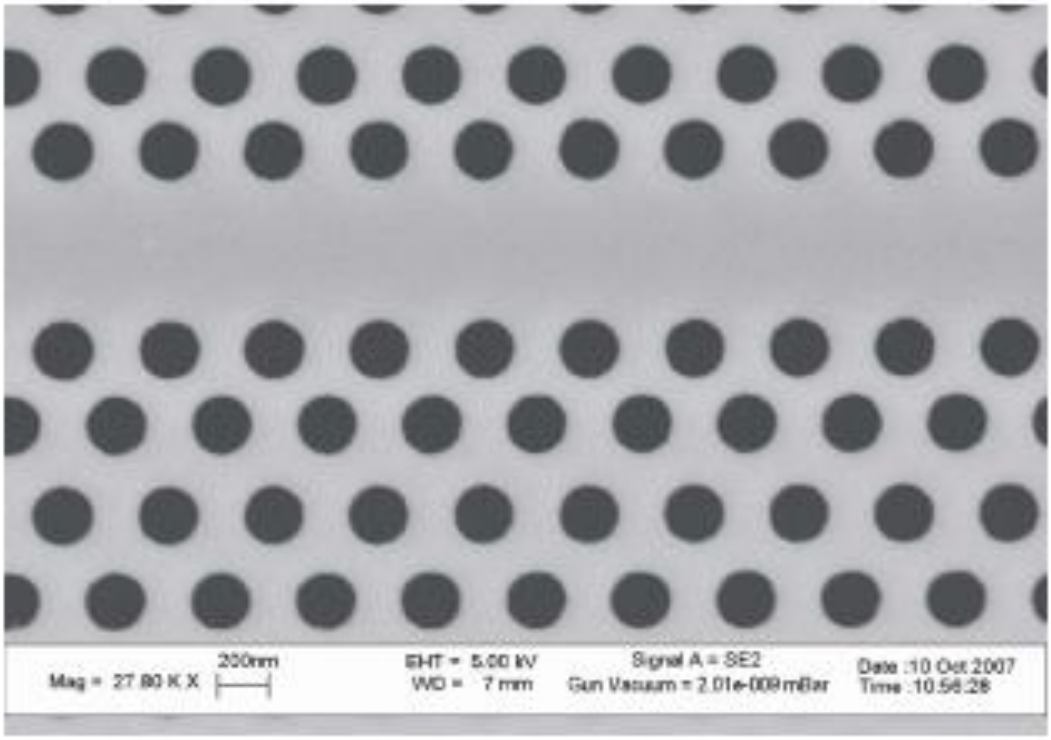

Figure 3(a): Dispersion free PCWG obtained by shifting of PC rows [1]

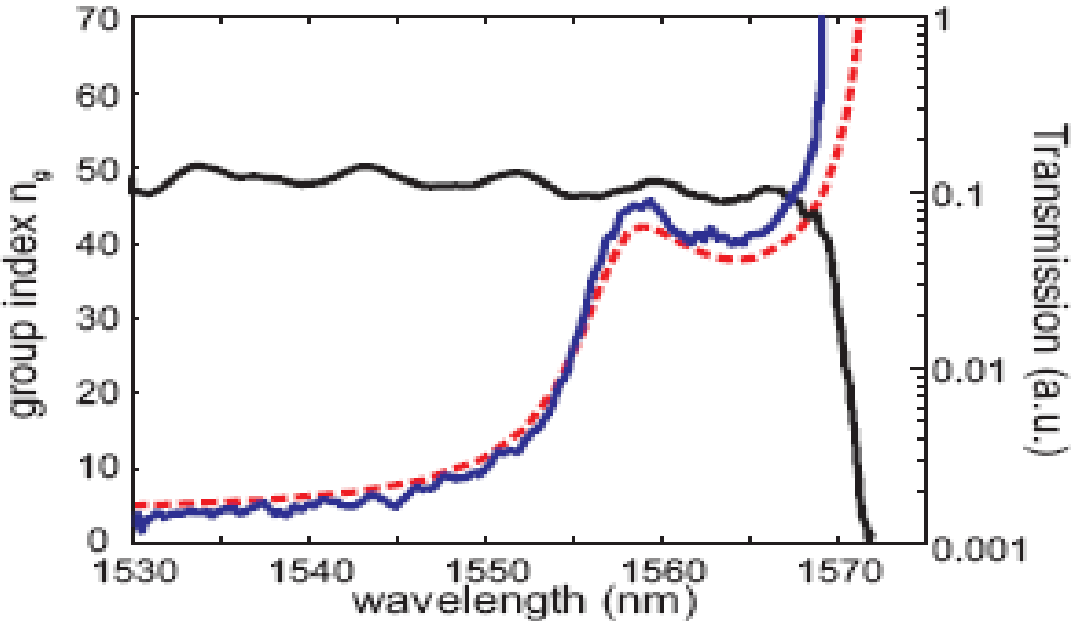

Figure 3(b): Group index (in blue) vs. Wavelength [1]

(Notice the flat dispersion free part of the blue curve between 1555nm and 1565nm)

In the aforementioned paper, the authors fine-tuned the position of the holes adjacent to the waveguide. This is shown on the figure 3(a). The result was a dispersion free slow light waveguide. Over a significant bandwidth, the waveguide showed a constant high group index. This can be seen in figure 3(b).

Photonic crystal waveguides can also be engineered for dispersion compensation and pulse shaping [2]. Figure 4 below, taken from reference [2], highlights how this can be done. Different sections of a PCWG can be designed in such a fashion that the dispersion characteristics in one segment complement and cancel the dispersion in another section. This can allow for dispersion free propagation of light since the spread of light pulse in one section is cancelled by pulse compression in the complementing section.

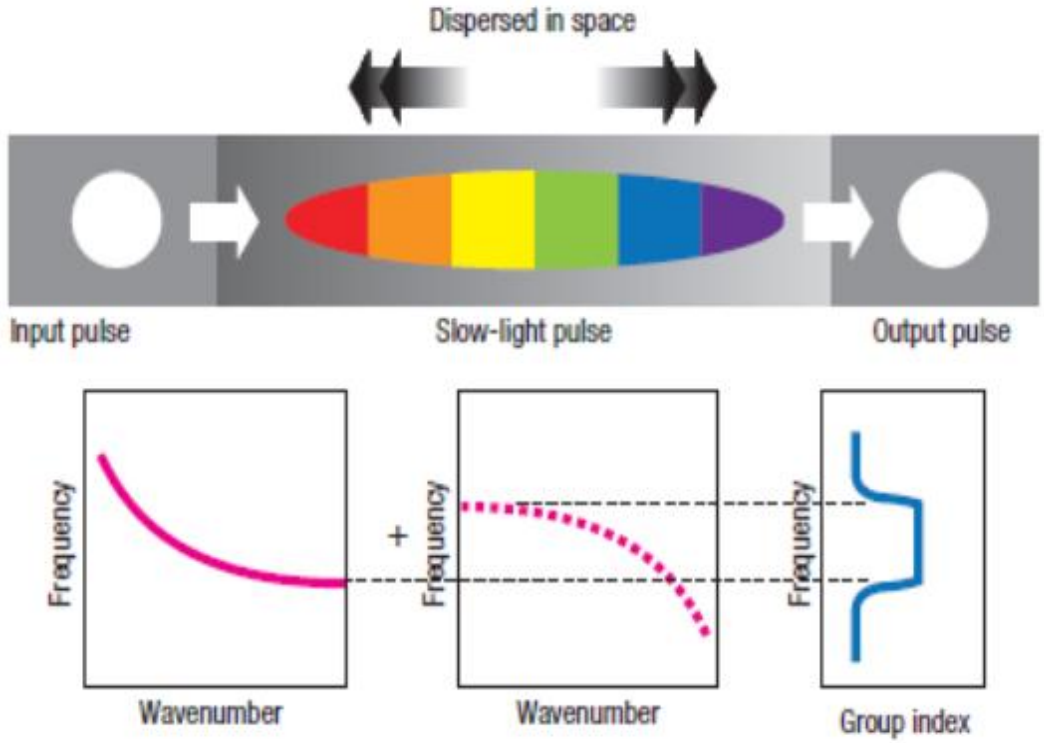

Figure 4: Dispersion compensation in PCWGs [2]

The available bandwidth in our lasers does allow for the compression of laser pulses to below a picosecond. Pulse shaping can potentially be used in our photonic crystal mode locked lasers and this can produce novel results.

Future work

There are many other exciting research avenues that can also be explored. Our proposed device has the photonic crystal along the complete length of the laser. Multi-segment MMLLs have been fabricated and it would be possible to add the photonic crystal to specific segments of the device [3]. For example a MMLL can be made where the photonic crystal is incorporated as a separate passive section. This section can be customized to produce slow light effect, pulse shaping etc. Another possible modification can be to incorporate the PC in the SA section only. Such a SA section will have better absorption cross-section due to the focusing of light by the PC. One possible hurdle in such schemes can be the optical impedance mismatch between sections with PC and the sections without PC. This may cause intra-cavity reflections.

For our lasers, we used QWs to provide optical gain in the gain segment and saturable loss in the SA section. Quantum Dots (QDs) can show much better performance in both of these roles. QDs have much faster carrier removal times [4]. This means that reverse biased QDs can provide us with a more effective SA section and give temporally narrower pulses. QDs can also show higher optical gain and provide us with more optical power.

The last step is to integrate our slow light lasers into the tiny microscopes made in the Schnitzer lab. The device would need to be packaged with the relevant drive circuitry and will also have to be mounted on an appropriate TEC cooled package. Since the footprint of each laser is less than 50 um wide, we can package and drive multiple lasers together. The light from these lasers can be focused into one beam and then can be used for illumination. This will help in increasing the total two-photon fluorescence obtained. At the same time it will reduce the thermal heating of each individual laser. Decreased thermal heating will in turn make each laser perform more efficiently.

Conclusion

Semiconductor mode locked lasers have been used for a variety of applications including in optical communication and for optical clock generation. Their use for two-photon microscopy has been limited though. In this work we have focused on the development of a novel semiconductor mode locked laser (MMLL) design, which can be effectively used for TPM. TPM is conventionally done using Ti:Sapphire mode locked laser that operate around 100 MHz. MMLLs on the other hand operate around a few GHz. To reduce the repetition rate of MMLLs we have tried to incorporate a slow light photonic crystal into the conventional passively MMLL architecture. Slow light PCWGs can be designed such that they show a high group index over significant bandwidth range. They can further be engineered to provide dispersion free light propagation in this high index regime. In this thesis work we have strived to combine such a slow light PCWG into the MMLL cavity in a monolithic fashion. The first step towards the development of such lasers was the integration of a PC lattice into an edge

emitting laser structure. We were able to accomplish this task successfully and demonstrated these unique narrow waveguide edge emitting lasers that have a 2D triangular photonic crystal lattice integrated into them. These lasers show very novel electrical and spectral properties and this thesis discusses these lasers in detail. This thesis also discusses the progress that we have made towards the slow light MMLL device that we have proposed. It also proposes some future avenues of research that can be pursued in this domain.

Reference for Chapter 8

[1] Juntao Li, Thomas P. White, Liam O'Faolain1, Alvaro Gomez-Iglesia, and Thomas F. Krauss, "Systematic design of flat band slow light in photonic crystal waveguides", Optics Express 6227, volume 16, number 9, 28 April 2008.

[2] Toshihiko Baba, "Slow light in Photonic Crystals", Nature Photonics, volume 2, August 2008.

[3] Brian R. Koch, Jonathan S. Barton, Milan Masanovic, Zhaoyang Hu, John E. Bowers and Daniel J. Blumenthal, "Monolithic mode-locked laser and optical amplifier for regenerative pulsed optical clock recovery", IEEE Photonics Technology Letters, volume 19, number 9, May 1, 2007.

[4] Rafael Aldaz, "Towards monolithic integration of mode-locked vertical cavity surface emitting laser", Thesis, Electrical Engineering, Stanford University, 2007.